PHOTOELASTIC ANALYSIS OF THERMAL STRESSES.

by

C.P. Burger.

A thesis presented for the degree of Doctor of Philosophy of the University of Cape Town

October, 1967.

The work for this thesis was performed in the Department of Mechanical Engineering of the University of Cape Town, during the years 1964 to 1967. It is the original work of the author, except where stated, and no part of it has been presented to any other university.

Signed by candidate

Rondebosch.
13th. October, 1967.

INDEX.

Section.		Page.
	List of Symbols.	3.
	ABSTRACT.	1.
1.	GENERAL BACKGROUND.	4.
	1.1 Historical Survey.	4.
	1.2 Three dimensional Photothermolelasticity.	6.
	1.3 Material Properties.	8.
	1.4 Principles of Photoelasticity.	9.
2.	THERMAL STRESSES.	13.
	2.1 Thermoelasticity.	13.
	2.2 Model prototype correlation.	18.
3.	EXPERIMENTAL METHODS.	21.
	3.1 Background.	21.
	3.2 Methods of imposing the temperature gradient.	24.
4.	DESCRIPTION OF APPARATUS AND EXPERIMENTAL PROCEDURE.	29.
	4.1 Overall description of system.	29.
	4.2 The photoelastic model.	31.
	4.3 The test tank.	36.
	4.4 The circulating liquid.	43.
	4.5 Hot kerosene system.	44.
	4.5A. Cold kerosene system.	47.
	4.6 Tank flow system and controls.	49.
	4.7 Temperature scanning and recording equipment.	55.
	4.8 Polariscope.	60.
	4.9 Photographic techniques.	66.
	4.10 Testing sequence.	69.
5.	EXPERIMENTAL RESULTS.	72.
	5.1 Model properties used in calculation.	72.
	5.2 Verification of model behaviour with theory.	73.
	5.3 Similarity scales; model to steel prototype.	74.
	5.4 Dimensionless stresses.	76.
	5.5 Stress concentrations.	76.
	5.6 Interpretation of photographic records.	77.
	5.7 Results and graphs.	78.
	5.8 Experimental errors.	107.
	5.9 General discussion of the results.	109.
6.	CONCLUSIONS.	113.
7.	ACKNOWLEDGEMENTS.	115.
	REFERENCES	116.

ABSTRACT.

Developments in the application of photoelastic techniques to the study of thermal stress problems are here briefly reviewed, then followed by a short introduction to the relevant photoelastic and thermoelastic theories.

A new method for the study of transient thermal stresses, as well as stresses due to the internal heating of nuclear reactor parts, is described. In this method hot or cold liquid is circulated continuously over the surfaces of a composite photoelastic model which incorporates the sandwich type of built in polariscope developed by Tramposch and Gerard. By varying the temperatures of the liquid and the flow rates to one or all the surfaces of a model, the temperature profile in the model can be controlled at will. The instantaneous temperature profile is sensed by banks of thermocouples which are scanned in sequence with a specially built rotary switch, and their outputs are recorded on a storage oscilloscope. The thermocouples here, are for the first time, mounted outside the sandwiched polariscope in a separate sensor block where they do not disturb the photoelastic fringe pattern of the thermally induced stresses. The stress fringe patterns are observed continuously and photographed according to a set time schedule in synchronism with the temperature pattern on the oscilloscope screen. Thus a simultaneous record of the thermal stresses as they develop in the model, and the temperature profiles that cause them, is obtained.

The test method is applied to the study of thermal stresses in an unconstrained thick plate with a temperature gradient across its thickness. Two models are used, one of uniform thickness and another which has a small change in thickness at a single radiused shoulder. The ratio of thick to thin section is 1.1 to 1. Three basic types of temperature gradient are induced in each model, i.e. firstly: equal heating

on both faces of a plate initially at uniform temperature; secondly: heating on one side only, of a plate initially at uniform temperature; and thirdly: heating on the cold side only, of a plate with an initial linear temperature gradient between a cold side and a hot side.

During the earlier parts of the last mentioned sequence, temperature profiles are included which are similar to those that exist as steady state conditions in nuclear reactor parts subjected to internal heating. The fringe patterns of all tests on the stepped plate also include information on the thermal stress concentrations.

Results are given which illustrate the extreme flexibility and adaptability of this new test method to different temperature conditions and model shapes. They present the first record of photoelastic techniques applied in such a general way to the study of transient thermal stresses. These results also include the first successful photoelastic study of stresses caused by temperature gradients which result from internal heating of plates, as well as the first photoelastic determination of stress concentration factors under such conditions.

Thermal stress concentration factors are found for the plate with a change in cross section during transient thermal conditions. These are of the order of 1.2 to 1.3 in comparison with the highest stresses in a similar plate of uniform thickness. They generally vary with time while the temperatures are changing.

The results are discussed and their relevance, as well as the general value of the test method, to design problems involving thermal stresses are emphasized.

Finally a typical model to prototype correlation is made for Araldite B(CT 200) and a low alloy steel plate of the same size subjected to the same range of temperature change. The relative times when conditions occur as well as the magnitude of stresses in each material are included with the general graphical presentation of the results.

List of Symbols.

C	stress optic coefficient; specific heat.
c	half plate thickness.
E	modulus of elasticity.
F	model fringe constant.
f	material fringe constant.
h	length of light path through model.
i, j	indicial tensor notation subscripts.
K	stress concentration factor; thermal diffusivity.
k	thermal conductivity.
N	photoelastic fringe order.
Q	photoelastic figure of merit.
T	temperature.
t	time.
V v	velocity of light through model.
x, y, z	Cartesian coordinates.
α	coefficient of thermal expansion.
δ	temperature scaling factor; relative retardation.
ε	normal strain.
λ	geometric scaling factor; wavelength of light.
ν	Poissons ratio.
ρ	density.
σ	normal stress.
σ_1, σ_2	principal stresses.
τ	shear stress.
ϕ	Airy's stress function.

SECTION 1: GENERAL BACKGROUND.

This section reviews the developments in photoelasticity which led to its use in studies of thermal stresses. It also presents the basic stress-optic equations.

1.1 Historical Survey:

The effect of temporary or stress birefringence by which certain materials which are not birefringent in an unstressed state, become so under the influence of stress, was first recorded by Sir David Brewster. The theoretical treatment of this phenomenon was developed independantly by both Neuman and Maxwell, although Neuman related the optical effects of strain, whereas Maxwell expressed his equations in terms of stress. Whether, in fact, the observed phenomena are strain based or stress based only becomes important when problems of a non-elastic nature are considered.

The use of photoelastic models for analysis of stresses in structures by analogy was first developed into a practical technique by Coker and Filon who, in over twenty years of research at University College, London, laid the foundation of modern methods of photoelasticity.

The wider use of photoelastic techniques was greatly assisted by the work of Frocht, whose two books on the subject[+](R1)are still the most widely used handbooks in the field.

Developments in methods of theoretical and experimental stress analysis have been considerable during the past few years. The scope of the photoelastic method, in particular, has been extended to cover almost the whole field of stress analysis. It has been fully established in the solution of three dimensional problems, and the technique of

+ Figures in brackets, e.g. (R1), refer to references on pages 116 to 119.

birefringence coatings is well established. Finally there are the more recent excursions into the fields of dynamic, thermal and non-elastic problems.

Although photoelasticity was first applied to the solution of thermal stresses by Weibel (R2) it was the work of Gerard, Gilbert and Tramposch (R3-8) which established it as a reliable method in this field. Photothermoelasticity, as they called the new technique, is concerned with thermal stress fields. In one major variation it employs two dimensional techniques in three dimensional models by using imbedded polariscopes in a way analogous to embedded strain gauges, except that, as in most photoelastic methods, the solution is for a full field.

Photothermoelasticity deals with a class of stress problem which is very difficult to solve analytically, even in this era of the computer. It is a small development in this method towards more flexibility and the easier simulation of temperature gradients which is presented here.

Three kinds of thermal stress problems have been solved by means of photoelasticity:

(1) Shrinkage stresses resulting from a uniform change of temperature in composite structures combining materials with different coefficients of expansion (R9-11).

(2) Stresses in multiply-connected cylinders subjected to a steady gradient of temperature (R12,13).

(3) Transient thermal stresses including thermal shock (R6,8,14,15).

The experimental methods used in these studies have been:

1) Adaptations of two dimensional techniques using transmission polariscopes on essentially two dimensional models (R5.9,11).

2) Reflection techniques to study surface stresses on large models (R16).

3) A combination of mechanical prestraining and three dimensional stress freezing techniques (R17).

4) Photothermoelasticity using a sandwich technique whereby the polariscope is built into a three dimensional model (R7,13).

1.2 Three-Dimensional Photothermoelasticity:

This term has been applied to the determination of thermal stresses actually induced in a photoelastic model by non-uniform temperature distributions (R7,8). From an experimental standpoint, essentially two-dimensional techniques are employed with the notable exceptions that the loading is thermal rather than mechanical. Since the observed fringe patterns representing the thermal stress fields are intimately associated with the conditions at the specimen boundaries, a most important experimental phase is the appropriate simulation and measurement of the desired temperature distribution.

Theoretical analyses of thermal stresses in three-dimensional bodies are relatively complex and available exact solutions are limited to a few configurations and loading conditions (R18,19,20). Gerard and Tramposch were the first to use a sandwich technique. They built a polariscope into a three-dimensional model by cutting a disc of photoelastic material from the centre of the model, placing it between two sheets of circular polarizing material, cut to the same size as the disc, replacing the combination in the original model and cementing all the parts together again. The sandwich was then effectively a built-in polariscope so that when the model was loaded the fringe pattern was confined to the preselected region of the model between the polarizers and could

be interpreted in the same way as other photoelastic patterns (R7). Thermocouples cemented into the sandwiched disc checked the temperature distribution. They compared their results with these models against known and reliable theoretical solutions, for amongst others, thick walled cylinders exposed to steady state heat flow with constant temperature distribution along the axis (R7,8), always with excellent agreement. Rothstein and Kirkwood (R12) modified this technique by bolting up the sandwich, instead of cementing it, between two thick Lucite end pieces, and applied it to an excellent analysis of the transient thermal stresses in ring assemblies for a nuclear reactor project. Emery and co-workers (R13) used the same method to study the thermal stresses in a partially filled annulus, but, following the same reasoning as was adopted by the author in this study, removed the thermocouples from the actual photoelastic sandwich and cemented them to the inside and outside surfaces of the Lucite end pieces, close to the test section. Again agreement with theory, where available, was excellent.

Since most photoelastic materials suffer large changes in elastic modulus and photoelastic fringe value when the temperature is appreciably increased above room temperature, it is general practice to induce thermal stresses by cooling rather than by heating the specimen. The type of coolant used depends on the number of fringes required and on the heat transfer coefficient between coolant and model. Dry ice placed in contact with a warm surface (R6,14,15), or immersion into a mixture of dry ice and alcohol or acetone have been most widely used (R7,13). Durelli and co-workers used a cold chamber in which they circulated chilled air around a model (R21,22).

The lowest temperatures encountered were around $-50^{\circ}C$ although with the availability of cryogenic fluids the lower

temperature limit could be reduced much more. The properties and behaviour of photoelastic plastics at these very low temperatures are however not yet known.

It is not necessary to cool to induce thermal stresses within the measurement range. Moderate heating to about 75°C is permissable and will induce stresses of a sufficiently high level for many investigations.

1.3 Material Properties:

Only a few materials, mainly the epoxies, have been evaluated for photothermoelastic application (R4,7,12). The index of merit used has been $Q = \alpha E/f$ (R23) which should be constant and as high as possible within test temperature range. The values of index of merit for most epoxy resins are reasonably constant, because, as the temperature is changed the elastic modulus and fringe constant change at approximately the same rate while the coefficient of thermal expansion stays nearly constant ($\pm$ 1 micro in/in °F) over the range of temperatures used (R4,12,39). The constance of Q eliminates complications in interpreting the model fringe pattern in terms of its stress distribution. Variations in E do of course, effect the stresses themselves so that correlation with theoretical computations and the prediction of prototype stresses from model measurements should take account of it. Fortunately the change in the modulus of elasticity is also small ($\pm$ 5000lb/sq.in) over the temperature range used and it is general to consider E constant when interpreting the stresses and correlating them to prototypes (R12,39).

These assumptions are not as alarming as may appear at first sight. In general thermoelastic calculations constancy of E and α are basic assumptions, yet, known values for steels show a remarkable variation. (Illustrated in table 1(R25).)

McCalvery (R24) similarly points out that the coefficient

of thermal expansion is usually taken as constant, yet it is not even reliably known, nor do metallurgists ever claim accuracies better than 1 part/million for their published figures. To the designer the difference between an average coefficient of 12×10^{-6} or 14×10^{-6} in/in ^{o}C means that for a temperature rise of 500^{o}C he may expect a strain of 0.006 in/in or 0.007 in/in!

Table 1: Mechanical and Thermal Properties of 3 Steels at different Temperatures.

Material	Modulus of Elasticity. ($\times 10^{6}$ lb/sq.in.)		Coef. Thermal Exp. (micro in/in^{o}C)	
	RT			
En 3	30.1	500^{o}C/19.9	100^{o}C/12.2	600^{o}C/14.4
En 40c, H&T	30.9	700^{o}C/21.2	100^{o}C/12.5	600^{o}C/14.0
En 55, soft	29.6	600^{o}C/22.2	100^{o}C/16.0	500^{o}C/17.0

1.4 Principles of Photoelasticity:

The principles of photoelasticity or photomechanics are adequately explained in several excellent books, notably Frocht (R1), Durelli (R21), Dally and Riley (R26). For a short summary of the methods used the reader is referred to the ASME Handbook (R27) and to the short treatment by Hendry(R46).

The following is given as a very brief summary of the principles involved and their application to thermal stress problems:

When linearly polarized light passes through a transparent substance that exhibits stress birefringence, it is split into two orthogonally polarized components, each parallel to a direction of principal stress. These components propagate through the material at different velocities. For light of a given wave-length (monochromatic light), the velocity of each component is proportional to the magnitude of the principal stress lying in its plane of vibration, i.e. $v_1 \propto \sigma_1$; $v_2 \propto \sigma_2$. Thus, on emerging from the photoelastic medium, the two com-

ponents will have suffered a relative change of phase or "relative retardation" that will be proportional to $(V_1-V_2)h$, where h is the thickness of the specimen. We can therefore say that the relative retardation $\delta \propto (\sigma_1-\sigma_2)h$ or, introducing the constant of proportionality $C\bar{=}$, the stress optic coefficient, we may write:

$$\delta = Ch(\sigma_1 - \sigma_2) \qquad (1).$$

If we view the emergent light through another sheet of plain polarizing material, called the analyser, with its axis of polarisation at 90^{o} to that of the polarizer, we shall see only one component of these rays. When the relative retardation is one wavelength of light, mutual extinction will occur, producing a black fringe at every point in the image of the photoelastic model which has a similar value, i.e. wherever the difference between the principal stresses is the same. These are the isochromatic fringes. Extinction also occurs at all points where the directions of the principal stresses in the model have the same orientation as the mutually perpendicular axes of the polarizer and analyser. These points form another set of dark lines called the isoclinics which appear at the same time as the isochromatics and obscure them. Isoclinics can be used to determine the directions of the principal stresses at any point in a stressed model by rotating the crossed polariser and analyzer simultaneously until an isoclinic line passes through the point. The directions of the stresses are then in the same orientation as the axes of the polariscope.

By using a circularly polarized set-up of the polariscope the isoclinic patterns are removed from the image of the stressed model and only the stress fringes, or isochromatics, remain. Since extinction occurs for every one wave length of retardation the observed pattern will consist of a series of dark fringes each representing an additional wave length of retardation. Equation (1) may then be written as:

(2)

$$\Delta = \frac{C}{\lambda} h (\sigma_1 - \sigma_2) \qquad (2)$$

where Δ is now the relative retardation in terms of the wave length λ of the monochromatic light used.

In engineering practice it is more convenient to write this equation as:

$$N = \frac{h}{f} (\sigma_1 - \sigma_2)$$

where N is the relative retardation in complete cycles of retardation, also known as the "fringe order" and $f = \lambda/c$ is defined as the material fringe stress value in lbf/in fringe. The form in which it is generally used is:

$$(\sigma_1 - \sigma_2) = Nf/h$$

and since the maximum shear stress $\tau_{max} = \frac{1}{2} (\sigma_1 - \sigma_2)$ we may write:

$$\sigma_1 - \sigma_2 \doteq 2\tau_{max} = \frac{Nf}{h} \qquad (3)$$

from which it is immediately apparent that the principal stress difference and maximum shear stress in the plane of a two dimensional model can be determined if the relative retardation N can be measured.
It is the function of the polariscope to determine the value of N at each point in the model.

From the two dimensional statement of Hooke's law it follows further that:

$$(\epsilon_1 - \epsilon_2) = \frac{Nf}{h} \left[\frac{1 + \nu}{E}\right] \qquad (4)$$

from which the principal strains may be found.

Isochromatic patterns therefore form the backbone of any photoelastic analysis. The fringe patterns present the direct evaluation of free boundary stresses ($\sigma_2 = 0$ at a free boundary) and of the interior maximum shear stresses in a model of a structure.

In the normal orientation of the polariscope elements described here, the background of the image is dark, and black

fringes appear at retardations of 0,1,2,....wave lengths of the light used. The arrangement is known as a "dark field set-up". With a small reorientation of the elements the background becomes light and dark fringes occur at retardations of $\frac{1}{2}$, $1\frac{1}{2}$, $2\frac{1}{2}$.....wavelengths. This is known as a "light field set-up" or a "mixed set-up" and is the orientation used for all stress patterns presented in this report.

SECTION 2: THERMAL STRESSES.

This section presents the thermoelastic equations for an unrestrained thick plate, such as used later in the experimental study. It then proceeds to give similarity relations for the thermoelastic model.

Thermal stress is stress arising from temperature effects. When a material is subjected to a temperature gradient, the various fibres expand different amounts. To enable the body to remain continuous, a system of thermal strains and stresses may be introduced which is dependent on the shape of the body and the temperature distribution.

Current interest in thermal stress is high and arises chiefly because of the many engineering components which fail because of it. The advances in rocket propulsion, high speed flight and nuclear engineering, all involve serious thermal stress problems. The same problems also arise in more familiar areas, such as the design of power generating plant, where modern advances in engineering are putting an ever increasing strain on the designer to know and design for the thermal stresses which are set-up in his plant.

2.1 Thermoelasticity:

Computations of elastic stresses is the first necessary step in any thermal stress analysis. Most problems encountered are, strictly speaking, three dimensional.

The equations for three dimensional thermoelastic problems are difficult to solve and it is very desireable to reduce as many of them as possible to a two dimensional form. If a body is very thin in one dimension, as in the case of a thin plate, it may be possible to consider the temperature

as a function of x and y in the plane of the plate only and to neglect any variation through the thickness. Normal and shear stresses in the z direction are neglected, and the problem is said to be one of plane stress. At the other extreme, when the z-direction of the body becomes very large compared with the other dimensions and the temperature does not vary with z, all planes perpendicular to the z-axis can be regarded as similar and may be analysed on the basis that $\epsilon_z=0$. This is the case of plane strain.

The formulation of thermoelastic problems is extensively treated in references 19, 20, and 30 and more specialised aspects in references 18, 28, 29, 31, 32 as well as in the shorter works 33 and 34. A short introduction is given here only to assist in the understanding of the problem of the semi-infinite thick plate which was used in the experimental investigation which follows.

If a body is imagined as being made up of a number of small cubical elements of equal size which fit together to form a given continuous body, then, if the temperature of the body is raised uniformly, and if its boundary surfaces are unrestrained, each element will expand an equal amount αT uniformly in all principal directions. The elements are thus still equal sized cubes; They still fit together to form a continuous body and no stresses will arise. If, however, the temperature rise is not uniform, each element will tend to expand a different amount proportional to its own temperature rise. The cubes can, in general, no longer fit together but since the body must remain continuous, each element restrains the distortions of its neighbours. Stresses therefore arise.

The total strains at each point of the heated body are thus made up of two parts: (1) A uniform expansion propor-

tional to the temperature rise T which, being uniform in all directions produces only normal strains and no shear strains. (2) Strains required to maintain the continuity of the body as well as those arising because of external loads. These strains are related to stresses in the usual way by the rules of linear isothermal elasticity. (R20).

The formulations employed in elementary thermoelasticity rest on a few principal assumptions: That the temperature can be determined independently of the deformations of the body, that the deformations are small, and that the material behaves elastically at all times. Elastic constants are assumed constant with temperature, the material is isotropic and inertia forces are neglected.

Free plate with temperature variations through the thickness only:

Consider a semi-infinite plate (fig.1) of constant thickness 2c which is completely free of surface traction and in which the temperature varies through the thickness only, that is T=T(y). It is reasonable then to suppose that the stress components will be of the form:

$$\sigma_x = \sigma_z = f(y); \quad \sigma_y = \tau_{xy} = \tau_{xz} = \tau_{yz} = 0 \qquad (5)$$

It can be shown (R20 pp277) that this is so:

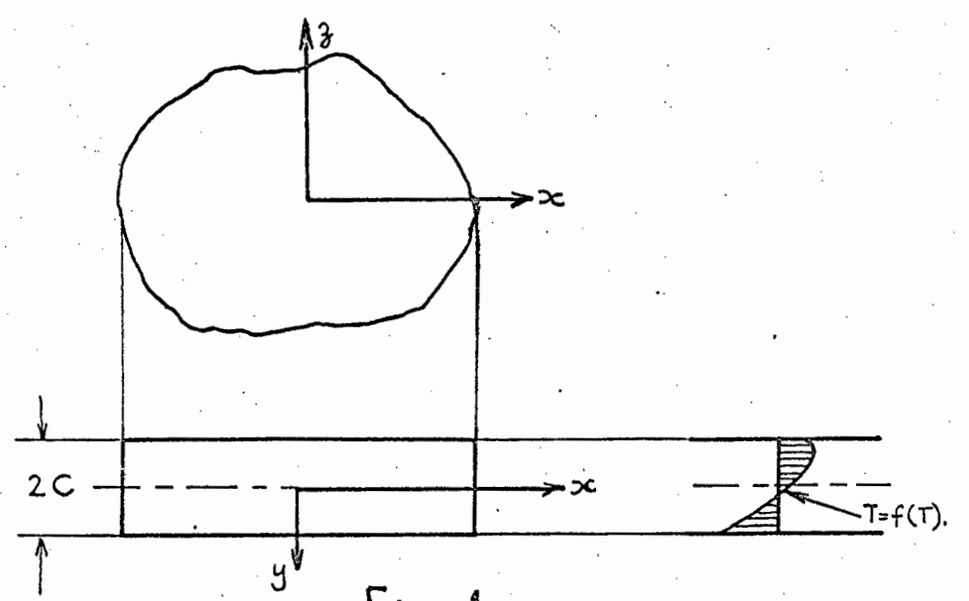

Fig: 1.

If the temperature T=T(y) is not symmetrical with respect to the x-axis there will be a resultant moment and the general stress equation will be (R18 pp 401; 20 pp 278)

$$\sigma_x = \sigma_z = -\frac{\alpha TE}{1-\nu} + \frac{1}{2c(1-\nu)} \int_{-c}^{c} \alpha TE dy + \frac{3y}{2c^3(1-\nu)} \int_{-c}^{c} \alpha TEy dy \qquad (6)$$

from which the thermal stresses in the plate can be calculated if the function T=T(y) over the thickness of the plate is known.

According to Saint-Venant's principle, this solution is an accurate approximation for traction free edges at distances from the ends larger than about one plate thickness.

The term $-\alpha TE/(1-\nu)$ in Eq. (6) corresponds to complete suppression of the thermal expansion in the plane of the plate whilst the other two terms which apply to a free plate, satisfy the conditions of zero net force and moment in the plate.

(a) Plate with a symmetrical temperature gradient: (R18 pp 402).

If a plate initially at a uniform temperature T_o is cooled by maintaining the surfaces $y=\pm c$ at a constant temperature T_1, then the temperature distribution at any instant t is given by Fourier's theory. This, substituted in Eq.(6) gives an expression of the form:

$$\sigma_x = \sigma_y = \frac{4\alpha E(T_o - T_1)}{\pi(1-\nu)} \left[e^{-p_1 t} \left(\frac{2}{\pi} - \cos\frac{\pi y}{2c}\right) + \frac{1}{3} e^{-p_3 t} \left(\frac{2}{3\pi} + \cos\frac{3\pi y}{2c}\right) + \frac{1}{5} e^{-p_5 t} \left(\frac{2}{5\pi} - \cos\frac{5\pi y}{2c}\right) + \ldots\ldots \right] \qquad (7)$$

in which $p_1, p_3 = 3^2 p_1, ---, p_n = n^2 p_1$ are certain constants.

Timoshenko says that "after a moderate time" the first term acquires dominant importance and subsequent terms may be ignored. There is however, good reason to be interested

in what happens to the material before the higher order terms can be ignored. Equation 7 must then be solved more fully. It represents a much simplified temperature history imposed on a body of very simple geometry. A step change in surface temperature such as assumed here, is not possible in practice. It implies that the surface of a hot body exposed to a cold shock immediately adopts the temperature of the cold medium i.e. the Nusselt number is much larger than unity, which means that the external (e.g. surface to fluid) thermal resistance is neglible compared with the internal resistance. Generally both kinds of resistance must be taken into account. Furthermore, the fluid temperature (in case of liquid to solid)heat transfer) does not usually change with a step function but more usually in a ramp (linear variation) or exponential function. Solutions of even the most elementary geometries then become very involved (R29).

It is therefore not surprising that exact solutions of thermal stresses in three-dimensional bodies are only available for a few configurations and loading conditions (19,20,29).

(b) Stresses in thick free plate with a symmetrical parabolic temperature distribution across its thickness:

Assume that in fig 1 the temperature distribution in the y-direction is given by the parabolic function

$$T=T_i(1-y^2/c^2) \qquad (8)$$

where $T(y=o)=T_i$, the internal temperature on the plate centre line.

The temperature is symmetrical with respect to y=O and there is no bending of the plate. The last term in Eq. (6) disappears and

$$\sigma_x = \sigma_z = \frac{\alpha E}{(1-\nu)}\left[-T + \frac{1}{2c}\int_{-c}^{+c} T\,dy\right]$$

$$= \frac{\alpha E T_i}{(1-\nu)}\left[\frac{y^2}{c^2} - \frac{1}{3}\right]_{(-c< y< +c)} \qquad (9)$$

For $y = 0.58c$; $\sigma_x = \sigma_z = 0$

For $y = \pm c$; $\sigma_{x\,max} = \frac{2}{3}\frac{\alpha E T_i}{(1-\nu)}$

For $y = 0$; $\sigma_{x\,min} = -\frac{1}{3}\frac{\alpha E T_i}{(1-\nu)}$

2.2 Model Prototype Correlation:

Since the photoelastic specimen represents a model from which stresses or strains in the actual part or prototype are deduced, it is important to consider the relation between the two stress systems.

The general equation governing the thermal stress problem is:

$$\nabla^4\phi + \alpha E\nabla^2 T = 0 \qquad (10)$$

in which ϕ is the stress function and the stresses are given as derivations of ϕ

$\nabla^4\phi$ is defined as $= \nabla^2(\nabla^2\phi) = \frac{\partial^4\phi}{\partial x^4} + \frac{\partial^2\phi}{2\partial x^2\partial y^2} + \frac{\partial^4\phi}{\partial y^4}$

It should be remembered that for the case of plane strain the equivalent value $E' = E/(1-\nu^2)$ and $\alpha' = \alpha(1+\nu)$ must be used. (R20 pp 259).

When $E\alpha$ is constant throughout the body, although not necessarily equal for model and prototype, the two systems can be correlated.

Eq. (10) may be written as: $\nabla^4\phi/E\alpha + \nabla^2 T = 0$

from which it is clear that if the temperature distributions in the two systems are identical, solutions for $\phi/E\alpha$ are also the same. Thus $\phi//E\alpha = f(T)$ or $\phi = E\alpha f(T)$. Since the stresses are given as derivatives of ϕ and since $E\alpha$ is constant the stresses in model and prototype are proportional to $E\alpha$.

Strains are determined as combinations of stresses divided by E, so that they are, for a given temperature distribution, proportional to α and independent of E. If then the temperatures in the prototype are chosen to produce identical distribution of thermal expansions, αT (instead of reproducing temperature), the two strain systems are equal (R23).

Photoelastic models, in general, have higher expansion coefficients than metal prototypes. Hence the simulation of αT can be achieved in plastics with lower temperatures. differences

However, two very important precautions must be observed:

1. The temperature range must be kept small enough so that $E\alpha$ is reasonably constant.

2. The thermal stress system must be separated completely from the effects of external loading, and each effect requires an independent investigation. In tests involving both thermal and mechanical loading the observed stresses in the model will of course, still represent the actual stress distributions in the model and if it is conducted to check a computational procedure, and the model is simply a vehicle for verification, the procedure is valid. Loads which are induced purely by external constraints in a body subjected to a temperature distribution must be considered as a thermal stress fraction.

In an excellent paper (R35) Hovanesian and Kowalski take the above arguments further and present complete similarity relations for time, temperature, displacements, strains and stresses between model and prototype for the uncoupled, quasi-static thermoelastic problem. Using the displacement formulation of the thermoelastic equation (R20 pp76, 260) expressed in terms of the usual indicial tensor notation (R20 pp 4; R36 pp 56) they derive amongst others, the following similarity relations:

1. For the generalised state of stress, or state of plaine strain:

$$\text{Strain:} \quad \varepsilon_{ij} = \frac{(1+\nu)\,(1-\nu m)}{(1-\nu)\,(1+\nu m)} \frac{\alpha}{\alpha m} \delta \; \varepsilon^{m}_{ij}$$

$$\text{Stress:} \quad \sigma_{ij} = \frac{E}{E_m} \frac{(1-\nu m)}{(1-\nu)} \frac{\alpha}{\alpha m} \delta \; \sigma^{m}_{ij} \qquad (11).$$

2. For the state of plane stress:

$$\text{Stress:} \quad \sigma_{ij} = \frac{E}{E_m} \frac{\alpha}{\alpha_m} \delta \; \sigma^{m}_{ij} \qquad (12)$$

3. Thermal similarity relations:

$$\text{Time:} \quad t = \frac{K_m}{K} \lambda^2 t_m \qquad (13)$$

Where: $\delta = \frac{T}{T_m}$ = temperature scaling factor.

$\lambda = \frac{x_i}{x_i^m}$ = geometric scaling factor

$\tau = \frac{t}{tm} = \frac{K_m}{K} \lambda^2$ = time scaling factor

t = time

K = thermal diffusivity

X = characteristic length

Sub- or superscript m refers to model variables

Prototype variables typed normal.

Considering the time scaling effect, it is interesting to note that the thermal diffusivity of a metal prototype is much larger than the thermal diffusivity of a plastic model and therefore $\tau < 1$ for an identically scaled model. A time dilatation occurs in the model which slows down transient phenomena, making it easier to note or record the events.

For a metal prototype and a plastic model, the temperature scaling term $\delta > 1$ so that by choosing δ properly the maximum stress and temperature in the model can be held within such limits that the elastic , optical and thermal constants of the model material may be considered constant.

SECTION 3: EXPERIMENTAL METHODS.

The problem of simulating the temperatures in parts subjected to internal heating is introduced. A general solution is offered and the various methods of obtaining it experimentally are discussed.

3.1 Background:

The experimental method reported here originated from a request by The South African Atomic Energy Board to explore the possibility of studying by means of photoelasticity, the thermal stresses in reactor components which are subjected to internal heating. An approximate steady state temperature profile through the thickness of such a part is given in fig 2(a).

It is not possible to impose a temperature gradient of this kind as a static condition on a model where heat transfer occurs only from the surface. However, if a steady state condition as shown in Fig. 2b(1) is first established and the one side, say T_1 is subjected to a change in surface temperature, the temperature profile will pass through a good approximation to 2(a) as a transient condition during its adjustment from initial condition 2b(1) to 2b(3). If the temperature gradient at any time t is known and a photoelastic pattern of the stresses can be obtained at the same instant, then the problem would be solved.

Probably the simplest model with which to establish a suitable technique was one of a free infinite plate with the required temperature gradient through its thickness. The temperature gradient is essentially one dimensional, and the stress gradient two dimensional (Fig. 3). The sandwich method for the photoelastic analysis of stresses in a slice from a

Fig: 2.

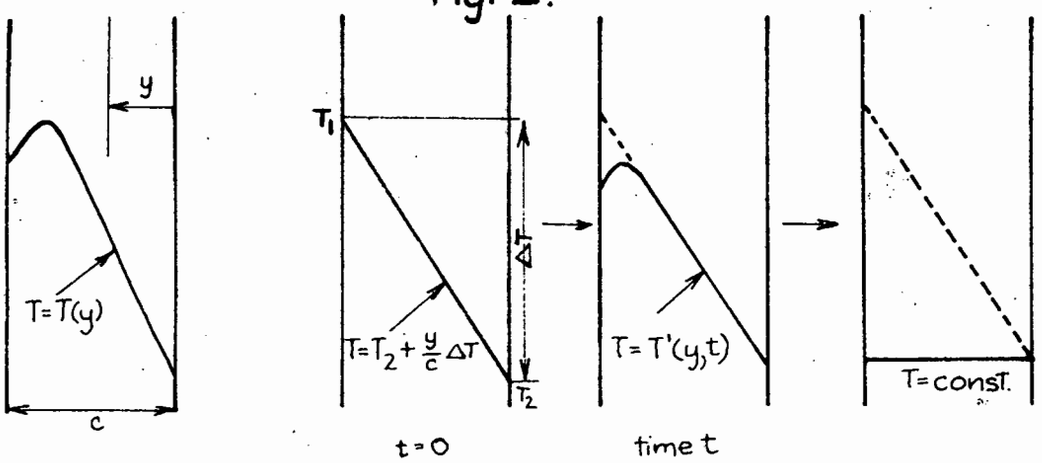

(a) start of test. (b)1. during test. (b)2. end of test. (b)3.

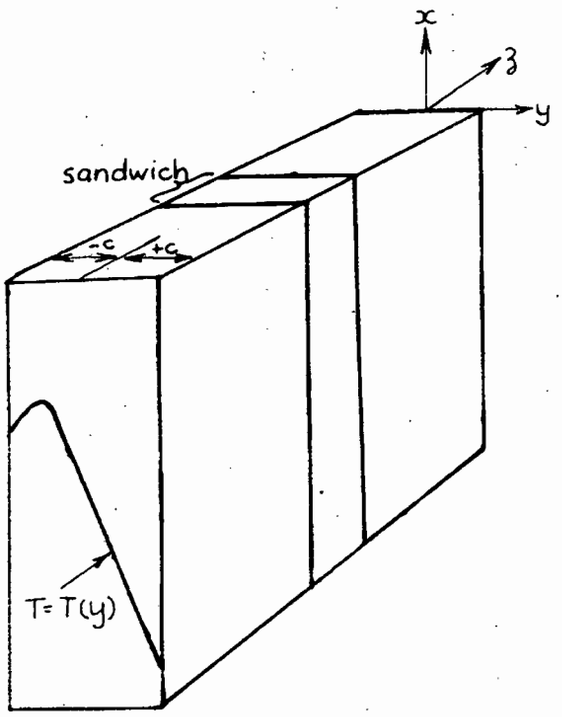

Fig: 3. Sandwich model of large plate with internal heating.

$x=z=\infty$; $-c<y<+c$
View in z direction.

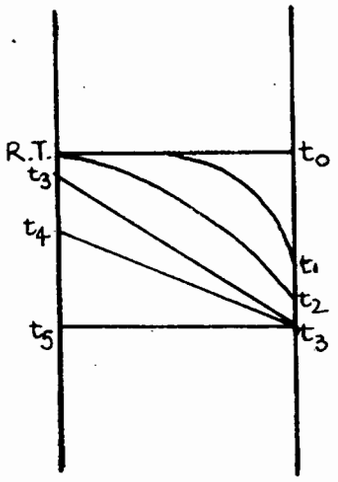

Fig: 4.

three directional body, as developed by Tramposch, was the most promising of existing methods and it was decided to base the study on this.

All previous methods of imposing a transient temperature gradient in sandwich models started either with a uniformly heated body cooled on one or both faces, or a uniformly cooled model immersed into a hot liquid bath (Section 1.2 pp 7). None of these would give the required gradient. In order to reach the condition in Fig. 3 the model had first to be soaked hot from the one side and cold from the other, until a linear gradient was established (Fig 2b(1)), at which condition the unrestrained plate would be free of stresses. Heating on the one side and cooling on the other is required to establish the steepest gradient within the operating temperature range of the model material. A gradient similar to Fig 2b(1) can be obtained by cooling one side only from room temperature, or from an uniformly heated condition, when from time t_3 onwards (see Fig 4) a linear temperature profile exists as a transient condition. This was not considered as suitable as starting from a known steady state condition.

The steady state linear gradient at the start of the test requires a long period of "soaking" (about 1 hr.) with a constant temperature differential between the two sides of the model, This rules out several of the previously used methods of heating and cooling. Dry ice would be expensive and difficult to handle for a long time, as would mixtures of dry ice and acetone or dry ice and alcohol. Brine solutions were ruled out because of the edge effects introduced by water absorption into the surfaces of the model, and also because of its corrosive nature. Immersion baths were obviously not suitable because they would not give the desired gradient. Finally there was the problem of keeping frost from forming on the model faces (edge effects) and on the

viewing ends where it would obscure the fringe patterns.

3.2 Methods of imposing the temperature gradient:

Three main systems for imposing the required temperature gradient were considered in designing the experiment. These are reviewed below and the reasoning behind the choice of the final design is given.

1. Hot and Cold Plates: (Fig. 5a)

At first this appeals as a good system. The heat transfer coefficient from plate to model surface is good, the plates can be made to maintain a uniform temperature and, with care, contact between model and plate can be even over the whole surface. The hot plate can be replaced by a cold one very quickly and the nearest approach to a step change in model surface temperature can be attained. The chief disadvantage is that it is really only suitable for flat surfaces. (The intention from the start, was to extend the technique to irregular, circular and even spherical models, once it has been established). There also remained the problem of frost on the faces of the cold plates and on the model itself, although a grease coating over the model could possibly reduce its harmful effects. The viewing ends would somehow have to be kept free of frost; probably with a flow of hot air. When the plates are pressed tightly against the model they may restrain its free expansion and contraction.

2. Hot and cold Air or Gas: (Fig. 5b).

Air or any non toxic gas has the big advantage of cleanliness. It adapts to any external profile provided the flow over the surface is controlled to prevent stagnant pockets of gas from forming. The cold air circulating over the model will be fairly dry, but the problem of frost still remains and the viewing ends will have to be kept clear with a blast

Fig: 5.

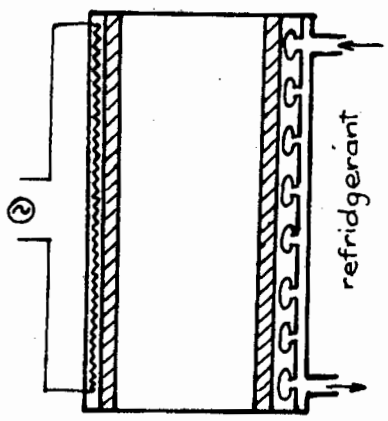

(a)
Hot and cold plates.

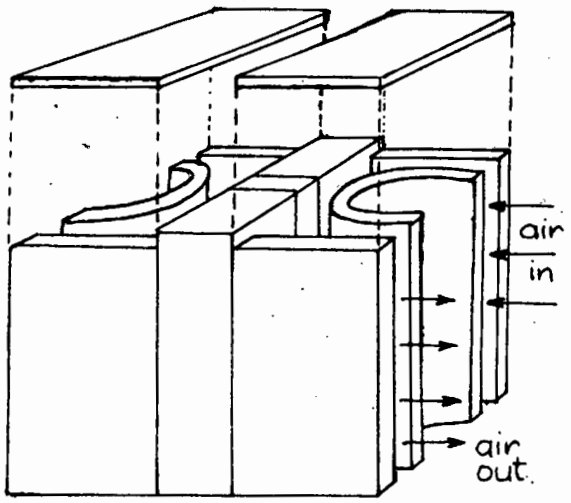

(b)
Hot and cold air.

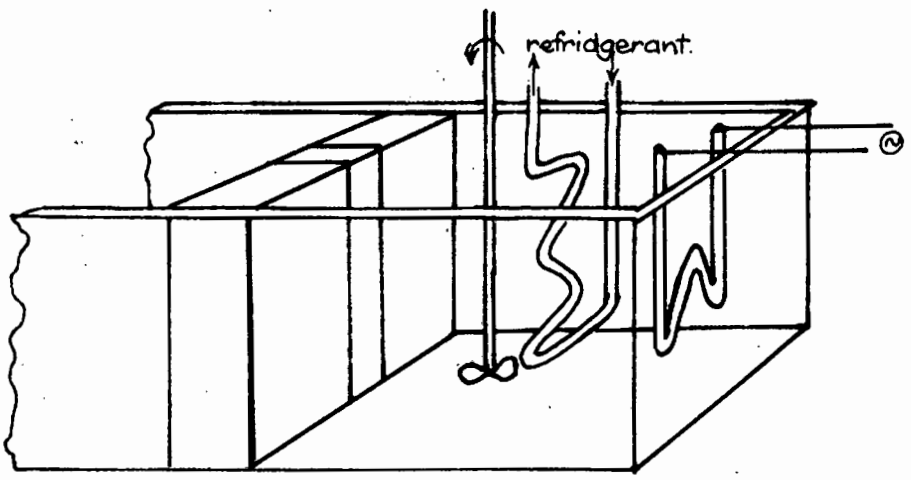

(c)
Liquid hot/cold bath.
(same layout on both sides of model)

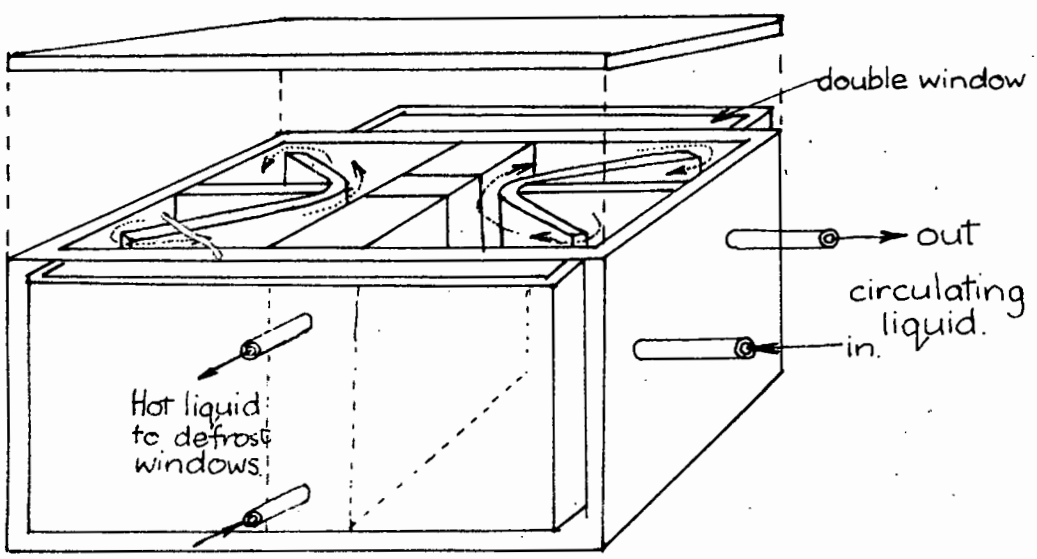

(d)
Forced circulation through tank.

of hot air. Since leaks are no problem the model can be made to be free from all external constraints.

The disadvantages are peculiar to a gas system. To chill air to the required low temperature will be difficult and even more so will be the problem of maintaining it at a constant hot or cold temperature for a sufficiently long time at various rates of flow. The chilling will be inefficient, which, added to the impractibility of using a closed circulation system, will require a low temperature refrigeration plant of comparatively large capacity. Feeder ducts will have to be large and well insulated. Finally the heat transfer coefficient, gas to solid, is lowest of all so that the temperature change in the model will be slow.

Cryogenic liquids, e.g. liquid Nitrogen, will impose very low surface temperatures but will be costly.

3. Hot and cold Liquids:

If a suitably low priced liquid can be found it may be used in two closed circuit systems, One hot and the other cold. Both the specific heat and the heat transfer coefficient of the liquid will be much higher than for the gas. The liquid flow can be controlled with pumps and valves. The system can have a large heat capacity which will help to maintain a steady temperature. Change from hot to cold, or vice versa can be done quickly; and since the liquid is in a closed system the capacity of the refrigerating plant need not be as large as with gas.

Several ways of using liquid as a heat exchange medium come to mind but only the two most suitable ones will be discussed.

(a) Large tank divided by the model with heating and cooling coils as well as a stirrer in both sides: (Fig 5c).

The model may divide a large tank into two compartments, each filled with liquid. Each compartment will have its own

immersion heater and cooling coil to heat or cool the liquid as required, a thermostat to control the temperature and a stirrer to keep it uniform throughout the volume of liquid.

The tank will have to be large to contain all the elements and to hold enough fluid so that each side will have a reasonable heat capacity under transient test conditions. The model cannot fit tightly in the tank otherwise free expansion is impaired; but since both sides have free liquid surfaces the pressures will be balanced and cross flow between them will be small. A rapid change from say hot to cold, is not possible unless the hot liquid is rapidly drained out and a supply of previously chilled liquid poured into the tank in its place. The cooling coils will have to be large to have sufficient capacity to maintain a low temperature during the test. The windows will need to be kept free of frost. Stirring must be vigorous to maintain a high rate of heat transfer between model and liquid. The whole system will be rather clumsy and is not easily adapted to other model configurations.

(b). Fully enclosed model in tank with forced circulation: (Fig 5d).

The model divides a tank into two compartments as before but the tank is compact and has a lid on. The liquid is pumped into either compartment under forced circulation from two separate systems, one hot, the other cold. Each system can be made to have a large thermal capacity, flow over the model faces can be rapid with consequent good heat transfer, and rapid changes can be made from hot to cold by the flick of a valve. By careful design of the tank the model will be free of external constraints or loads and the whole method is easily adaptable to many model configurations.

Apart from the starting condition of "skew soak" it is adaptable to any other test condition. In fact, by manipulating the flow and the reservoir temperatures almost any desirable temperature profile can be imposed on the model as a transient, and many different ones as steady states. External control through valves in each circuit makes it a very flexible system. Viewing ends can be kept clear of frost simply by bypassing some of the hot liquid through double walled windows.

This is the system which was adopted and which is described, in its present state of development, in the following section. It is novel in the exactness of control and the flexibility which it offers over the temperature profiles which can be imposed on a model and also in its adaptability with a minimum of trouble, to a wide range of models. The whole design proved so successful in use that it is presented here as a significant advance in the methods for studying thermal stresses in photoelastic models. A single installation of this kind will enable any photoelastic laboratory to perform a wide range of thermal stress studies without the need to develop a new system for each one.

SECTION 4: DESCRIPTION OF APPARATUS AND EXPERIMENTAL PROCEDURE.

This section discusses the developments towards, and the final design of, the composite photothermoelastic model together with the test tank used to impose the temperature gradient in it. Each major section of the apparatus is described in detail, followed by a short summary of a typical test procedure.

4.1: Overall Description of System:

The equipment as a whole was designed and built to give the highest degree of flexibility in generating thermal gradients, and their associated thermal stresses in models of many shapes.

Fig. 6 shows the general system as used with a rectangular model in place in the testing tank. Hot or cold liquid can be circulated through each of the two compartments according to any test plan. It flows along the sides of the model to heat or cool them as required.

The heat exchange fluid is commercially available jet fuel - Kerosene JP1. (because water-free!)

Hot liquid is supplied by an immersion heater/circulation system, known as the "hot system" and cold liquid is produced in a refrigeration plant or "cold system". The supply from either source is handled by small vane pumps with individual speed control which pump the kerosene to the test tank via a distribution box and control panel. Liquid temperatures, flow rates, and tank pressures can be controlled to give almost any desirable temperature gradient in the model within the upper (70°C.) limit of the model material, and lower (-35°C,) limit of the plant.

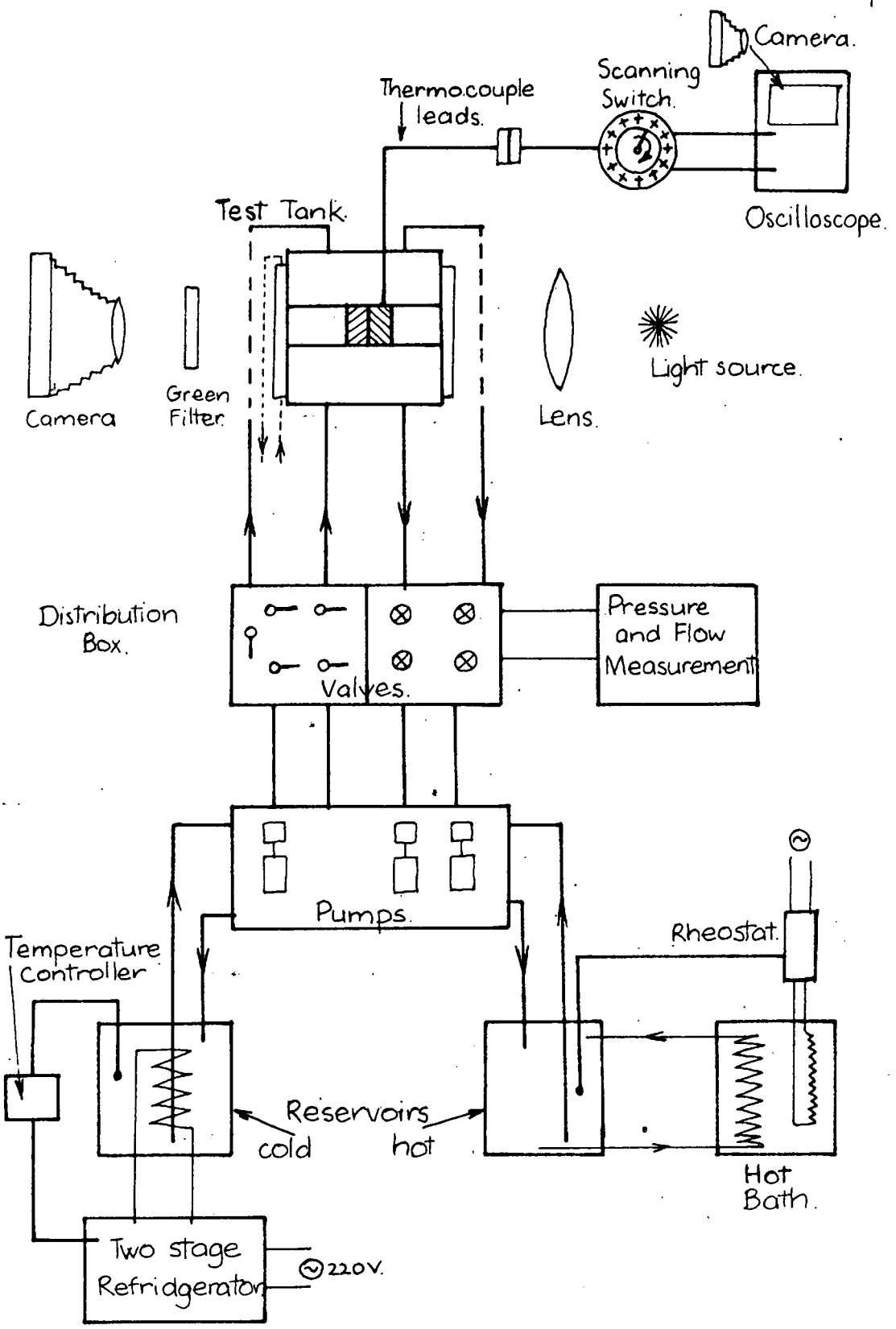

Fig: 6.

Complete Layout of Test System.

The exact temperature gradient is sensed by one or more banks of thermocouples embedded in a separate sensing element bolted together with the model. These thermocouples are continually and rapidly scanned with a specially built rotary switch and are finally recorded on the screen of a storage oscilloscope from where they may be photographed if required.

The test tank is in the parallel field of an ordinary transmission polariscope which makes the thermal stresses in the model visable as photoelastic stress fringes which may be either observed directly or photographed, as the need may be.

By synchronizing the two cameras, one on the polariscope and the other on the oscilloscope, coincident stress and temperature records are obtained. These are then used to study the thermal stresses set up in the model.

4.2 The Photoelastic Model:

The photoelastic model was based on the type first used by Tramposch (R27). The final version described here grew by a process of evolution through several stages, each of which was tested for the validity of its results against the theory, described in section 2 page 17 , for a thick plate, free of external constraints, subjected to a symmetrical parabolic temperature profile through its thickness. Agreement was invariably good and the confirmation of results for the models is presented in section 5 on page 73.

The stages of development were:

1. A model approximately 6 inches high, 4¼ inches long and 1¼ inch thick made completely in epoxy resin and with all elements glued together. It was very dark in the direction of viewing.
2. A model of similar size with epoxy stress element

and filters, as well as an epoxy thermocouple block or temperature sensing element, glued between perspex blocks to make up the overall length. It was much more transparent along its length than the previous model.

3. Similar to (2) but with all elements bolted, instead of glued together. The Perspex and pieces were made up from ½" thick blocks. Correlation with theory was still excellent.
4. Similar to (3) but with the thermocouple block made of perspex. Light transmission was excellent, photographic definition of the fringes in the epoxy element very sharp, and correlation with theory excellent (Section 5.2pp 73).

Models (1) and (4) had various thermocouples imbedded in the end pieces on their central (x z) planes as shown in fig.7 to determine how far the end conditions affect the temperature along the centre line of the model. These were distributed as follows(Fig 7c):Model (1): Points A,C,D,E and F. Model (4): Points A,B and E. In each case point A represents the row of thermocouples which record the temperature profile across the thickness of the model. Point C recorded temperatures slightly different (about $2^{o}C$).from D. All other points recorded identical temperatures during test runs, confirming that a reliable and uniform temperature field exists over the central section of the model, and that the temperatures in the Perspex are not significantly different from that in the Araldite.

In two additional tests with model(4) the epoxy photoelastic assembly was placed ½" towards each end from the mid-position in the model and the stress patterns obtained under a symmetrical parabolic temperature distribution compared with each other and with theory. There was no difference.

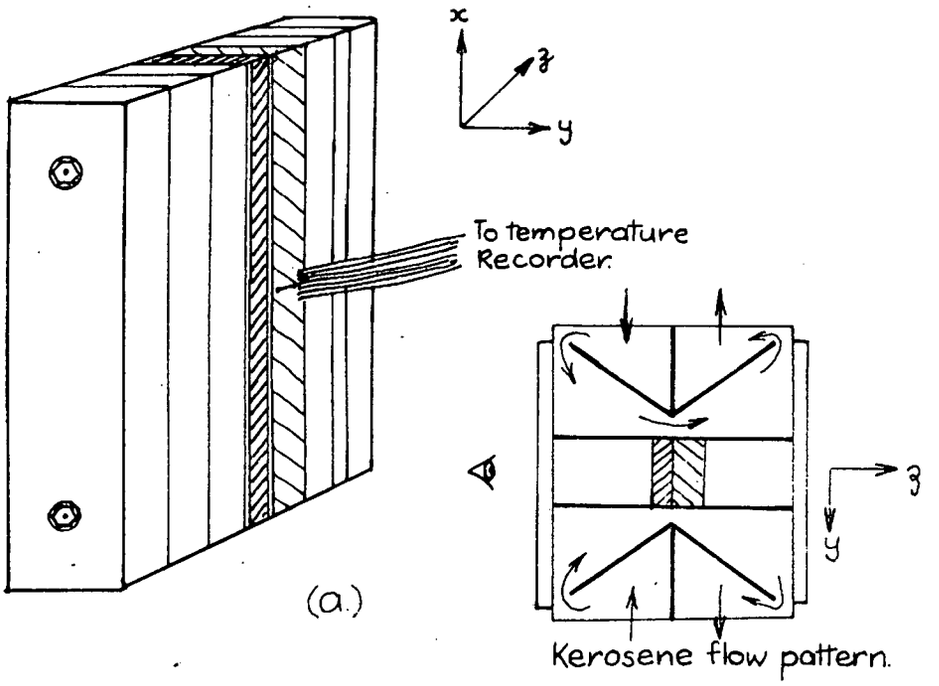
x
z
y
To temperature Recorder.
(a.)
z
y
Kerosene flow pattern.

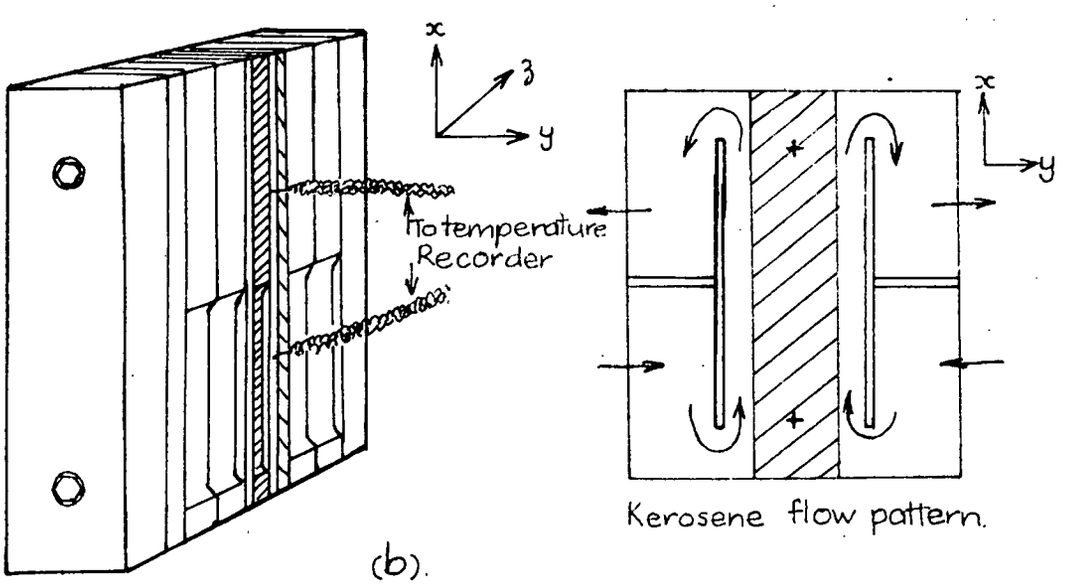
x
z
y
To temperature Recorder
(b).
x
y
Kerosene flow pattern.

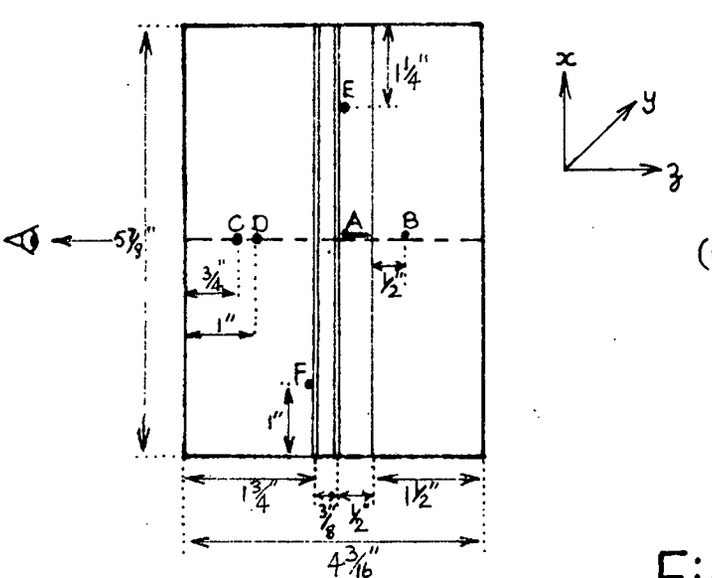
E
1¼"
C
D
A
B
5⅞"
¾"
1"
½"
F
1"
1¾"
⅜"
½"
1½"
4 3/16"
x
y
z
(C).

Fig: 7.

The stress pattern was also identical at any value for x, until disturbed by the stresses around the holes through which the bolts passed. It was clear that there existed a reliable "test section" over at least the central $2\frac{1}{2}$ inches vertical and $1\frac{1}{2}$ inch horizontal, i.e. for $-1\frac{1}{4} < x < 1\frac{1}{4}$; $-\frac{3}{4} < z < \frac{3}{4}$.

The final design for the model was then as shown in fig. 7a and plate 1. The central portion consisted of a $\frac{3}{8}$ inch thick epoxy section which was sandwiched between two circular polarizers. Next to it was mounted a temperature sensing block which carried from 11 to 15 thermocouples. The overall length of the model was made up with perspex spacers so that it fitted loosely into the tank between the two windows and the whole assembly was bolted together with two long through-bolts. The bolts passed through clearance holes to prevent the danger of constraints, and their ends were countersunk into two perspex end pieces.

This proved to be an extremely versatile arrangement which saved many hours of work in re-making a whole assembly for each change of model geometry.

The thermocouple block was a piece of precision work. It had a grid scribed on it to indicate the exact positions of the thermocouples relative to the stress pattern, and each thermocouple bead was cemented into place within very close tolerances - They were actually placed to $\pm$ 0.002 inch of their desired positions. All leads from this block passed through a silicon rubber seal in the lid of the tank, after which their free ends were soldered to pin connectors which led to the switch. Since this sensor block was separable from the model assembly it could be used for many tests, on various rectangular models without the need to remake either the model or the lid seal and connections.

The model length (z) could be adjusted to fit correctly into the tank for a wide range of test piece thicknesses. It could also be readily disassembled and reassembled with plain polarizing filters for observation of the isoclinics.

The tank design was such that merely by changing a set of replaceable baffles, the flow over the model face could be changed, e.g. from washing across the face in the z -directions to flowing in the x -direction(Fig. 7)

The most important novel features in the design of this composite model are : (a) The use of thermocouples mounted outside the photoelastic element where they do not disturb the fringe pattern. (b) The simulation in a compact model of a large infinite thick plate free of external constraints. (c) Improved light transmission through the length of the model.

Model Materials:

The photoelastic element was machined from a $\frac{1}{2}$ inch thick sheet of "Araldite Casting Resin B" produced by a suitable mixing and curing cycle to give stress free plates without mottle or inclusions. The mixture used was 100 parts Resin to 30 parts hardener 901 by weight.

Properties of Araldite B (100 parts resin /30 parts H 901)

Supplied by CIBA, Basle, Switzerland.

Modulus of Elasticity (E) (lbf/sq.in.):

Test: Deflection of thin ring (R37,38):

at 21°C - 4.15×10^5 ; at 61°C - 3.80×10^5 (all $\pm$ 10%)

CIBA: VSM 77111: 4.27 to 5.7×10^5

DIN 53455: 5.4×10^5

Poissons Ratio (ν): 0.35

Linear Coefficient of Thermal Expansion (α) (in/in °C)

Test: $16\frac{5}{8}$ inch rod: at -5°C; 5.2 to 5.4×10^{-5})
30°C; 5.7 to 6.1×10^{-5}) (all $\pm$ 5%)
50°C; 6.0 to 6.2×10^{-5})

at 20°C by inter-extrapolation: 5.6 to 6.0×10^{-5}

CIBA, VSM 77110: 6.0 to 6.5×10^{-5}

Coefficient of Thermal Conductivity (K)(Btu/ft h ^{o}F)

Test: Hot plate and calorimeter: at 65^{o}C; 0.125($\pm$ 5%)

CIBA, DIN 52612: at 20^{o}c; 0.12 to 0.13

Photoelastic Fringe Constant: (f) (lbf/ in fringe)

Test: Disc in diametral compression

from 21^{o}to 78^{o}C : 56.4 to 57($\pm$ 2%)

CIBA: 57.6

Properties of Perspex:

Supplied by ICI, England

Modulus of Elasticity (E)(lbf/sq.in)

Test: Thin ring at 21^{o}C; 3.97×10^{5} (R37 & 38)

ICI tangent modulus; 4.2×10^{5}

1% secant Modulus; 3.9×10^{5}

Poissons ratio: ICI; at -25^{o} to + 50^{o}C; 0.35

Linear Coefficient of Thermal Expansion (α) (in/in^{o}C)

Test: $16\frac{5}{8}$ inch rod: at 29^{o}C ; 7.3×10^{-5}

ICI, ASTM D 696; at 20^{o}C ; 7.3×10^{-5}

Coefficient of Thermal Conductivity: (K)(Btu/ft h ^{o}C)

ICI: at 20^{o}C ; 0.195

4.3 The Test Tank:

The test tank design, together with the model, comprises the central feature of that which is novel in this experimental method developed to study thermal stresses in bodies, by the photoelastic method. The tank was designed for the highest degree of versatility in terms of both the temperature profiles which can be simulated in the photoelastic model and the shape of the models which can be tested. The detailed description given here applies to the set-up as used for testing rectangular models which simulate sections of infinite thick flat plates subjected to a temperature gradient through their thickness.

Essential requirements:

The basic requirements for a test of this kind may be

1. MODEL ASSEMBLED IN POSITION IN LID OF TANK. NOTE THE ADJUSTABLE CLAMPS WITH SEALS WHICH HOLD MODEL.

2. MODEL FITTED IN LID. NOTE SEAL WHERE THERMOCOUPLES PASS THROUGH.
A=GOOSENEK TO SUPPORT WIRES.
B=CANON CONNECTOR.
C=THERMOS FLASK WITH 0°C REFERENCE COUPLES.

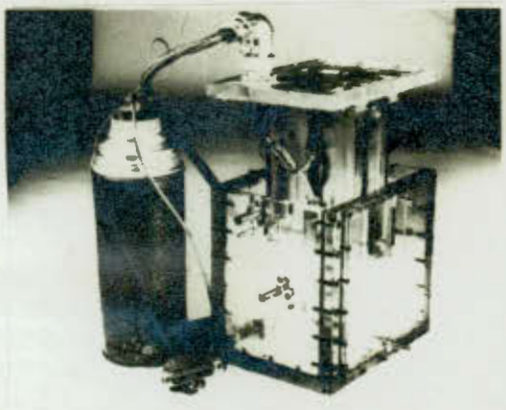

3. MODEL HALF ASSEMBLED IN TANK.
A=NEOPRENE SEALS ALONG EDGES OF MODEL.

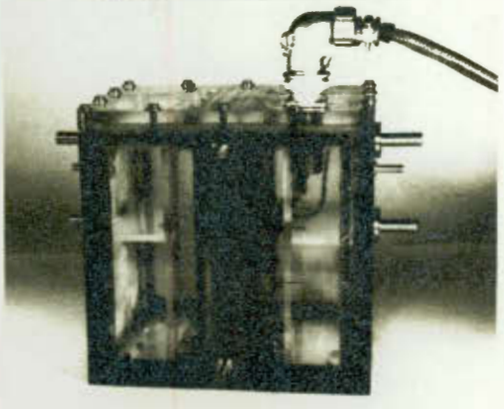

4. TANK CLOSED WITH MODEL IN PLACE. VIEW THROUGH ONE WINDOW. THE BAFFLES DIRECT FLOW VERTICAL UPWARDS OVER FACES OF MODEL.

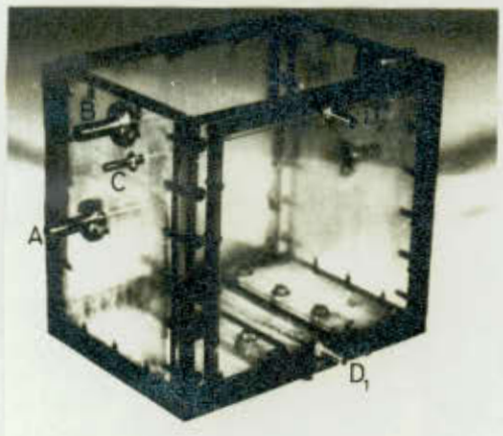

5. DETAIL OF TANK: A=MAIN INLET; B=MAIN OUTLET; C=VENT AND MANOMETER TAPPING; D_1 AND D_2=WINDOW INLET AND OUTLET.

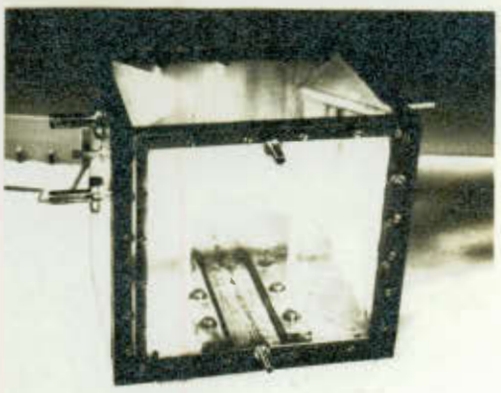

6. TANK WITH BAFFLES FOR FLOW DIRECTED HORIZONTAL ALONG FACE OF MODEL. NOTE ADJUSTABLE SEAL CLAMPS ON FLOOR OF TANK.

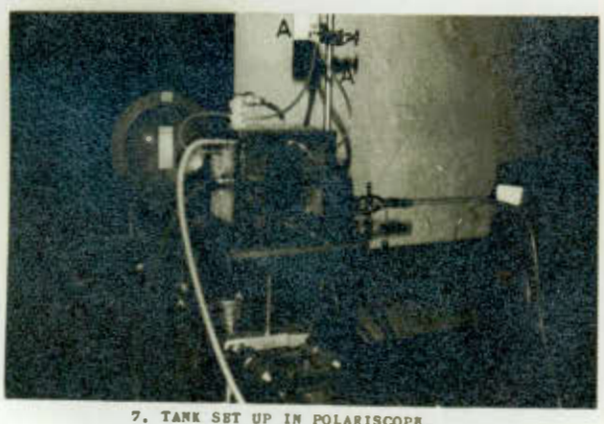

7. TANK SET UP IN POLARISCOPE.
A=MANOMETER AND VENT TUBES.

PLATE 1

listed as follows:

The tank must contain the model and direct the flow of the heating/cooling liquid around, over or through the model. It must not impose any constraints on the free expansion of the model, other than those specifically required by the test being conducted, while at the same time sealing effectively against leaks to the outside, as well as against cross leakage between the hot and cold systems at all test temperatures.

The tank must further be optically clear in the direction of the light path through it, and these properties must not change with temperature. It must remain optically transparent under all conditions, including continuous operation at sub-zero temperatures.

The materials used in the construction of the tank must not be adversely affected by the kerosene used as heat exchange medium and the whole construction must have a long life despite many rapid changes of temperature.

Finally the tank must be easily adaptable to the testing of a wide range of models.

During earlier tests it was found to be very desireable to have a completely transparent tank so that the behaviour of the model and the flow of the liquid could be seen.

Two comparatively crude tanks, one made in steel and the other in brass, were used during earlier tests. The experience gained with these tanks was used in the design of the satisfactory version described below. Apart from being opaque, the main problem with metal tanks is the large difference in the linear coefficients of thermal expansion between the metals ($\pm$ 15 x 10^{-6} in/in ^{o}C) and the model materials ($\pm$ 60 x 10^{-6} in/in ^{o}C) or glass ($\pm$ 8 x 10^{-6} in/in ^{o}C). It was obviously better to make the whole tank out of the same material as the "windows" and preferably one that had a coefficient of expansion near to that of the epoxy resin used for

the photoelastic model.

Perspex satisfied this requirement as well as all those listed before. It is also readily available in various thicknesses, has good optical properties and is easily machined, drilled, tapped and glued.

Final Design:

The detail design of the tank as it evolved is shown in fig 8 and several views are given on plate 1. A rectangular model is shown in place.

The whole tank was made of ½ inch Perspex sheet, held together with countersunk screws tapped into the side walls. Permanent seals were made with "stag" sealer. This form of construction facilitates repairs or structural changes which would not be possible if the whole assembly was glued together.

The model divided the tank into two identical compartments, each with a brass inlet connection just below the horizontal centre-line, and an outlet connection of slightly larger diameter, to prevent an excessive pressure build-up in the tank, near the top. Also included in each side wall was a small brass manometer tapping used to vent the tank to atmosphere and to read the pressure in each compartment. In operation each side was fitted with baffles to direct the flow of the kerosene past the model.

The rectangular models were located against transverse movement and sealed against cross flow, with two adjustable clamping blocks fitted to the floor of the tank. Each block had a round synthetic rubber seal mounted in a groove on the faces adjacent to the model. This clamped the model lightly and sealed against cross flow while at the same time providing a minimum of restraint against expansion or contraction of the model relative to the tank.

The lid closed on to the tank and sealed on an O-ring

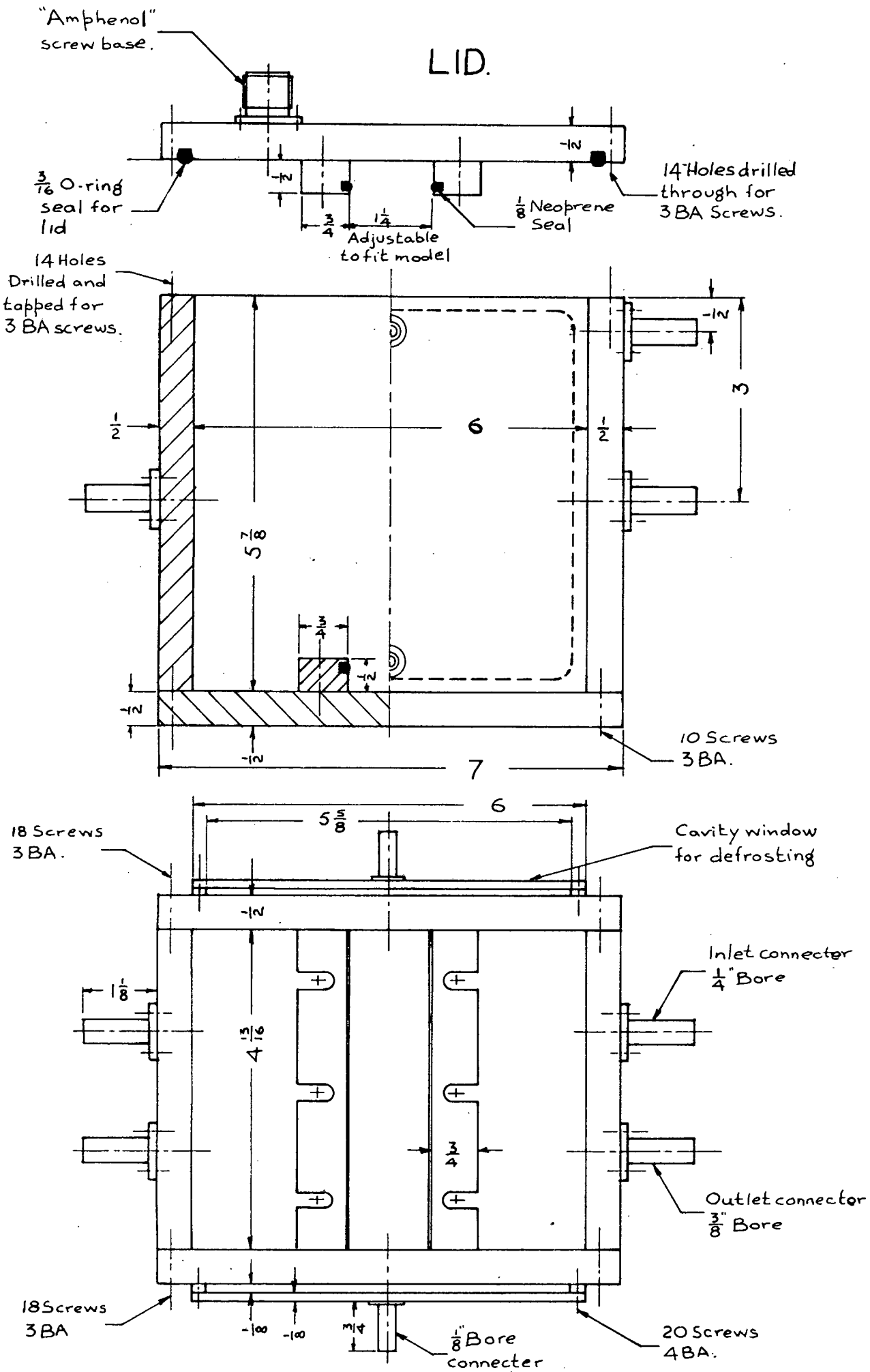

Fig. 8: TESTING TANK.

located in the lid. The model was located in the lid in exactly the same way as on the floor of the tank and the thermocouple leads passed through a special gland screwed into the lid and sealed with a cast in plug of Silastic 589 RTV silicone rubber.

During tests at sub-zero temperature a thick layer of ice formed on the outside of the tank. For this reason double walled windows were fitted which were defrosted by circulating hot kerosene up through the cavity.

The O-ring in the lid was larger than the groove so that the seal did not require the lid to be tightly screwed down on the box as would have been required by a "face seal". The screws were taken up just sufficiently to provide an effective seal against leaks. Under these conditions the clearance between the model and tank was about 0.08 inches at the top and the bottom. The model rested on a thin strip of expanded polythene "sponge" on the floor of the tank. A double bead of soft Silicone rubber adhesive (Silastic RTV 732) was placed between the two clamping blocks on the lid. It stretched from O-ring to O-ring and effectively prevented cross flow over the top of the model. Both cushions are very soft and did not limit the free expansion of the model significantly.

The model could furthermore not be a tight fit in the tank between the windows. To seal against cross flow between the ends of the model and the windows special seals were cemented on to the edges of the model. These were round sections, of the same material used for the O-ring and clamping seals, which were glued to the corners of the model. Soft silicone rubber adhesive (RTV 732) was used and the seals protruded 0.05 inches past the end faces of the model. The

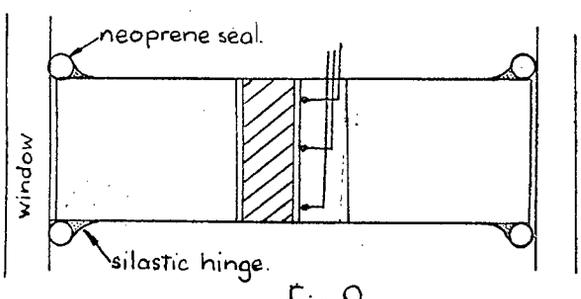

Fig:9.

silastic acted as a stiffish hinge and kept the synthetic rubber strips in good contact with the inside surfaces of the windows. This design sealed adequately against cross flow between the two tank compartments, provided the pressure difference between them was not excessive. Photoelastic observation of the free model and the model in the tank, both hot and cold, showed no stresses due to constraints against free expansion.

It should be remembered that, although allowing for free expansion in all directions, any differential expansion between tank and model is entirely due to temperature differences, because both the tank and the larger part of the composite model are made of the same material. The coefficients of expansion for Araldite B, and Perspex are very alike.

The tank was made so that the whole of the two "viewing ends" were clear windows without any obstructions. In this way it is readily adapted to house almost any shape of model with an outside diameter of up to 5 inches. Various wall thicknesses and geometrical shapes can be handled after only slight modifications to the tank, mainly in respect of guidance for the required flow of the heat exchange fluid.

If, for example, it is decided to study the radial stresses in a circular thick walled pressure vessel subjected to any temperature gradient, including the case of internal heating, through the thickness of the wall, the test could be accomodated in the tank as follows:

Make a composite model, with a built in photoelastic sandwich polariscope, of the correct length to fit freely between the windows of the tank and with end seals as before. Build a manifold into each end of the model to introduce and collect the liquid which flows axially along the inside.

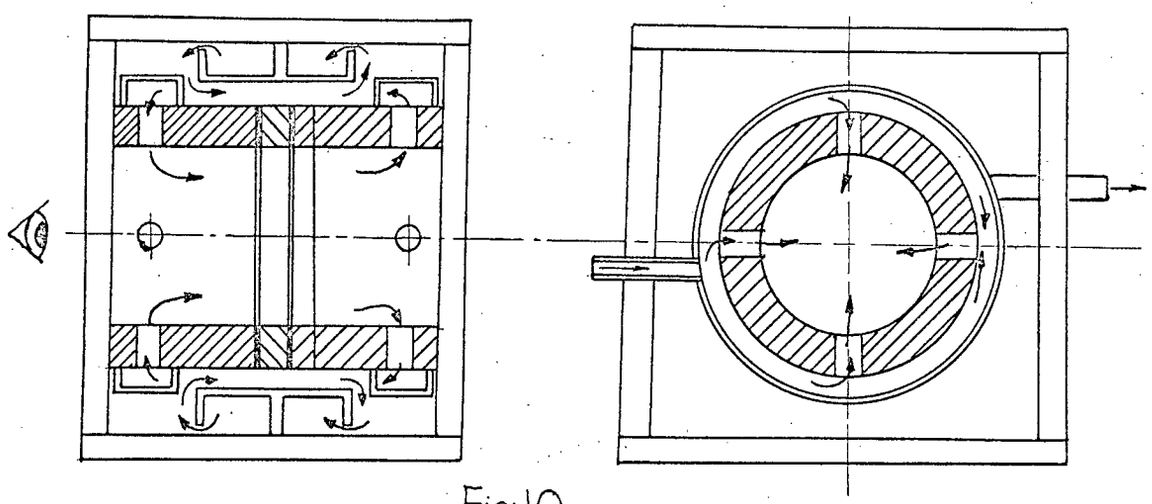

Fig:10.

Place baffles inside the tank to direct the liquid flow axially over the outside of the model along the surface at high velocity. The model will then have a central section of at least 1½ inches with a reliable temperature profile, not affected by the end conditions. All liquids are taken into and out of the tank through existing connections in its side. One of the pressure tappings will connect with the inside of the model.

As before any temperature gradient can be studied as a transient condition, and the test section may include stress concentrations or be made up of dissimilar materials.

Temperatures are sensed and recorded as before with thermocouples embedded in the model.

4.4: The Circulating Liquid:

The liquid used to cool or heat the model is standard kerosene type jet fuel (JPI).

Since the upper temperature at which the epoxy model material retains its elastic and optical stress properties within reasonable limits is about 80°C, the only way to maximize the temperature gradient in the model is to use a liquid which is heated in the one instance to 80°C and in the other cooled to a low temperature. Small refrigerating plants still have reasonable capacities at -40°C to -50°C so that a suitable fluid should still flow easily at these temperatures.

Water affects the models, which should be kept dry to avoid "edge stresses" or residual stresses which will interfere with any imposed stress pattern. Brine solutions are therefore not suitable. They are also corrosive.

Commercial JPI jet fuel has all the required characteristics. It is not excessively volatile and is still safe to use at 80°C. It has a pour point of -45°C maximum. It is dry; in fact fully stress relieved models can be stored indefinitely by immersing them in kerosene. It is optically clear and neutral to epoxies and to Perspex. It is freely available and relatively cheap so that the inevitable losses which occur do not constitute a financial burden. It is relatively non-toxic when handled with a minimal amount of care, and still has a low viscosity at -35° to -40°C. It pumps easily at these temperatures. Flow over the model is rapid and the heat transfer rate high. Specific heat is high.

Since kerosene is non-volatile it does not form gas bubbles on hot model surfaces. It can be used at higher temperatures than other low temperature liquids, all of which are rather volatile (e.g. Acetone and Alcohol).

Its one disadvantage is high solvent power and a resultant tendency to attack seals and similar parts. This presented serious problems in the selection of valves and plastic tubing as well as in the design and sealing of the test tank. Most synthetic rubbers swell when immersed in the hot kerosene. Products which proved reasonably useful were certain grades of Neoprene and also the two Silicone products "Silastic 589" and "521".

4.5: Hot Kerosene System:

Hot jet fuel was supplied to the test tank and windows from a two stage heating system shown in Fig. 11.

The object of the hot system is to provide a large reservoir of hot kerosene at a constant temperature of about

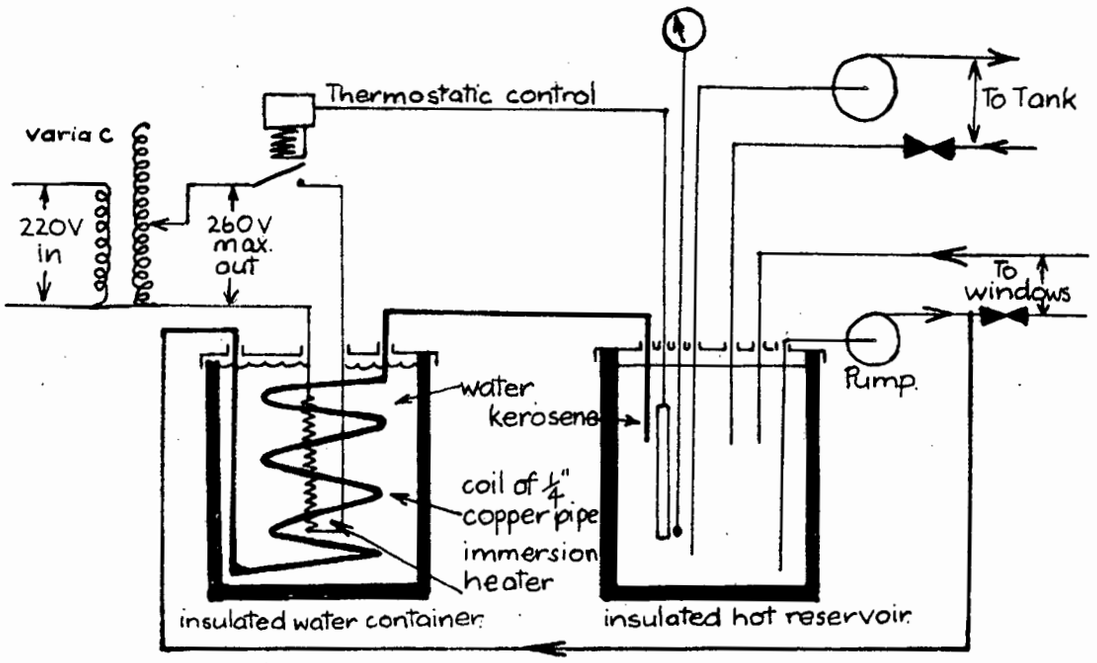

Fig: 11. Hot System.

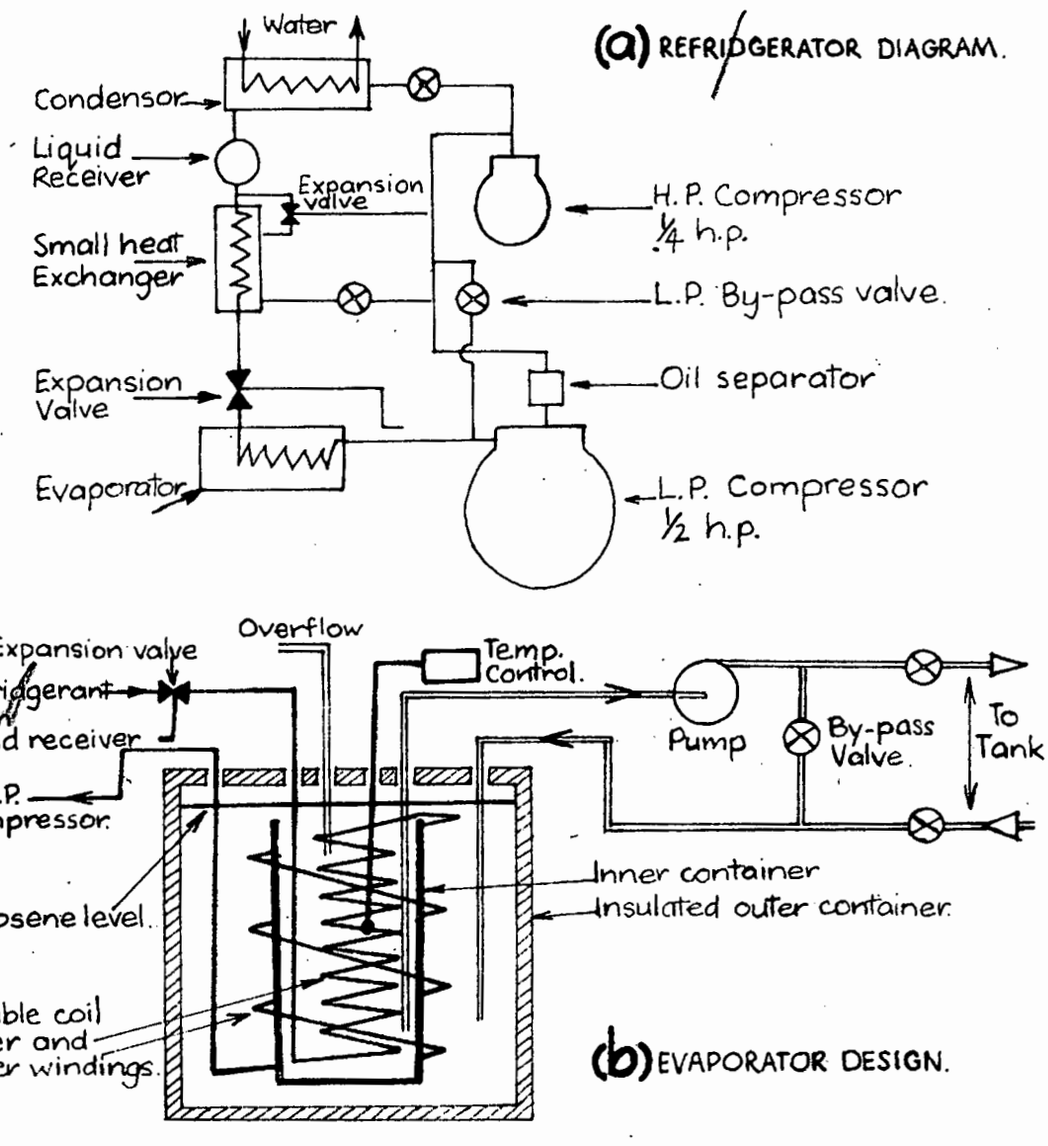

Fig: 12. Cold System.

80°C. to the test tank and tank windows. The system should be versatile, safe and insensitive to variations in the level of kerosene in the reservoir. The last requirement arises because in operation there is frequently a slight transfer of liquid between the cold and the hot systems due to cross flow in the tank. The tank capacity is in itself about 3 pints, or the equivalent of about 1½ inches in the reservoir. During start-up and while the system is being adjusted small and even large leaks are inevitable. All of these taken together lead to severe fluctuations in the fluid level of the tank, and since the cold system is of necessity a closed system, and fully insulated, the whole circulation system is so arranged that fluctuations in the total liquid content of the plant is, as far as possible, taken up in the hot system, where make-up and external manual control is comparatively easy. The simplest system of heating would have been an immersion heater placed directly into a can of kerosene, with a stirrer, if necessary. This has the danger of hot and cold pockets in the bath, the possibility of high local temperatures on the heater, and is especially dangerous if the level drops below a point where an active portion of the heater breaks through the surface of the kerosene. Any failure of the controls may furthermore lead to a highly dangerous condition when the bath overheats.

The system as finally used is in two stages. An immersion heater, heats a stationary hot water bath. A variable speed pump (see Section 4.6 page 50 for a description of the pump controls) draws kerosene from a 4 gal. reservoir and pumps it through a long double wound coil in the water bath and back to the reservoir. In this way the highest temperature to which kerosene can possibly be subjected is 100°C and the highest reservoir temperature recorded during a period of severe malfunctioning was 90°C. The worst that can happen is for the water bath to boil dry, under which condition the

kerosene temperature would actually drop as the effective heat transfer surface in the water bath decreases.

The power supply to the immersion heater was through a variable transformer, which had a range of from 0 to 260 volts. A thermostat control in the kerosene reservoir cut the heater in and out to maintain a constant reservoir temperature. The temperature of the reservoir was read on an ordinary dial thermometer. Continuous circulation of the kerosene ensured an even temperature throughout the reservoir.

During tests this system operated very well. It was flexible, handled some severe emergencies with complete safety, and required very little supervision. It had one weakness: There was a long time lag in the temperature control system.

The hot kerosene supply to the windows of the test tank was also taken from this circulating system. It was important that the window supply should be independent of the hot supply to the tank. Since the hot circulation system had to be kept running to keep the kerosene for the windows warm, the supply to the windows could just as well be taken from it. A small valve after the pump delivery bled a sufficient amount of kerosene off to the windows. The flow rate to and pressures inside the windows was under complete control, and the windows never "frosted" over during a test.

4.5 A. Cold Kerosene system:

Cold jet fuel was supplied to the tank from a small refrigerating unit. Fig 12a shows the refrigerator design and Fig. 12b the details of the evaporator design and cold circulation system.

Earlier tests in this series were run with a cold system which consisted of a single stage ex-naval refrigerator adapted for this work. The lowest temperature which could then be achieved on the model was $-10^{o}C$. The unit required

continuous supervision. Since the only way of getting a larger temperature difference in the model was by lowering the cold side, a new two stage refrigerator plant was built. This unit was used in the last part of the tests reported here. It operated very smoothly, was completely automatic after initial start-up and gave cold kerosene temperatures in the test tank as low as -42°C under full load. The model wall temperature could be held constant at -35°C.

Component details:

The evaporator was designed to give a maximum heat transfer area and a minimum temperature at the pump suction. It consisted of an inner and an outer container with cross flow between refrigerant and kerosene.

Circulation of the kerosene within the evaporator reservoir (cold reservoir) was with the cold supply pump via a by-pass valve. The cold pump was thus kept running throughout a test, recirculating the cold liquid through the by-pass valve when the tank was isolated. When cold fluid was being supplied to the test tank, the by-pass valve was closed.

The cold system performed well. The only problems which occurred were when there was excessive transfer of hot liquid into the cold system by cross-flow in the test tank. The plant maintained a constant cold side temperature under normal testing conditions even with a moderate cross-flow of hot liquid into the cold system.

Refrigerant: Freon F -12.

Compressors: Bitzer air cooled.

L.P. Type 1: 700 rpm: ½hp.

H.P. Type O; 500 rpm: ¼hp.

4.6 Tank flow system and controls:

The main object of circulating hot or cold liquid through the test tank, is to heat or cool the faces of the composite photoelastic model, as the case may be. Such a circulation system however, must meet other specifications. Generally stated these are:

1. It must provide for quick changes in temperature at any time during a test cycle, between any one of the following four conditions:

Condition	Liquid flowing to tank.	
Number	Side A	Side B
1	hot	hot
2	hot	cold
3	cold	cold
4	cold	hot

All changes should be quick and must at all times be under complete control of the operator, who will adjust the flow to either side according to the information which he receives from the temperature recorder.

2. The pressure on the two sides of the model must be balanced for two reasons:

a) So that the model is not subjected to bending effects and stresses other than thermally induced ones.

b) To reduce cross flow from one compartment to another. As explained in section 4.2, the model should not fit too tightly in the tank. Cross flow, or a transfer of fluid from one side to the other, between model and window or over the top or bottom of the model is therefore likely if a large pressure difference exists between the two sides. This disturbs the even temperatures and fluid levels in the fluid systems.

3. The flow rates to the two sides must be fully variable and must be known. The temperatures of the liquid going into each side of the tank, together with the flow rates, determine the rate of cooling or heating of the model face. When monitoring the temperature profile across the model, adjustments of the controls are frequently necessary to maintain the correct pattern and this can only be done by watching for small variations in the individual flow rates. When a symmetrical temperature change is required (e.g. tests 1 and 4 figs. 20-22) it is particularly important to balance the rates of flow to the two sides of the model.

4. The back pressure of the hot system needs to be variable: The back pressure, or return line pressure head is different for the hot and cold systems and for each of the two sides of the tank. A control on this is necessary in order to prevent a vacuum from forming in the tank under conditions when the return flow may act as a syphon. It will also help to equalize the flow rates and pressures. Since the hot reservoir was mounted about 24 inches lower than the cold reservoir, it was found most convenient to control this return pressure with a small restricting valve in the hot drain line to the reservoir. In practice this was found to be a most useful control.

5. It must be possible to defrost the windows: In all tests where cold liquid was flowing into the tank, the windows would freeze up rapidly and become opaque if they were not specially heated.

Description of System.

Figure 13 shows a diagrammatic layout of the pumps, valves and controls involved. A valve chest housed eight flow control valves in two compartments, separately insulated, and so constructed that heat flow from the "hot" side to the "cold" side was small. The valves enabled the flow

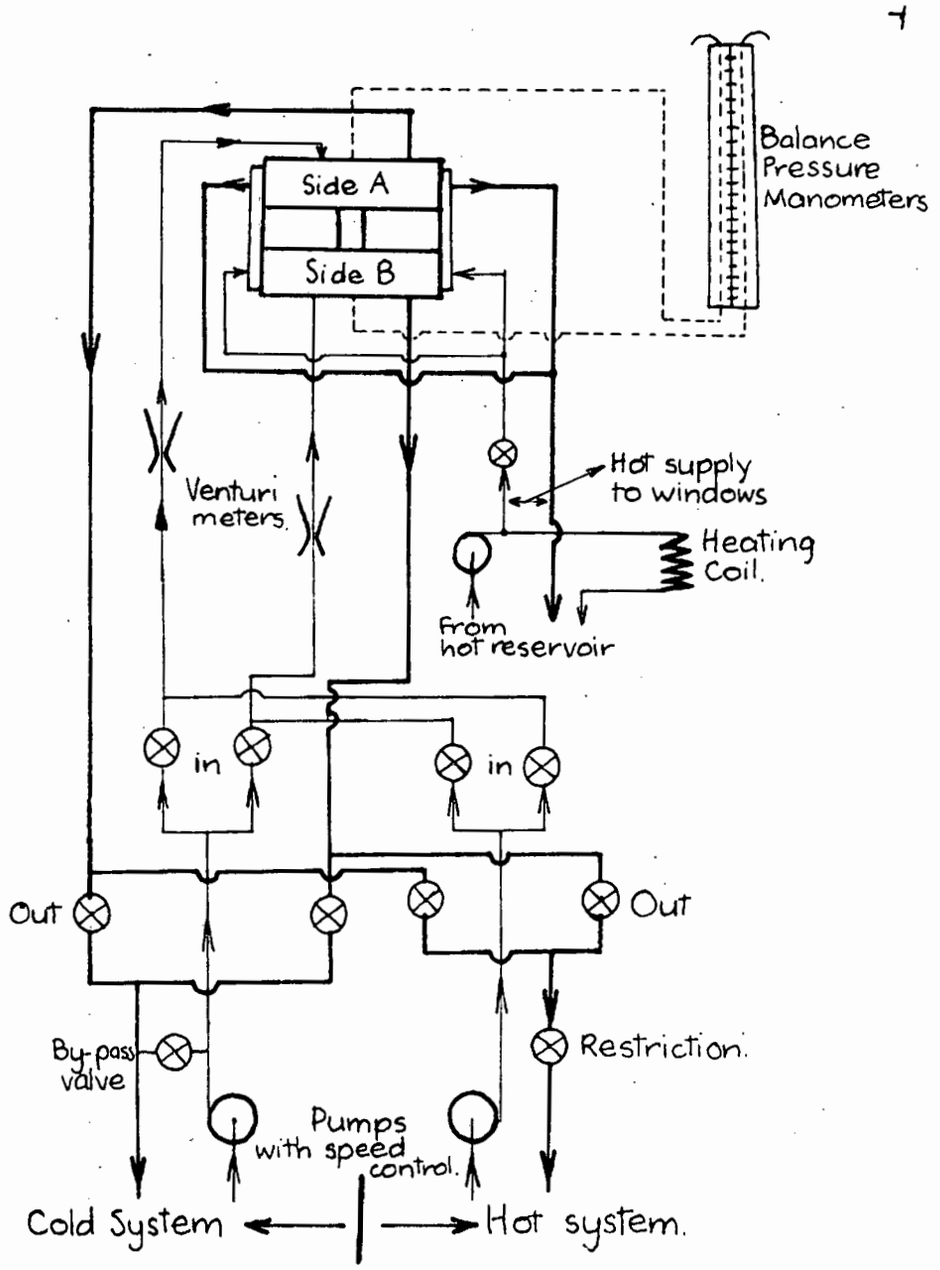

Fig:13. Tank circulation system and flow control.

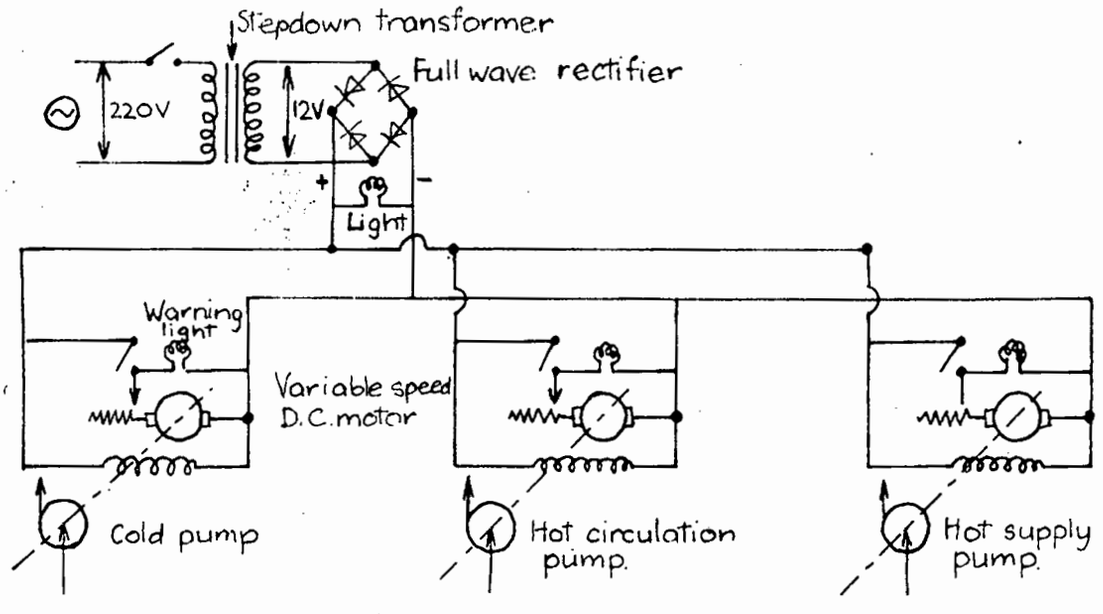

Fig:14. Circuit diagram for variable speed pumps.

to be controlled according to any of the patterns stated under requirement number 1 above. Initially all valves were of the "rubber" diaphragm type but the diaphragms became hard at low temperatures so that the valves had to be heated before they could be closed. They were replaced with special plug valves which remained free at all temperatures. The diaphragm valves were retained on the hot side for reasons of cost only. They worked well but had a higher flow resistance than the plug valves.

Balancing of the pressures on the two sides of the model proved to be difficult. When the leaks were large the pressures were naturally balanced and there was no indication of cross flow other than rapid changes in the relative levels of the kerosene in the two reservoirs. This upset the stable temperature conditions of the system. A prior requirement to the effective balancing of the pressures was therefore an adequate seal against cross leaking between the two compartments in the tank. Once a reasonable pressure difference could be maintained between the two sides, cross flow could be eliminated by balancing the pressures.

Initially the differential pressure between the two sides of the model was read on an inclined manometer connected directly to the manometer tappings in the sides of the tank. Unfortunately the tank had to be drained and opened frequently to change or adjust the model and every time this was done the leads to the manometer trapped air, which then had to be removed. A painstaking operation. Another difficulty arose when either side of the tank operated under a vacuum caused by too rapid a return flow to the hot drain. This put an effective "suction" on the one side of the model, which caused cross flow to occur and also put a transverse load on the model.

By connecting two long open polythene pipes to the

pressure tappings and mounting them on a long vertical board above the tank, each compartment was at once vented to atmosphere and, when under pressure, the level of the kerosene which pushed up into the pipes indicated the pressure in the tank in "inches of kerosene". Pressure differences between the sides could thus be read with great accuracy. This "manometer" was by far the most useful single indicator used in controlling the flow through the tank.

Flow rates were measured with a small venturi-tube in the supply line to each side. They connected with two inclined mercury manometers mounted on the valve box. The flow was controlled by varying the speeds of the individual pumps. Fig 14 shows the control system for the motors: The normal 220 volt A.C. supply was stepped down in a transformer to 12v after which it was rectified in a full wave four arm bridge. The small DC motors/vane-pumps used were constant speed ex-aircraft stock. They were modified for speed control by separating the field and armature windings. The field exitation was kept constant and the armature voltage varied with a reostat. In this way they had complete speed control from zero to full speed. Small indicator lights were built into the control panel to show when (a) the fields were on, (b) each of the three pump motors was on.

The pumps were small vane type aircraft igniter fuel pumps with built in variable relief valves. They were driven through a small gear box. The "cold pump" was further modified by mounting the gear box/pump unit on an extended shaft away from the motor. In this way a considerable heat load caused by the hot motor was removed from the cold system and the pump could be individually insulated together with the cold pipes. With these modifications the pumps and motors ran smoothly for long uninterrupted periods and handled the hot and cold kerosene with ease. The flow rates

were at all times under exact control.

All parts including the hot system, pumps, valves and flow motors were built into a single cabinet and control panel. Special care was taken to insulate all "cold" lines and valves to reduce the load on the refrigerator. All cold pipes were insulated with 5/16th. in. thick foam-rubber sleeving and the valves were modified to have long stems so that they could be mounted deep down in an insulated box. This box was divided into two compartments and the valves were arranged logically into "cold" and "hot" sections, and those controlling the "far side" of the tank were mounted furthest away from the operator.

Window heating was with hot kerosene drawn from the heating circuit and was controlled through a small valve at the side of the main control panel. This "defrosting" system worked extremely well.

EQUIPMENT SPECIFICATIONS.

Valves: Diaphragm type: Saunders 3/8in.
Plug type: Hattersley Floreat ⅛in.
} Modified with long stems.

Pumps: Vane type driven by geared motor.
Plessey "Torch" igniter pump. EP3.
Modified for speed control with rheostat in armature circuit.

All Rigid Pipes: Copper.

All Flexible Pipes: Polythene Tubing - Fibre glass reinforced to prevent them from collapsing when hot.

All seals, diaphragms, pipes and valves must be resistant to hot and cold kerosene.

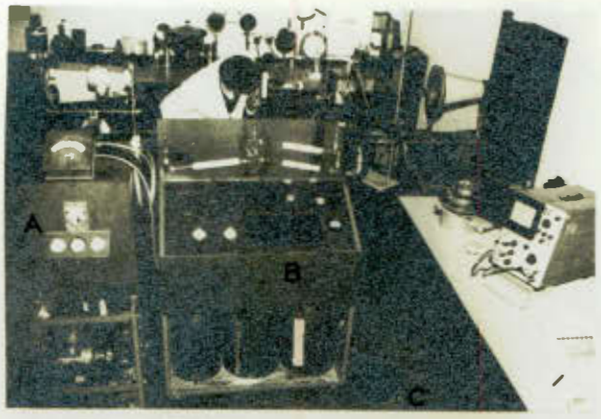

8. VIEW OF APPARATUS
A=REFRIGERATOR AND COLD TANK;
B=CONTROL PANEL AND HOT TANK;
C=VARIABLE TRANSFORMER.

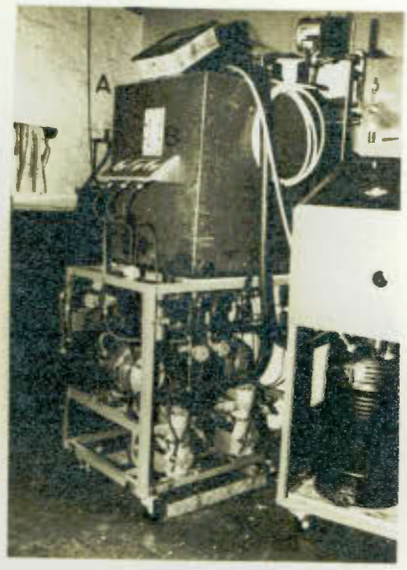

9. CLOSE UP OF TWO STAGE REFRIGERATOR PLANT.
A=EVAPORATOR AND COLD RESERVOIR
B=LEVEL SIGHTGLASS.

10. VIEW INTO CENTRAL PANEL:
A=COLD PUMP MOTOR; B=HOT CIRCULATING PUMP;
C=HOT SUPPLY PUMP; D=RECTIFIER BRIDGE;
E=FLOW MANOMETERS.

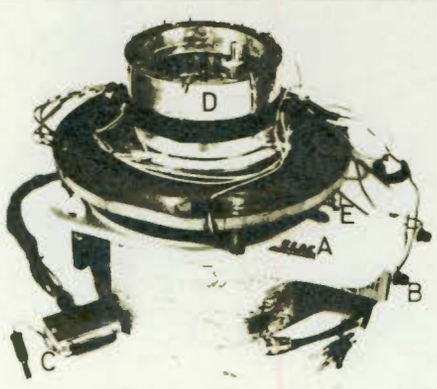

11. FIFTEEN POINT SCANNING SWITCH.
A=RECORD TURNTABLE ON SHEET METAL BASE & SCREEN
B=BATTERY FOR TRIGGER. C=CANON CONNECTOR.
D=MOUNTING RING (SCREENED) FOR SWITCHES.
E=CONTACT BREAKER ADJUSTMENT.

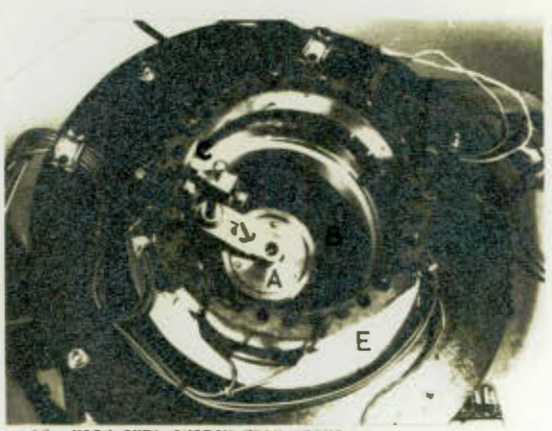

12. VIEW INTO SWITCH FROM ABOVE.
A=15 LOBED CAM.
B=CONTACT BREAKER POINTS.
C=ROTATING MAGNET.
E=SWITCHES.

13. OSCILLOSCOPE, CAMERA AND SWITCH.

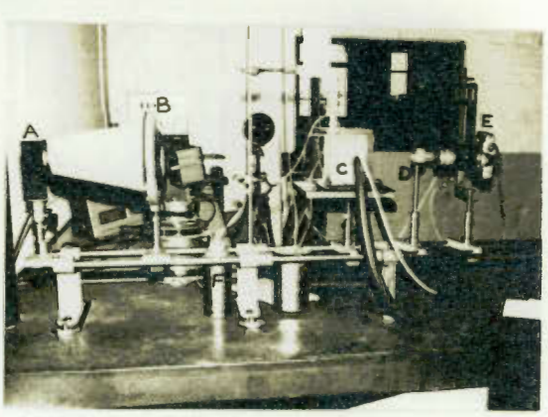

14. POLARISCOPE SET-UP.
A=LAMP; B=FIELD LENS; C=MODEL IN TANK.
D=GREEN FILTER. E=CAMERA.
F=ICE POINT

4.7 Temperature Scanning and Recording Equipment.

The sensing and recording of the instantaneous temperature profile in the model presented the most difficult problems in the development of the apparatus. The electrical signals which have to be monitored are extremely small (resolution of 50 micro-volt is required) demanding a high level of performance throughout the system.

The overall requirements of a system for recording the temperature profile in the model are to sense the temperatures at closely spaced points in the stressed model and to record them for easy study, and especially in such a form that at any instant during an actual test the temperature profile can be reliably related to the stresses.

Since the temperature differences are small, (biggest difference anticipated between the two sides was 120^{o}C) the resolution was set at 1^{o}C i.e. a 1^{o}C change in temperature must be noticable in the final record.

This is not a severe requirement for reading temperatures on a semi-static basis, but in this case the temperatures of many points in the model had to be read rapidly before a significant change could occur in any of them.

Fortunately epoxy resins are relatively poor conductors so that temperature changes do not occur as fast as in metals, yet preliminary tests showed that all points should be sampled in less than one second. Many of the usual means of recording small temperature changes are therefore unsuitable.

Finally the sensing elements in the model must not themselves disturb the temperature profile.

Iron-constantan thermocouples were chosen to sense the temperature because they gave the highest output at small temperatures, were available in thin wires and had lower heat conductivity than copperconstantan wires.

These thermocouples, made of 32 gauge wire, were glued into a special temperature sensing block with their beads immediately next to the polarising elements, but outside the polariscope. They therefore

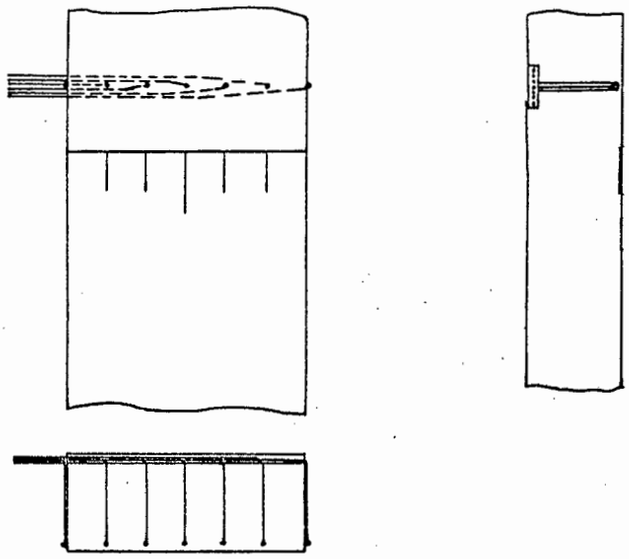

Fig. 15.

measured the temperature of the outer face of the polarizing filter which, being thin and of a material similar to the model meant that they effectively measured the temperature of the photoelastic model. The wires were led along an isothermal for at least one eighth of an inch, but usually for three eighths inch, before leading out of the model. In this way heat conduction along wires, as it passes through the temperature gradient, will not effect the formal reading at the bead. They were cemented into small holes with "Araldite Adhesive".

The accuracy of this method of measuring is confirmed by the results in section 5 fig 20.

The bunched thermocouple wires left the tank through a kerosene tight seal in the lid and were all connected to one end of a special CANON multi point connector. The other half of the connector points were soldered to multi-stranded screened copper wires which were connected with the switching unit. The 25 point CANON connector had gold plated pins and sockets with very low contact resistance. It was mounted about 15

inches from the box in an area where there was no sudden temperature changes, and was built into a comparatively heavy brass(connector) box which ensured that all the soldered joints were held at the same temperature, thus introducing no errors in the recorded values of the temperature differences in the model.

After emerging from the model, but before passing through the lid, the bunch of wires was insulated with soft Urethane rubber to reinforce them and to reduce the rate at which they would conduct heat into the model during periods of rapid temperature changes.

All temperatures were read with reference to that of melting ice ($0^{o}C$) and the reference couple was soldered to the connector in exactly the same way as the others. An extra thermocouple was also mounted in melting ice and scanned together with those in the model to act as a continuous calibration for the system. The full layout is shown diagrammatically in figure 16.

The leads from the CANON connector were individually screened, and they passed to a scanning switch which switched them in turn to the input of a storage oscilloscope which had it's time base adjusted so that a full horizontal sweep coincided with a single cycle of the switch. The signals from the thermocouples were thus drawn in sequence on the screen where they could be observed and recorded during the test.

The whole system was carefully screened and constructed to reduce "noise" to a minimum. During tests the noise level on the signals was less than 50 micro volts. One cycle of the switch lasted 0.7 seconds, during which time a complete "graph" of the temperature profile was drawn on to the screen of the oscilloscope.

Description of Switch:

Various switching methods were tried but the version as described here was by far the best. It has an extremely low

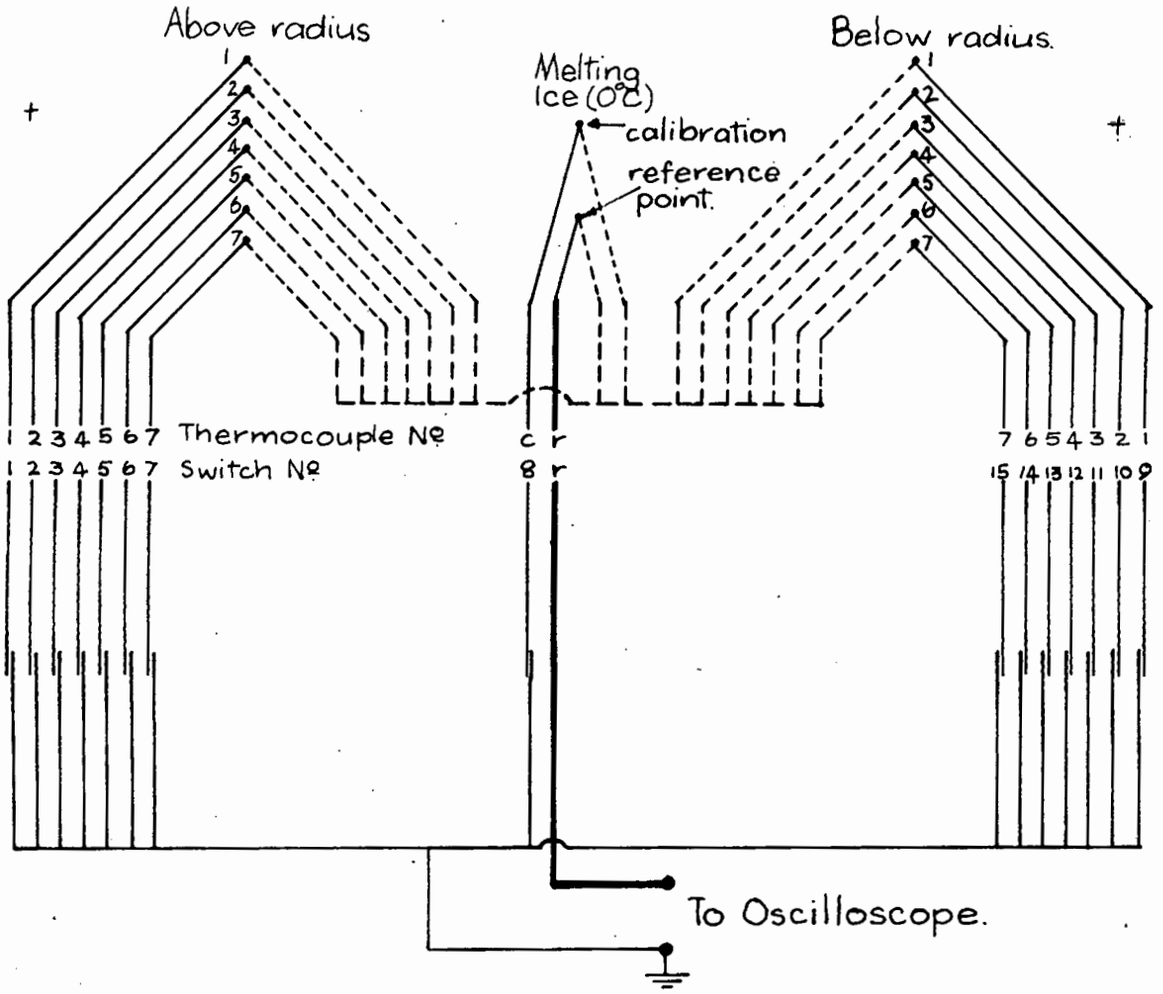

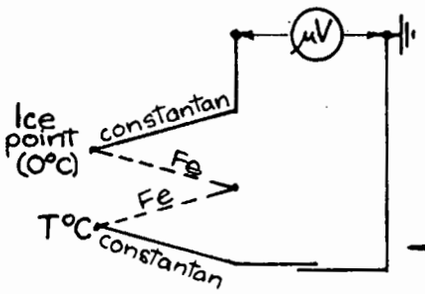

FIG 16: Thermocouple and Switch connections.

Equivalent circuit.

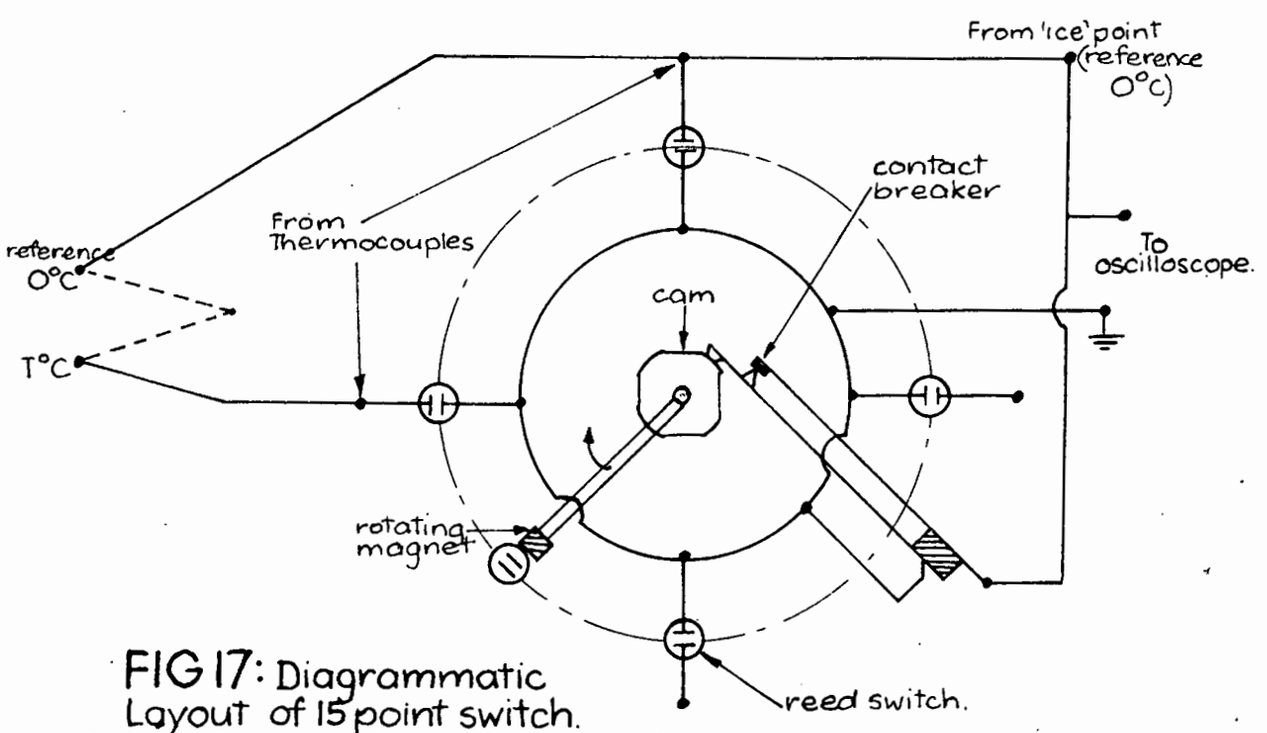

FIG 17: Diagrammatic Layout of 15 point switch. (only 4 cam lobes and 5 switches shown)

contact resistance, excellent performance at high switching speeds for long periods of operation (no thermal emf's) and is readily adaptable to the sampling of almost any number of input signals. The present number of inputs is fifteen but the switch can be easily modified to sample a larger number, if required.

The switch consists of an ordinary three speed record turntable, over which is mounted a cylindrical ring drilled to support, in an annular array, the required number of mercury wetted reed switches, to each of which is connected the output from one thermocouple. The switches are sampled in sequence by a small bar-magnet which is mounted centrally on the turntable and rotates past each switch in turn (Fig 17 and Plate 2). In between each switch station the input to the oscilloscope is connected to "earth" through a cam operated contact breaker. This not only "chops" the signals into a square wave which can be handled by a high gain A.C. stabilized amplifier, but it also provides a continuous "base line" for use with high gain D.C. amplifiers which may tend to drift unexpectedly.

The oscilloscope input has a high impedence of 1 megohm which puts virtually no load on the thermocouples. This is a prime requirement for the reliable recording of thermocouple signals of this kind.

The oscilloscope has an 8cm by 10cm rectangular storage screen. Its calibrated time base can be adjusted to sweep in synchronism with the switch. The time base was triggered externally by a 4½" volt signal from an additional switch mounted in between the last and the first switches in the ring. The recorded pattern therefore repeated consistently with thermocouple No. 1 at the left and No. 15 at the right hand end of the screen.

The thermocouple signals were fed into either of two

plugin amplifiers, the one a stabilized A.C. and the other a high gain D.C. unit, Both functioned well but generally the stable D.C. amplifier was preferred.
When required the stored graph of the temperature gradient was recorded by photographing it with a 35mm oscilloscope camera.

Although the system described above evolved through many intermediate stages, the final version not only performed smoothly and reliably but also presented the required information in a very useful way. Because it appears in the oscilloscope screen almost as a "graph" of the temperature profile it can be interpreted directly and adjustments can be made to the flow control system without first having to plot a graph.

Specifications.

Switches: Flight research "Hamlin" mercury wetted reed switch Type HRC -1.

Oscilloscope: Tektronix type 564
Time base: 2B67 operated in single sweep mode and external trigger.
Input amplifier: 3A3 two channel D.C. differential operated at 1mV per cm. and 0.5 m V per cm.

Camera: Tektronix/Robot Recorder operated on F/2.8 and $\frac{1}{4}$ second exposure.

4.8 Polariscope:

The stresses set up in the model by the temperature gradient were studied by placing the "sandwich"-type photoelastic model in a modified transmission polariscope shown in Fig. 18a.

The light source was a Mercury arc lamp with a compact 3mm arc of average brightness, 20,000 candeles.

It was mounted near the focal point of a single element double convex lens which was meant to produce an evenly illuminated parallel light field down the test section. Unfortunately this parallel field was not of even brightness; it contained a very troublesome "hot spot" of about ½" diameter, which although not objectionable during visual observations, made any photographic study extremely difficult. The exposed plates or films would be overexposed in certain areas and underexposed in others. Detail is then lost in c critical areas. By mounting the lens a little further than one focal lenght away from the light source a slightly divergent field was produced but the "hot spot" was considerably expanded in size. A small screen of optical quality etched glass mounted immediately after the lens further diffused the light slightly and improved the evenness of illumination over the whole field of view. With this set-up negatives were produced which were of sufficiently even exposure for reasonable results to be obtained by special processing techniques (see Section 4.9.for detailed discussion of photographic techniques.) The final photographic records of the stress patterns were of an overall quality which was adequate for the studies involved.

The composite model assembly was at once photoelastic model, polariscope and temperature sensor. The two polarizing filters were built into the model by mounting them immediately adjacent and on both sides of the epoxy resin stress sensitive element. Any disturbances in other parts of the test tank and model assembly could therefore not produce stress patterns. (See sections 4.2 and 4.3 for detailed discussion of the test tank and model set-up.) The stress fringe pattern in the model was photographed directly with either a 35mm camera or a 4in.x5in. plate camera. Alternately it was projected onto a screen with a

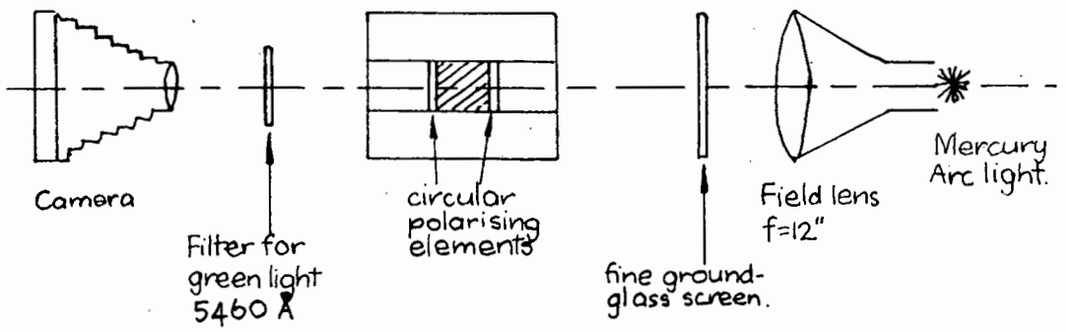

Fig:18(a) Photo-thermoelastic polariscope arrangement.

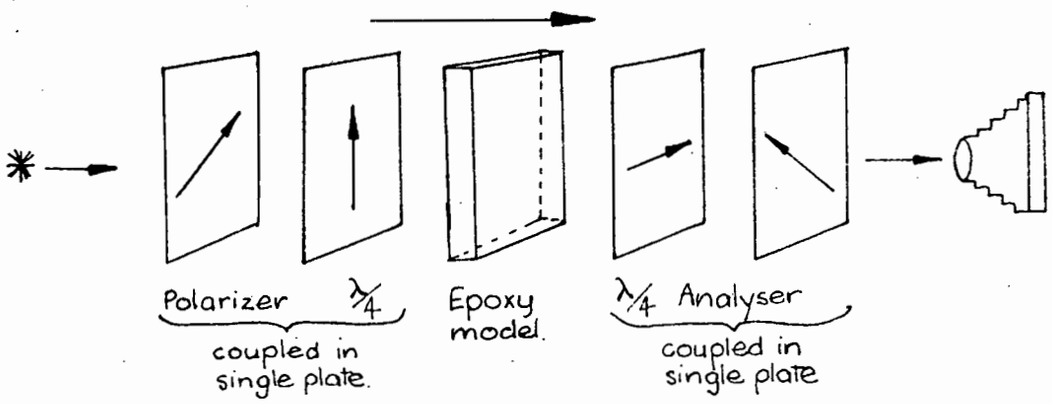

Fig:18(b) Equivalent polariscope for isochromatic studies—light field only.

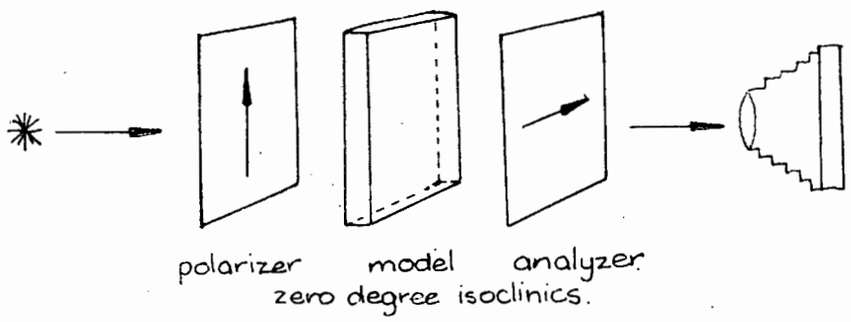

Fig: 18(c) Equivalent polariscopes for built-in studies of isoclinics zero degrees ≡ polarizing axes vertical and horizontal.

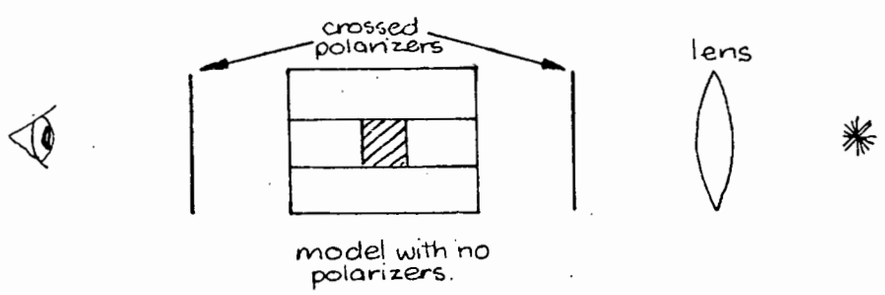

Fig: 18(d). Set-up used for observation of isoclinics at angles other than 0° and 45°.

multi-component projection lens for visual studies. It is normal in transmission polariscopes to collect the light from the "parallel" field with a large diameter lens of similar dimensions to the field lens. Such lenses, however, introduce abberations unless they are of unusually high quality. Since a lens of this quality was not available it was preferred to record by direct photography, or projection, in order to exclude these distortions.

Set-up used:

For isochromatic fringe studies (Stress fringes) two sheets of combined polarizer-quarter wave plate were used. Because of the fixed orientation of the polarizing and quarter wave plate axes in each plate, it was not possible to obtain a dark field set-up. All observations were therefore in the light field set-up, i.e. the dark lines observed are half-order fringes. The normal orientation of the polarizing axes were at 45° with the horizontal, with the polarizer analyzer axes crossed.

Combined circular polarizers were used in preference to separate polarizer and quarter wave plate filters, in spite of their limiting observations to light field only, because they formed the thinnest possible sandwich in the composite model. This is important in the constructions used because the thermoelastic properties of the polarizing material were not known and all temperature measurements were made "outside" the polariscope immediately adjacent to the filters.

Isoclinic studies are not easily made with built in polarizers. Each angle-setting requires a specially cut filter, with the required orientation of the polarizing axes. The model has to be disassembled, the "old" polarizers removed and the "new" ones substituted. These are very

costly and time consuming procedures and it was therefore decided to limit the internal observations of isoclinics to zero and 45 degrees from the vertical. The former were obtained by using filters cut from plain polarizing sheets and the latter by turning the composite circular polarizers inside-out. In this way the quarter wave plates were placed "outside" the polarized field, where they have no modifying effect on the plain polarized character of the light.

In most models the zero degree isoclinic covered almost the whole field and generally there were no dark isoclinic bands left in the model at angles greater then 20 degrees from the vertical.

In order to observe the stress-directions (isoclinics) at angles other than zero and 45 degrees a series of test runs were made to investigate the possibility of using "external" polarizers as in a normal transmission polariscope.

It was known that, although small, perspex has temporary birefringent (Photoelastic) properties, However, because this was small, it was thought possible that the effects of the tank Windows and of the ends of the composite model on the isoclinics, may be small enough for reasonable estimates of the stress directions to be obtained by mounting the polarizers outside the tank. This proved to be so.

Firstly, the epoxy element and filters were removed from the model and replaced by an equivalent thickness of perspex. The stressed model was thus pure perspex. The model was then mounted in a normal circular transmission polariscope, both light and dark field, and the isochromatic fringes observed when thermally stressed. They had very approximately the same distribution as in the epoxy sheet. but the modifying effects of the ends and of the windows were clearly visible. When the polariscope was converted to a plain polarized set-up the isoclinics were present.

The zero and 45° isoclinics compared well with those found in the sandwich set-up, but were much more diffuse because of the long optical path through the model (about 5 inches). The windows in the box, introduced their own sets of isoclinics, but they were very faint and it was reasoned that if the camera or projection lenses were used with maximum apperture, the very short depth of field (about ½in.) would put them out of focus. This was confirmed in subsequent tests, but they still cast shadows which further reduced the sharpness of the already poorly defined isoclinic areas.

Although not entirely satisfactory, this method yielded sufficiently clear information on the stress directions, outside areas of high stress concentration, to confirm the assumptions made in the interpretation of the test results, and to give a general idea of their orientation.

Details of Equipment.

Light Source: Clear glass compact source mercury vapour lamp; 250 watt; 220/250 Volts with associated choke and condenser. Lamp type Mazda MB/D 250; 20,000 candeles /cm^2; 3mm arc length.

Field Lens: Single element double convex; 10" outer diameter focal length 13in.

Polarizing Filters: Polaroid circular polarizers used as a light field set-up. Polaroid plain polarizers used for plain polarizing set-up.

35mm Camera: Single lens reflex - Minolta SR1 camera back and shutter, 1/500sec. to 1 sec., Meyer Optic Primoplan 58mm lens, apperture F/1.9 to F/22.

Extension Bellows: Minolta.

Converter Lens: Vincor 2 time convertor. Thus the camera was effectively a single lens reflex with a long focal length (equivalent 116mm) lens system set-up to take close-up photographs in the model. The field of view was about 2½

inches in the longest dimension.

4" x 5" Plate Camera: Calumet 4x5 professional camera with modified mountings to adapt it for "bench-type " operation. Schneider "Symmar" lens f=150mm, appeature f/5.6. With the rear half-section of the lens removed, it had a focal length of 265mm, apperture f/12 which is the form in which it was used. The full field recorded on the 4" x 5" film back was 2¾in. on the model in the longest dimension. (See section 4.9 for detailed discussion of photographic techniques, materials and exposures.)

4.9 Photographic Techniques:

The materials and techniques used in the photographic recording of stress patterns are special. The aim is for the highest contrast between the black "fringes" and the white intermediate areas when viewing in green light, and also for the best resolution between the fine closely stacked fringes which occur in areas in which the stress gradient is steep. Normally film-speed is not important, because the stresses are static. In this study however, conditions were transient so that, at certain times during a test run the fringes were "moving" across the field of view of the camera fast enough to blur the definition on the photographic negatives if exposure times exceeded ½second. This was particularly troublesome where the fringes were fine and close together, because the resultant picture would not show individual fringes but a grey blur instead.

Further problems arose because of the uneven light intensity over the field viewed by the camera. This is an optical characteristic of the polariscope which has a "hot spot", or bright central area from which the intensity tapers off radially towards the edges of the field. The methods used to reduce the undesirable effects of uneven illumination were discussed in section 4.8 pp 61. Hot spots occur in many

polariscopes but are not troublesome in the usual static photoelastic studies where the overall stress field can be photographed separately from the small field studies of areas of high fringe density. High resolution in the region of stress concentrations is not required in the overall view, and for the studies of detail the polariscope is adjusted so that the bright spot covers the whole of the small area which is being observed, making the light intensity over this portion comparatively even.

This two-stage type of observation is not possible under transient stress conditions, such as those studied here, A given set of conditions prevails only once, and the same negative which records the overall stress field must also provide the detailed information of the stresses in regions where the stress gradients are steep.

With the polariscope set-up used, the variation in light intensity over the field photographed by the camera was equivalent to almost two apperture stops or a factor of four. High contrast photographic materials generally have only a small latitude in exposure if good working negatives are required. The technique described below was therefore developed to reduce the films sensitivity to variations in exposure so that the required detail of the whole stress pattern would be available from a single photograph.

Because of the rapid sequence in which photographs had to be taken during the early parts of each test, a through the lens reflex 35mm camera was used. This has a rapid wind-on mechanism so that exposures can be taken at 5 second intervals if required.(Exposure time used was 1 sec.) This rate of exposure was not possible with a plate camera. Another important feature of a through the lens reflex camera is that the model can be viewed through the camera at all times excepting the 1 second of exposure time when the shutter is actually open.

A few 4in. x 5in. photographic plates were taken to study details such as isoclinics which were more conveniently viewed on the ground glass screen of a professional plate camera.

Materials and techniques found most useful were as follows:

35mm Photography of Stress Patterns:

Kodak microfile film exposed for 1 sec. at F/1.9 and F/2.8, developed in Kodak D-8 developer (mixed according to instructions and diluted 2 parts stock solution to 1 part water) for times varying from 20 seconds to 35 seconds. Washed in water and fixed in a bath of Kodak Acid Fixer. All chemicals at 20°C.

This technique is equivalent to overexposing the negatives and compensating for it by decreasing the developing time.(normal time is 2 minutes).

Printing paper Agfa Agepé developed for best results in Kodak developer D163, washed and fixed. All at 20°C.

It was found that the variation in negative density due to the uneven illumination of the model was considerably reduced by "overexposing" the negative and then developing it for a short time. Under such conditions the exact developing time is obviously critical and it was standard procedure to expose a short series of trial negatives for each test after the camera and bench set-up was adjusted and during the time when the test conditions were being stabilized. These would then be developed separately for times varying from 20 to 40 seconds (5 test negatives) and the best one selected. In this way adjustments can be made for variations in illumination and in the strength of the developer.

4in. x 5in. Photographs of Stress Pattern:

Du Pont Chronar/Ortho S Litho .004 in. thick plates developed for 2 minutes in Chronalith liquid developer mixed at extra strength (1 part liquid to 1 part water).

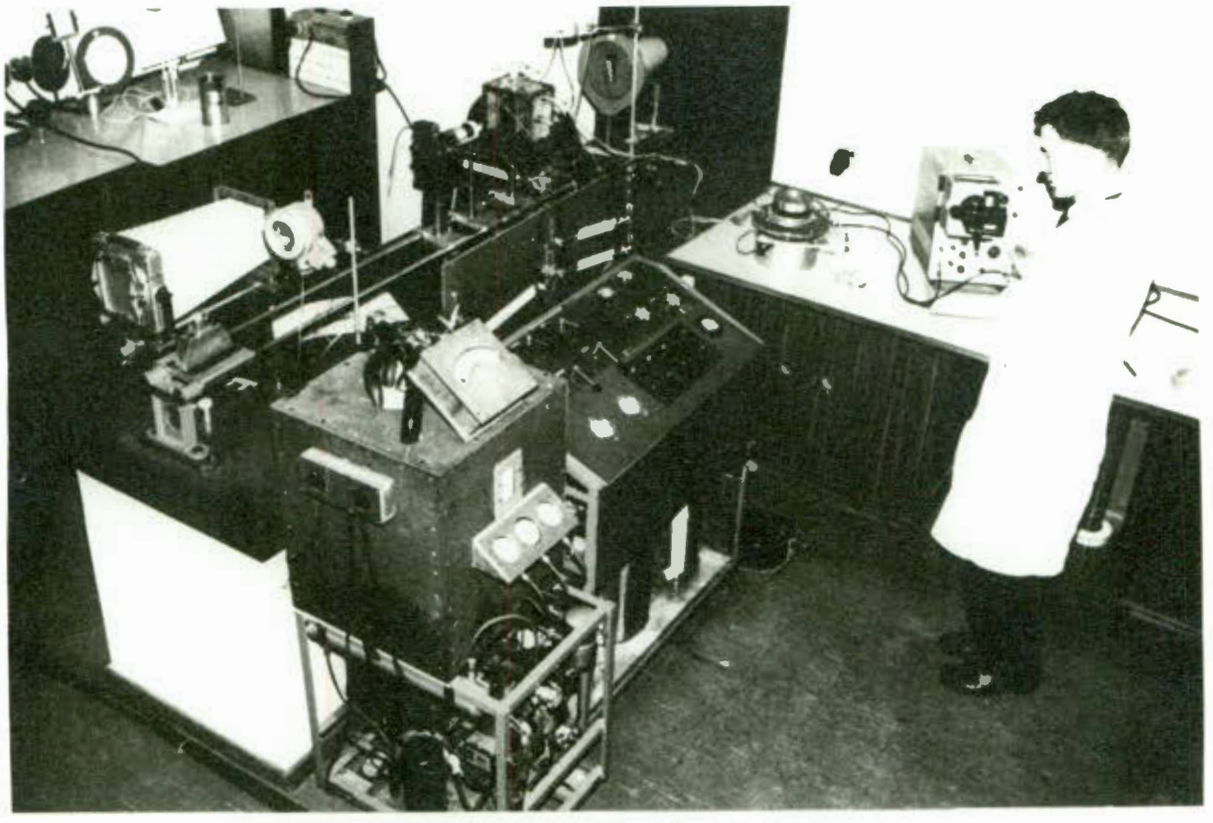

15. OVERALL VIEW OF APPARATUS.

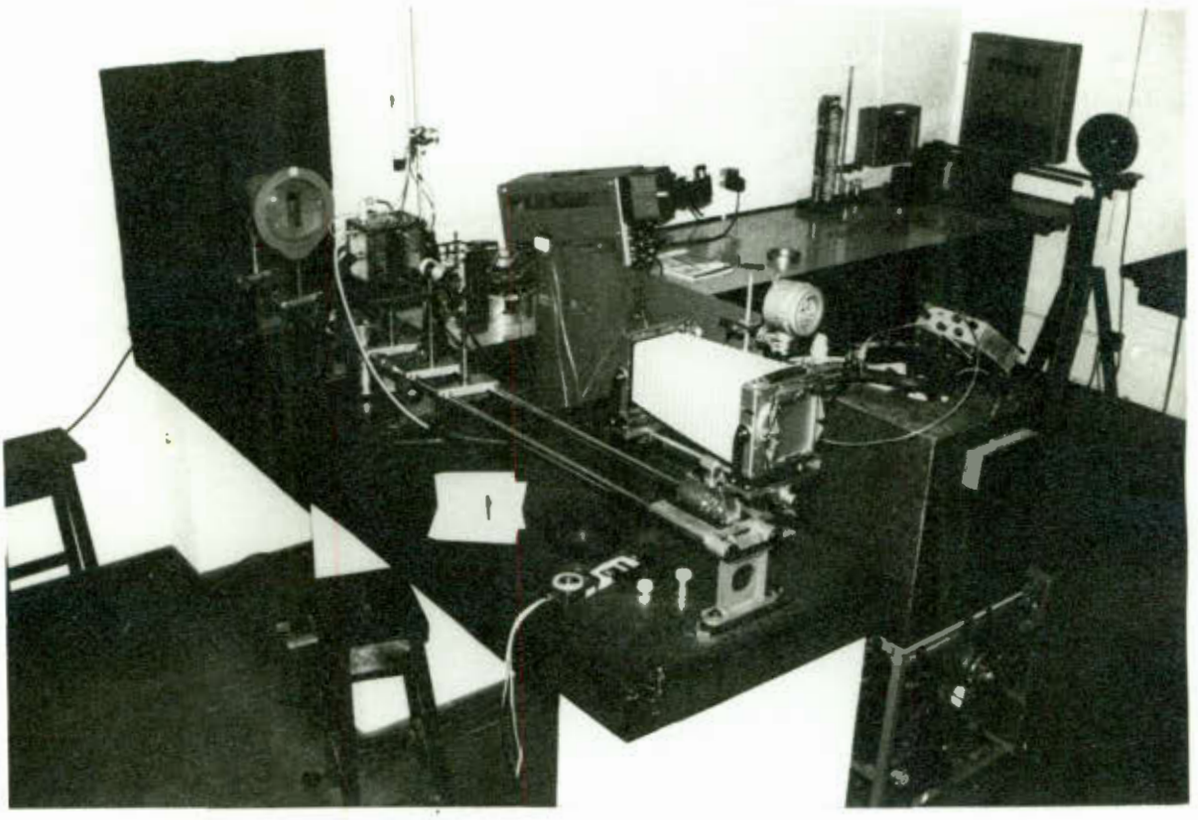

16. VIEW DOWN THE POLARISCOPE.

PLATE 3

Washed and fixed. All chemicals at 20°C.

35mm Photography of Oscilloscope record:

Kodak Tri-X 35mm film developed for 2 mins. in Kodak D-8 developer mixed 2 parts stock solution to 1 part water. Washed and fixed. All chemicals at 20°C.

The much faster Kodak Tri-x film was used here because the camera had a maximum shutter timing of only $\frac{1}{4}$ second. Settings were: $\frac{1}{4}$ second at F/2.8; Oscilloscope in stored mode, trace intensity to just write and graticule light intensity at "9".

4.10. TESTING SEQUENCES.

The sequence of operations for a typical experimental run is given briefly below.

Two operators are required, one for each camera. They can perform all other functions at the same time.

Test: Soak hot one side, cold the other. Then change to cold both sides.(This is the test described in section 3.1, pp21).

1. Start refrigerator and immersion heater and circulate hot and cold liquids through by-pass systems until constant temperature controls operate - i.e. until test temperatures are reached. Prepare model, cameras, oscilloscope and thermocouple scanning system. Start polariscope lamp.

2. Circulate hot kerosene to one side and cold kerosene to the other side of the tank. Adjust flow rates and pressures to prevent cross flow and pressure loading on the model. Circulate hot kerosene through windows to keep them clear of frost. Focus camera on fringes which occur during the soak period. Take sample exposures to determine correct developing time. Check temperature gradient at intervals and continue soak until steady state conditions are reached. The

temperature profile will now appear as a straight sloping line on the oscilloscope screen and the model will be free of fringes.

3. Take photographs of this starting condition.

4. Change flow to cold on both sides of model. When first signs of stresses appear in model which is usually after about 15 seconds, start taking photographic exposures of the stress pattern as well as the temperature profile, with the two cameras synchronised, at 15 second intervals until 90 seconds have passed, then every 30 seconds until 4½ minutes; every 1 minute until 12 minutes and then every two minutes until 20 minutes have passed since the start of the sequence.

During this period the flow rates and pressures must be adjusted to remain equal on both sides of the model and the flow of hot kerosene through the windows must be maintained. The temperature of the hot reservoir must also be kept constant.

5. Continue the run until the new steady state, cold right through the model, is reached and check that the model is again free of stresses.

Once the time sequence for taking photographs is every minute, the fringe pattern must be studied and notes should be taken of the position of the zero fringe, which can be distinguished from the other fringes when the model is viewed in "white" light.

This information is valuable when the black fringes on the developed negatives are being interpreted. Unfortunately it is quite impossible to obtain this information in the early stages of a test run, when it will be most valuable, because the eye cannot destinguish that clearly nor that quickly where this zero fringe is in the very closely stacked and fast moving fringes in the model.

A single test as described takes about 4 hours;

1 hour for the preparation, 1½ hours for the soak, ½ an hour for the test and another ½ hour to 1 hour before stable conditions are once more reached.

One test can be run in a day, because films have to be processed and small adjustments inevitably need to be made to the model and the apparatus before the next test can be performed.

The normal sequence of studies for a model which is symmetrical about its vertical centre line is:

1. 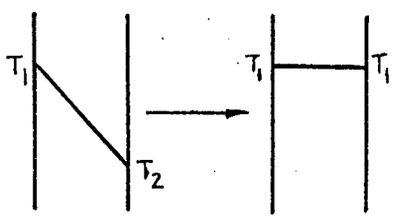

From hot on one side, cold on the other, to hot on both sides.

2. 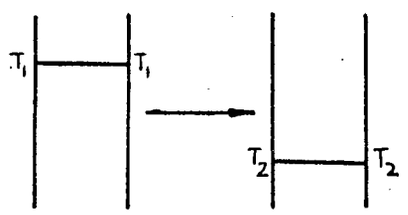

From hot on both sides to cold on both sides.

3. 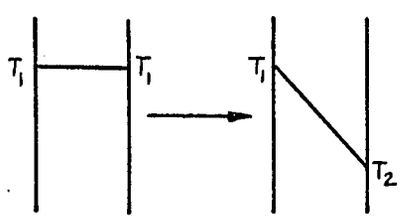

From hot on both sides to hot on one side cold on the other.

For models which are not symmetrical about the vertical "centreline" two more tests are taken.

4. 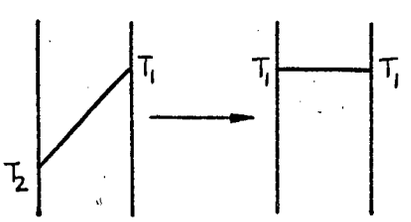

and 5. 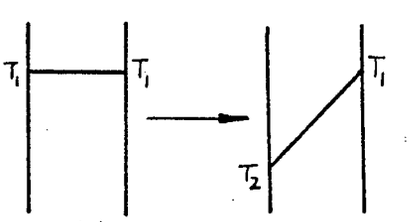

Tests 1 and 4 represent conditions when there is a "change in load" and also simulate conditions of "internal heating". Tests 3 and 5 represent conditions during "start up" of equipment.

SECTION 5: EXPERIMENTAL RESULTS.

This section presents the experimental results obtained from a series of seven tests on two models. It compares experimental results with theoretical predictions, where possible, and gives time and stress scales for correlating model results to those expected in a steel prototype. The salient points of each set of graphs are discussed and the sources of experimental error are reviewed.

The tests reported here were performed on two different models (Fig. 19). The one representing a plate of uniform thickness and the other a similar plate but with a change in thickness.

5.1: Model properties used in calculation:

As explained in section 4.2 (p35) the model material properties vary with temperature. The values chosen as representative for each set of tests, and which were then considered constant for the test are given in table 2.

The correctness of these values could be checked in tests 1 and 4 where these basic assumptions are shown to be justified.

Table 2: Properties of photoelastic models.

Property	Units	Model A.	Model B.
E	lbf/sq.in	3.75×10^5	3.9×10^5
α	in/in$^{\circ}$C	54×10^{-5}	5.5×10^{-5}
ν	—	0.35	0.35
f	lbf/fr.in	58	56.4
Figure of merit $Q = E\alpha/f$	fr./in$^{\circ}$C	0.35	0.38
Model thickness h	in	0.432	0.435
Model fringe value $F = f/h$	lbf/in^{2}fr	134	130

5.2 Verification of model behaviour with theory:

The temperature and stress profiles were compared with theory at three points during the test sequence.

Firstly, a carefully contrived symmetric parabolic temperature profile was established in model A. This profile (Fig. 20), was compared with the theoretical one of equation 8(p17) and the experimental stress profile was compared with the distribution given by eq. 9(p17). Agreement is seen to be excellent.

From amongst the sequences in tests 1 and 4 two reasonably symmetrical temperature profiles were then chosen for comparison with the theoretical predictions of equation 8. The related experimental stress fringe profiles were further compared with the theoretical fringe profile (Figs. 21 & 22) based on eq. 9, as follows:

From eq.3(p11))and eq.9:

$$\sigma_x = \frac{E\alpha}{1-\nu}\left[\frac{y^2}{c^2} - \frac{1}{3}\right]\Delta T = \frac{Nf}{h}$$

$$N = \left(\frac{E\alpha}{f}\right)\frac{h}{1-\nu}\left[\frac{y^2}{c^2} - \frac{1}{3}\right]\Delta T \qquad (14)$$

where ΔT is the difference between the internal and boundary temperatures($59^{\circ}C$ for fig.21 and $58^{\circ}C$ for fig.22).

With the values from table 2 put into eq.14 the parabolas marked "theory" were drawn. Agreement between theory and test is good near the boundaries and reasonable (10% low) internally. General sources of experimental errors are discussed in section 5.8(p107) but the three mainly responsible for the present variations are pointed out here:

1. The temperature profiles associated with the "test" curves of figs. 21 and 22 are not fully symmetrical parabolas.
2. The material properties,Q,and Poissons ratio are assumed constant through the model.
3. Experimental uncertainty in reading partial fringe orders at internal regions where the fringes are broad and ill defined.

Further comparisons between test and theory are made on graphs 1D and 4D for surface stresses and on 4E for internal stresses, at times when the temperature distributions in the model were such that equation 14 could be applied without serious misgivings. Values for the figure of merit (Q') for the model material were calculated over the same time ranges and are plotted in graphs 1F and 4H. For these eq.14 was used at the boundary where y/c =1. Then

$$N = \frac{2}{3} Q' \left(\frac{h}{1-\nu}\right) \Delta T \qquad (15)$$

$$\text{or} \quad Q' = 1.5 \left(\frac{1-\nu}{h}\right) \frac{N}{\Delta T} \qquad (16)$$

from which Q' can be calculated, if the experimental values of N and ΔT are known. In both graphs the figure of merit remains reasonably constant which fulfils the requirements of section 1.3(p8).

Both these results (for Q' and the boundary stresses) lend support to the reliability of the material properties chosen as representative over the range of temperatures encountered in the tests.

5.3 Similarity scales; model to steel protype:

The similarity laws of section 2.2(p18) were applied to the experimental values to determine the time dilatation when converting test results to a steel prototype and also to afford an indication of the level of stresses which could be expected in such a prototype.

Table 3 lists the relevant properties for the model material (see section 4.2 p35) and further figures supplied by CIBA, Switzerland) and also for typical low and high alloy steels (Smithells, R25).

Table 3: Properties for Araldite B(CT 200) and Steel.

Table 3:

Property	Model	Steel Prototype	
		low alloy	high alloy
For time scale:			
Thermal conductivity, k, (cgs units)	$.39 \times 10^{-3}$	.11	.08
density, ρ,	1.2	7.8	7.9
Specific heat, C, (cal/ ^{o}C)	0.35	0.12	0.12
With diffusivity $K = k/\rho C$			
The ratio K_m/K		8.0×10^{-3}	12.5×10^{-3}
For Stress scale:			
E (lbf/in^2)	As per table 2	30×10^6	
α (in/in^{o}C)		$1.2 \times .0^{-5}$	
ν		0.30	

Averaging the ratios K_m/K for low and high alloy steels at 10×10^{-3} the time dilatation of equation 13 becomes

$$\frac{t_{Steel}}{t_{Model}} = 0.01(\text{geometric scaling factor})^2 \qquad (17)$$

For a model the same size as the prototype the time scaling is then 1/100 which is the value used in all the graphs.

The stress scales of the two models have to be calculated separately. Thus:

Model A (tests 1 to 3)	Model B (tests 4 to 7)
$\sigma_{st} = 16.5\,\delta\,\sigma_m$	$\sigma_{st} = 15.5\,\delta\,\sigma_m$
but: $\sigma_m = 134N$	$\sigma_m = 130N$
therefore:	
$\sigma_{st} = 2210N\delta$	$\sigma_{st} = 2020N\delta$

Small variations in the values for α and ν for steel have a large effect on the equivalent stress ratio so that a rounded off scale was chosen to compare stresses in a steel part with those in a part made of Araldite B. This was:

$$\sigma_{st} = 2000\ N\frac{T}{T_m}\ \text{lbf/in}^2 \qquad (18)$$

and the equivalent stress scale for a temperature scaling factor $\frac{T}{T_m}$ of 1 was drawn on the stress curves for each test.

5.4 Dimensionless stresses:

In a fully constrained plate which is uniformly heated or cooled, by an amount ΔT from its initial condition, the stress would be:

$$\sigma^* = \frac{\alpha E}{1-\nu} \Delta T \qquad (19)$$

This can be used as a reference stress to develop a dimensionless stress ratio σ/σ^* By choosing a suitable reference value for ΔT such a ratio can be developed, but this only simplifies the interpretation of the results, if the temperature difference is of some logical value. Nowhere in these tests did the surface temperature change by a step function so that ΔT could not be taken as constant throughout a test. In tests 4 and 5 however, the difference between the boundary and the lowest internal temperature at each instant, had a direct relationship to the stresses. These instantaneous values for ΔT were set into equation 19 and the ratio σ/σ^* was plotted against time. (Graphs 4G and 5G).

5.5 Stress concentrations:

The stress photographs for tests 5 to 7 show clearly the existence of a stress concentration, on the boundary as well as internally. Unlike the stress concentrations caused by tractions or body forces under isothermal conditions, these "thermal stress concentrations" are not always constant, nor are they a function only of the geometry of the stressed component (Graphs 4F and 5F). There is also no "mean Stress" in terms of which the stress concentration can be expressed. A logical ratio to use is, however, a comparison between the highest stress in the region of the radius and the stresses ruling in those parts of the model which are undisturbed by the change in geometry. Thus the instantaneous maximum boundary stress in the radius is compared to the instantaneous boundary stresses far removed from it. Similarly the highest internal shear stress

in the region of the radius is compared to the internal stresses far removed from the disturbance. The ratios are then plotted as "thermal stress concentrations", which may be used as reliable guides in the design of components subjected to similar thermal loads.

5.6 Interpretation of photographic records:

The complete record of each test is contained on two matched photographic sequences each comprising from 20 to 38 negatives. These are "read" by direct viewing through a microfile reader or 35mm projector. Because of the difficulties introduced by the uneven illumination of the model (see section 4.9 p66), and the processing techniques used to correct them, the negatives most suitable for direct reading are so dark in certain critical areas that the detail which they contain is not readily reproduced on a positive photographic print. The prints presented on the following pages are therefore only meant to show how the stress patterns developed with time. They are not a full record of the test, nor are they meant to contain sufficient detail for accurate reading in areas where the stress gradient is steep.

On some negatives the position of the zero order fringe can be seen quite easily but not so on others. In the latter cases the complete stress profile has to be plotted on graph paper so that the position of the zero order fringe can be found by balancing the "positive" and "negative" areas under the curve. The intersection of the stress curve and the"zero line" must obviously coinside with the position of a full order fringe. This method constitutes a very valuable check on the extrapolations for the boundary and internal stresses, where such extrapolations were necessary; It also shows up any errors in the stress distribution during the very early stages of a test when the behaviour of the stress pattern, at the boundary opposite to the one which experiences the temperature

change, is not at all obvious. The presence and effects of residual stresses in the model are also clearly shown.

Whenever there was uncertainty about the exact fringe count at a point under study, the range of probability was plotted on the graph paper. In some frames the range may be wide (as much as one full fringe) whilst in other subsequent frames the count may be very exact. In this way a series of dots and bars of varying length is developed through which a representative mean curve can be drawn, with a large degree of confidence. These are the curves presented in graphs D and E for each of the tests. Unless otherwise stated they may be taken as representative of the true stresses in the model within a tolerance of 0.5 fringe for the boundary stresses and 0.2 fringe for the internal stresses.

The time from the start of each test is plotted on a log scale. In this way the earlier events, when changes occur rapidly, are expanded, and the later events, when conditions change very slowly are compressed. The rapid movement of the densely spaced fringes near the boundaries, during the first 20 to 40 seconds of a test, leaves only a blurred area on the photographic negative. It is not then possible to read the boundary stresses with any degree of accuracy. This study is, however, not concerned with these early conditions of "thermal shock", so that the results of very early frames are not presented in the graphs. There is, of course, no reason why, with improved illumination these regions can not be included in studies using the same techniques.

5.7 Results and Graphs:

In the following pages the results of the tests are presented in sequence. Each set of graphs is then discussed briefly. An overall discussion is given in section 5.9.

Test 1(Model A): Plate initially at uniform$_a$ Temperature cooled symmetrically on both sides.

FIG. 19.

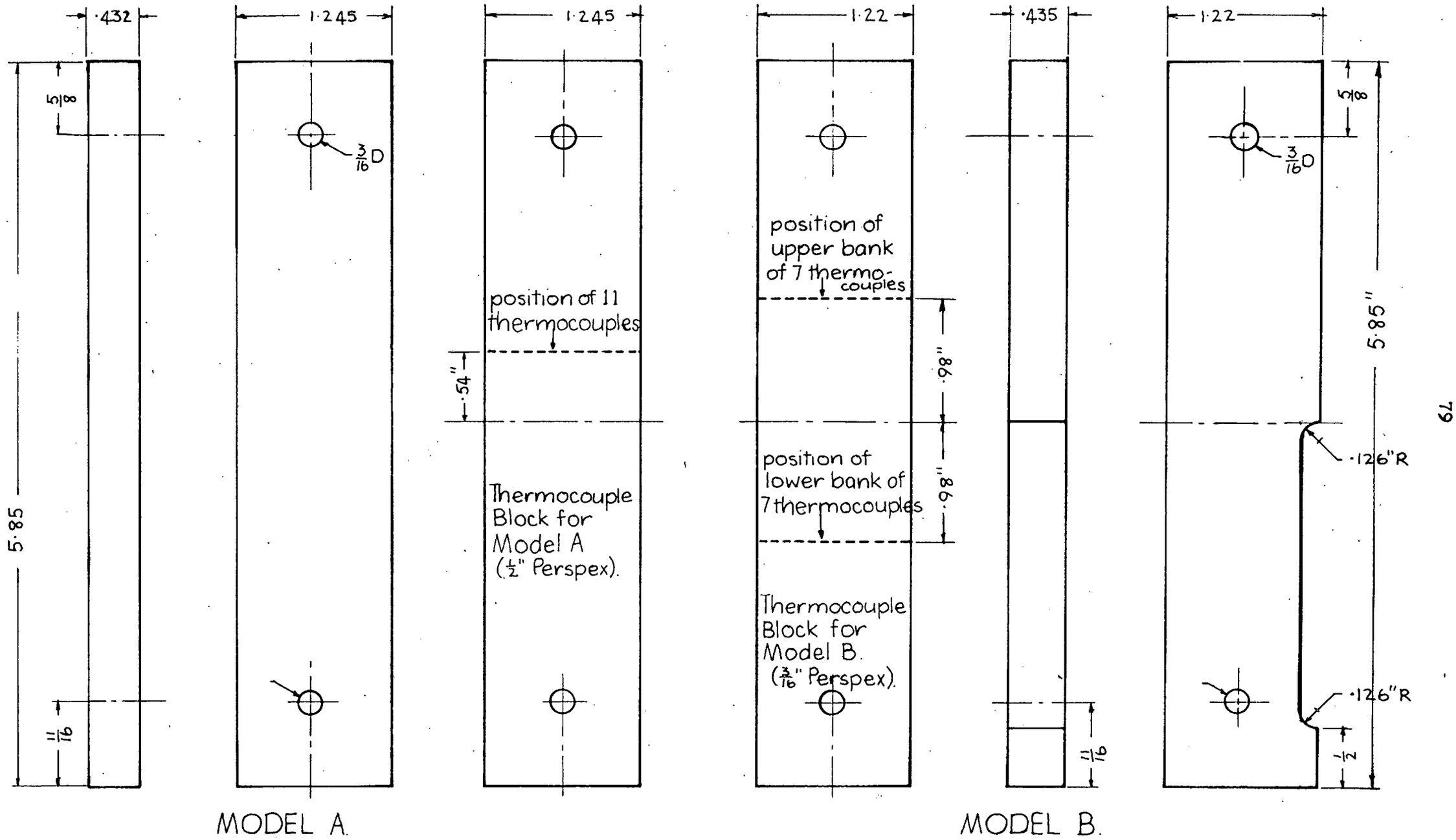
·432
1·245
1·245
1·22
·435
1·22
5/8
3/16 D
position of 11 thermocouples
·54"
Thermocouple Block for Model A (½" Perspex).
position of upper bank of 7 thermo-couples
·98"
position of lower bank of 7 thermocouples
·98"
Thermocouple Block for Model B. (3/16" Perspex).
5·85
11/16
5·85"
·126"R
·126"R
½
MODEL A.
MODEL B.

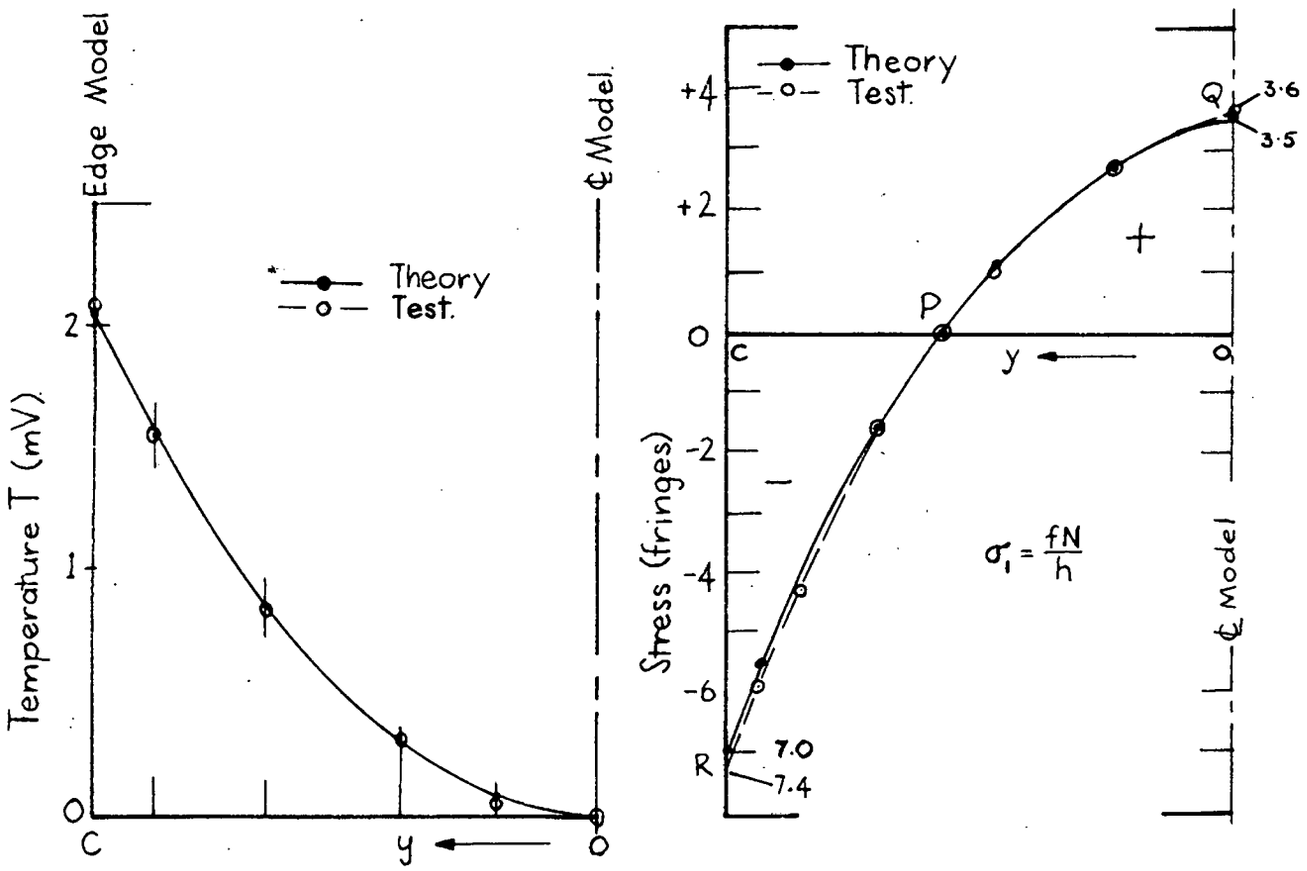

FIG. 20: Correlation with theory, (Equations 8 and 9, page 17) for model with Perspex end pieces and Araldite thermocouple block.

Error: Point P for position of zero order fringe 2%
Point Q for stress at centre of model 2·9%
Point R for stress at boundary of model 5·7%
(extrapolated to edge)

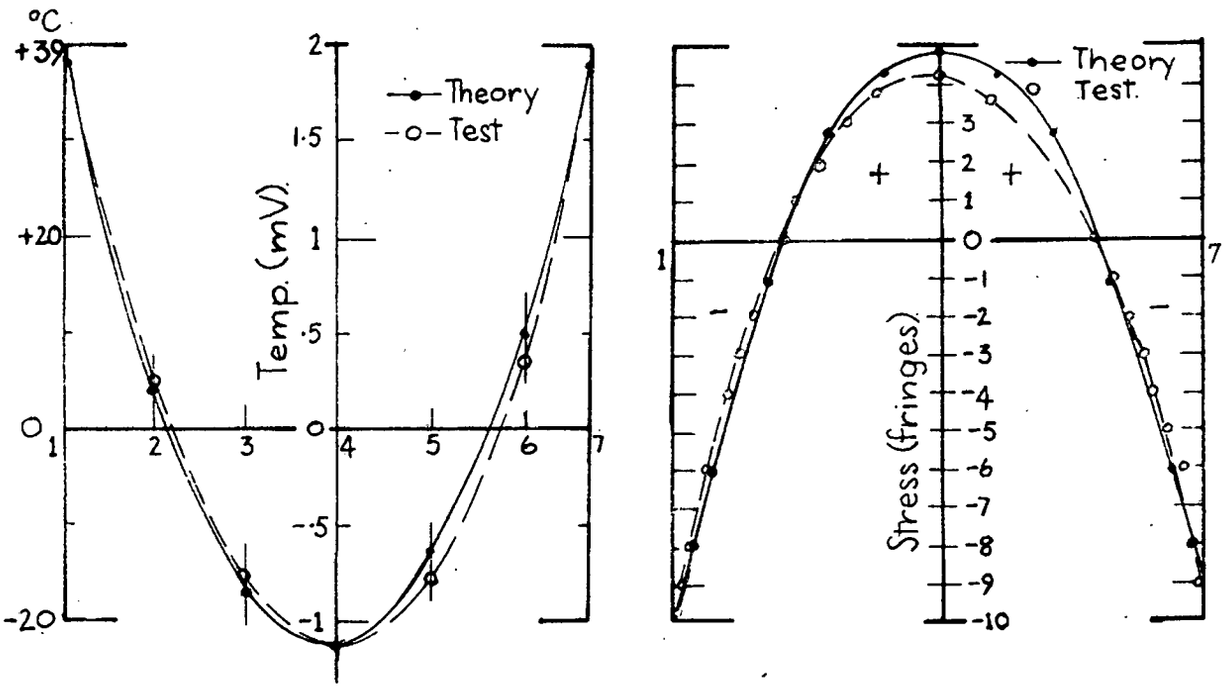

FIG. 21: Correlation with theory (Equations 8 and 14) for Test № 4, 3 minutes after start, on the section below the radius.

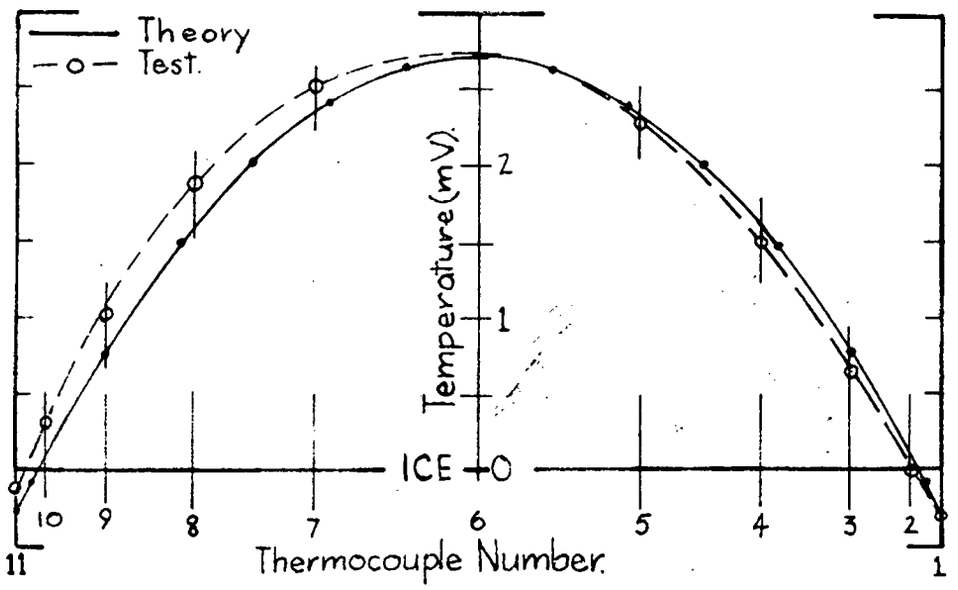

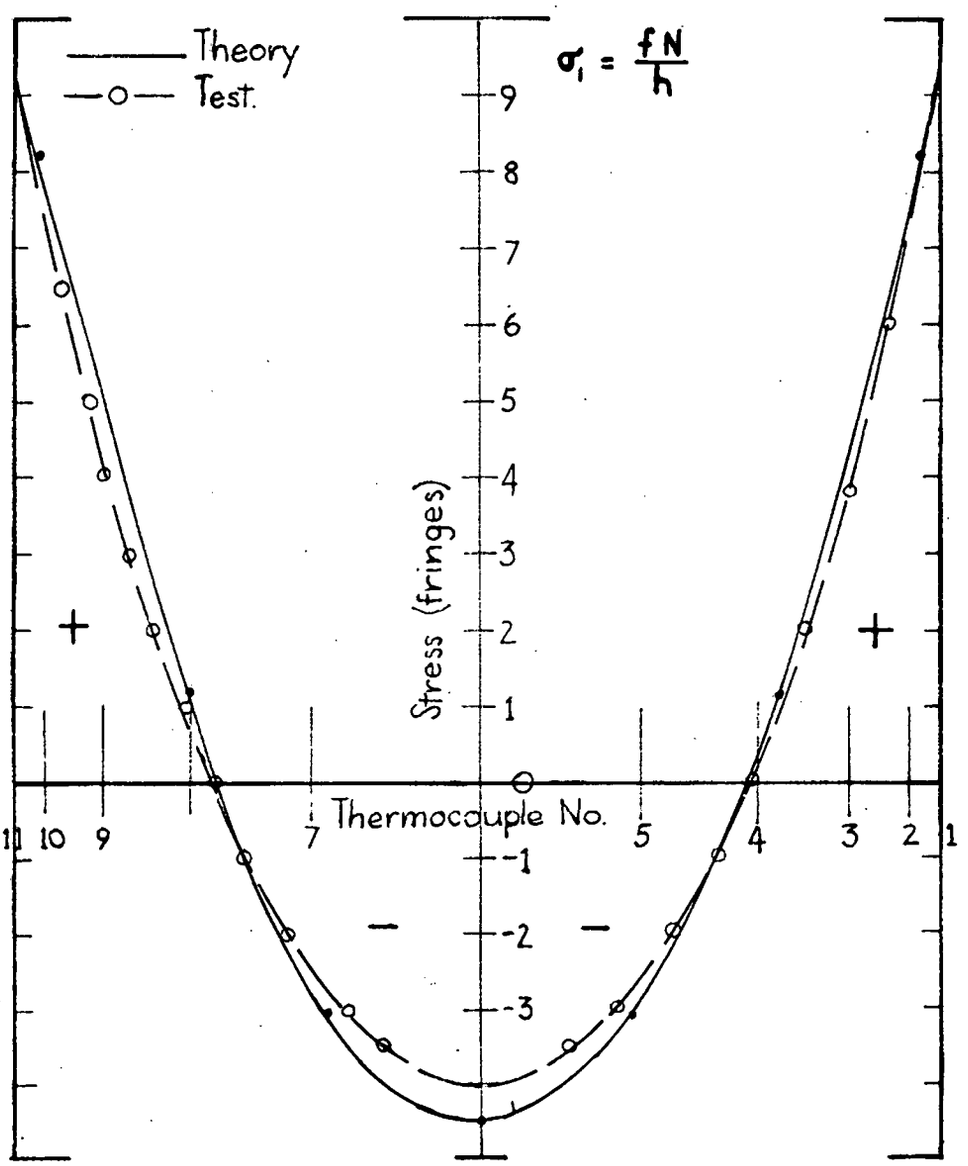

FIG. 22: Correlation with theory (Equation 8, page 17 and Eq. 14 page). for Test Nº 1, 5 min 5 sec. after start.

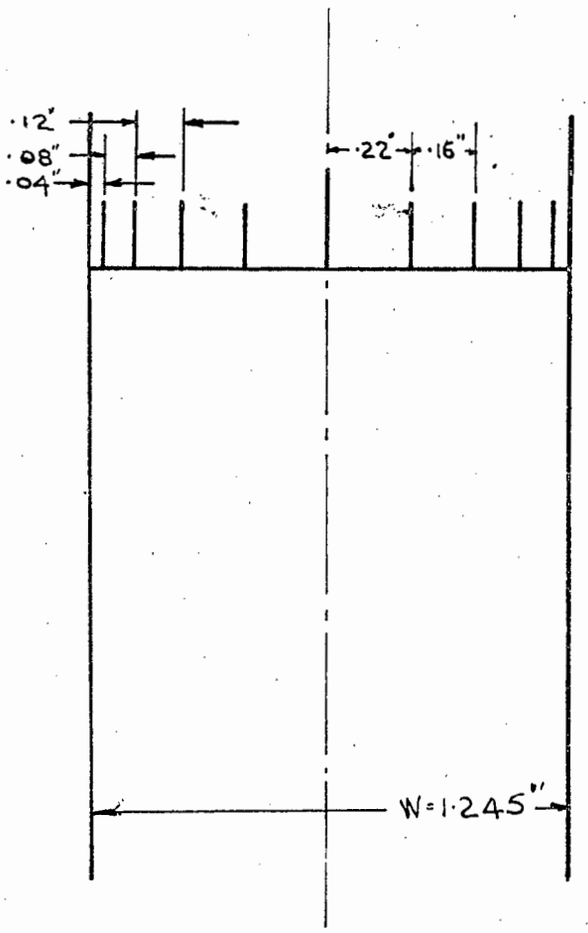

MODEL A
TESTS 1, 2, 3.

NOTATION.

σ	= normal stress	Subscripts.	
τ	= shear stress	1 to 11	indicates points across the width of the model.
W	= model width		
N	= fringe count	i =	internal
σ_m	= model stress	o =	starting condition at time zero
σ_{st}	= equivalent stress in steel.	f =	final condition at end of test.

Examples: T_{o11} = Starting temperature at side 11.

T_6 = Instantaneous temperature at point 6 in the model.

T_{min} = Lowest temperature inside the model at the time of observation.

TEST Nº1

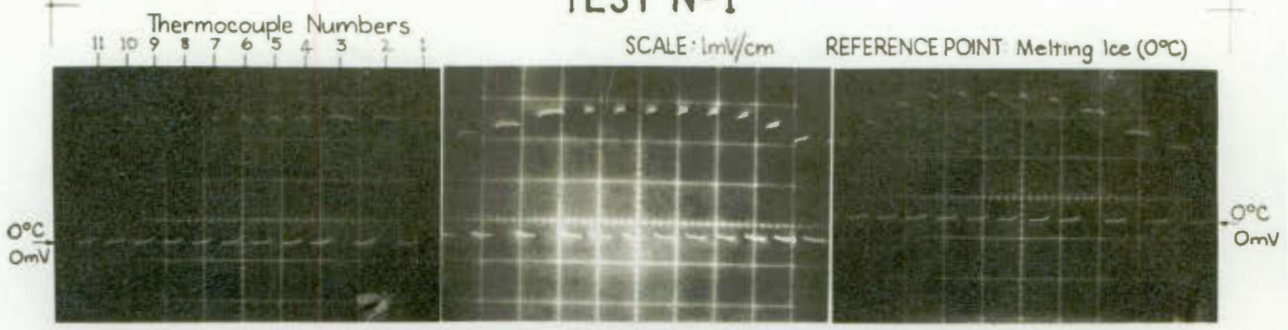
Thermocouple Numbers
11 10 9 8 7 6 5 4 3 2 1
SCALE: 1mV/cm
REFERENCE POINT Melting Ice (0°C)
0°C
0mV
0°C
0mV

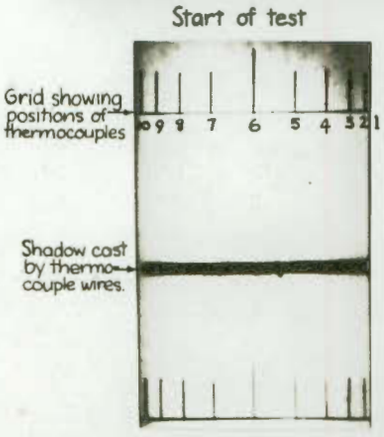
Start of test
Grid showing positions of thermocouples
10 9 8 7 6 5 4 3 2 1
Shadow cast by thermo-couple wires.

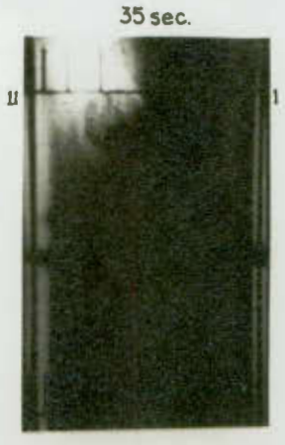
35 sec.
11
1

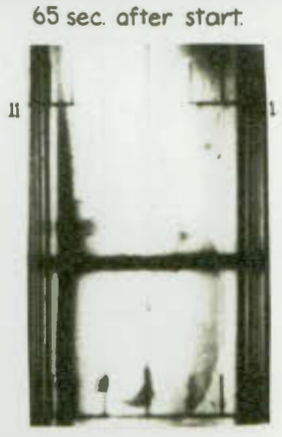
65 sec. after start.
11
1

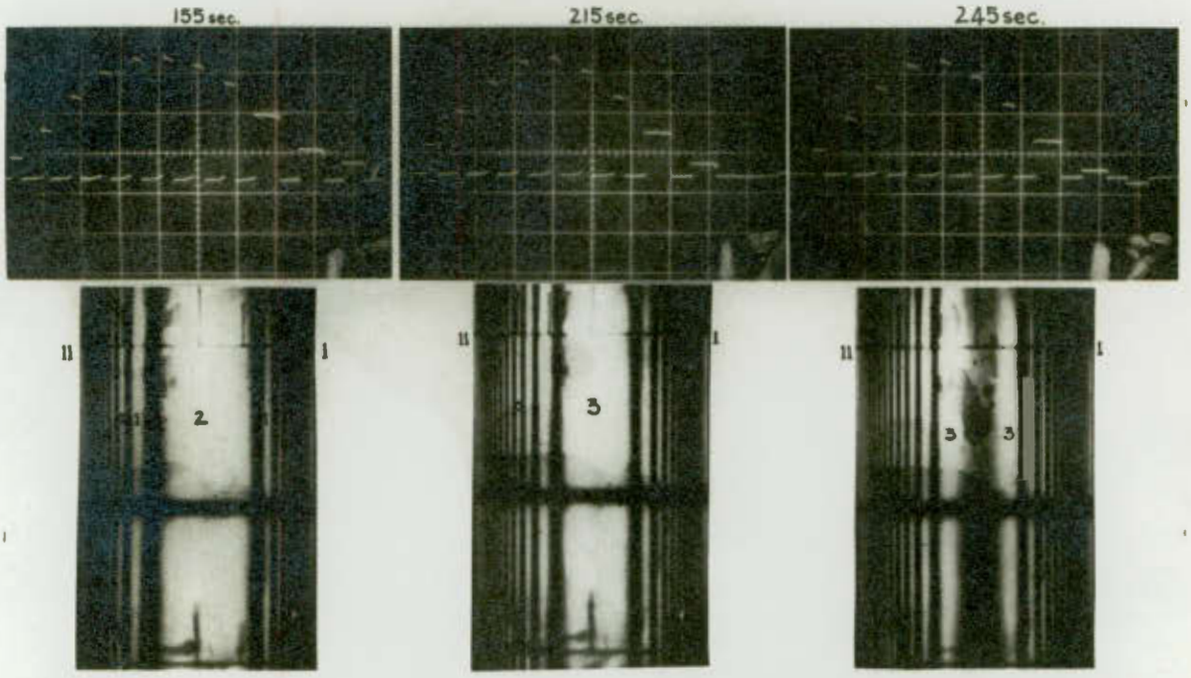
155 sec.
215 sec.
245 sec.
11
1
2
3
3 3

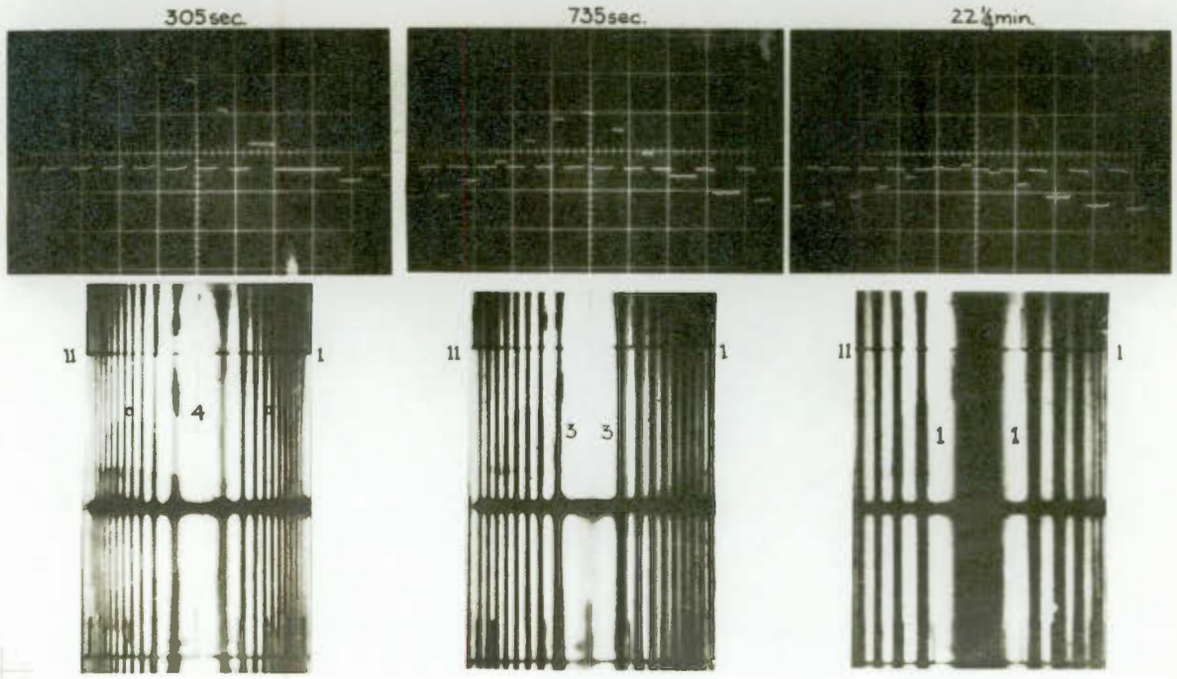
305 sec.
735 sec.
22½ min.
11
1
4
3 3
1 1

TEST Nº 1

NOTATION: page 82.

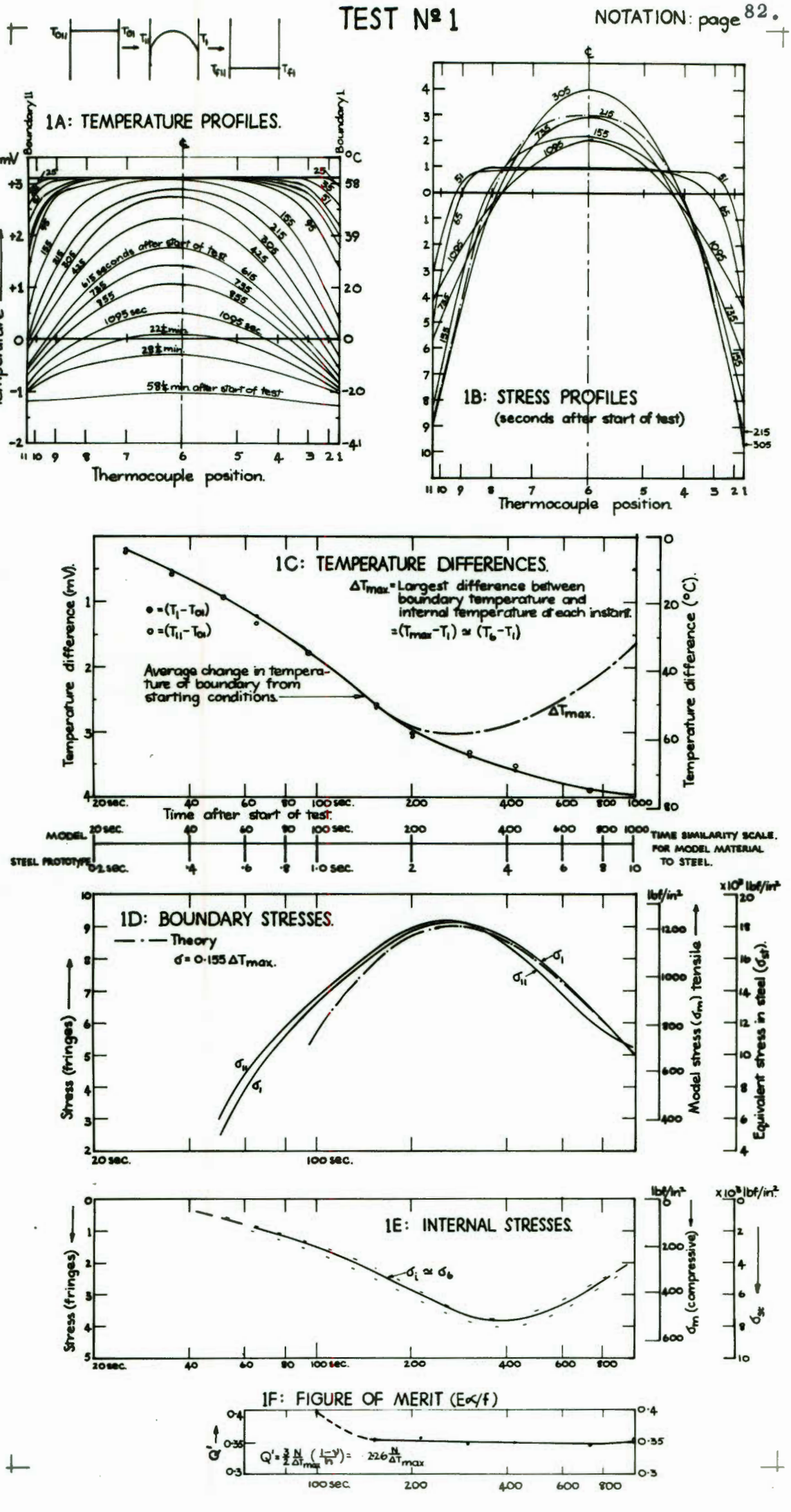

TEST Nº 2

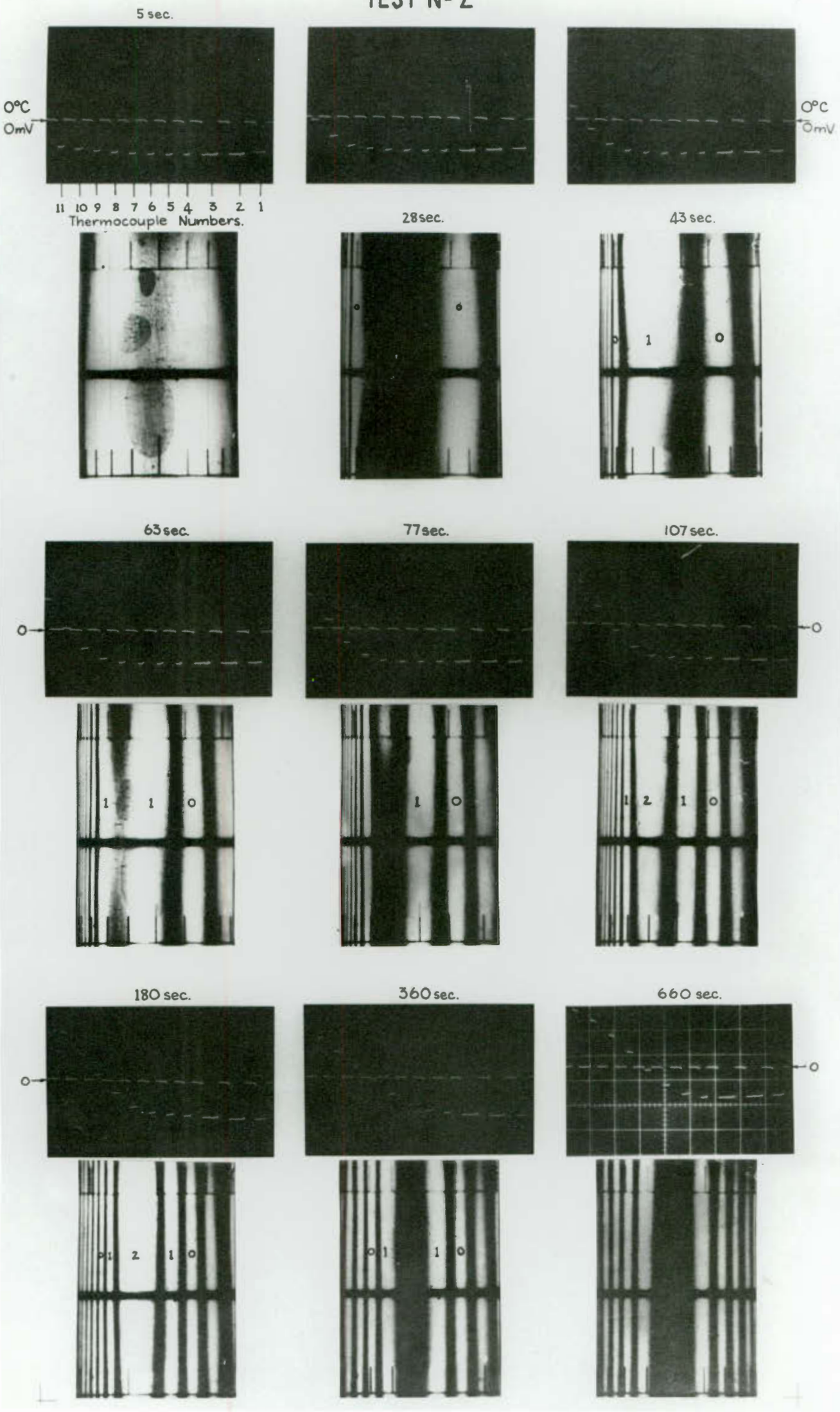
5 sec.
0°C
0mV
11 10 9 8 7 6 5 4 3 2 1
Thermocouple Numbers.
0°C
0mV
28 sec.
43 sec.
63 sec.
77 sec.
107 sec.
180 sec.
360 sec.
660 sec.

TEST Nº2

NOTATION: page 82.

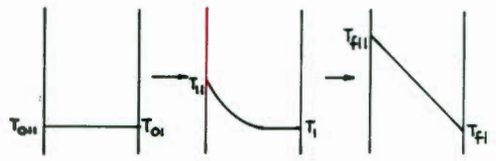

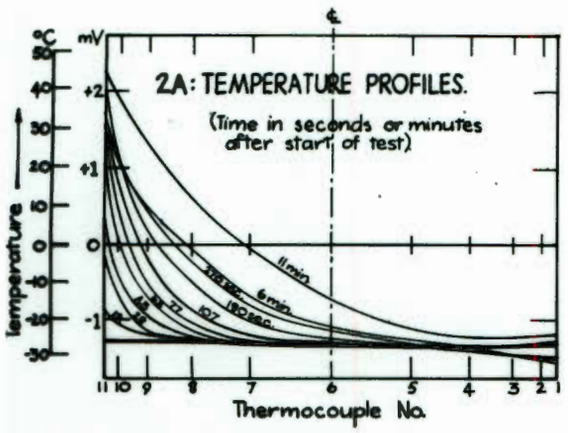

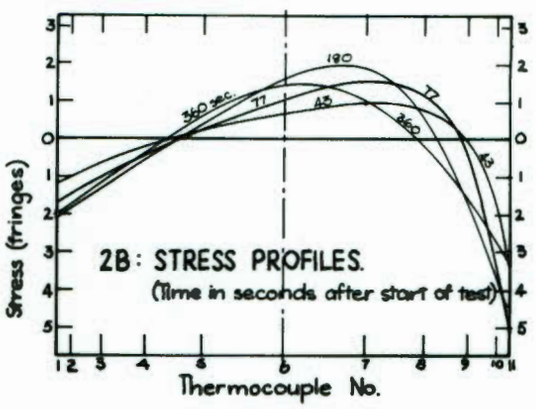

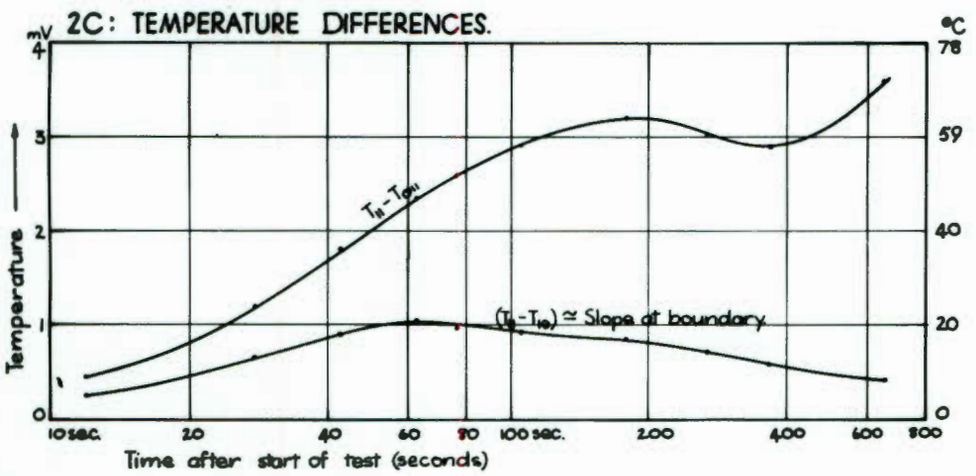

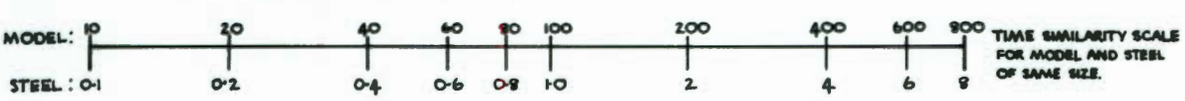

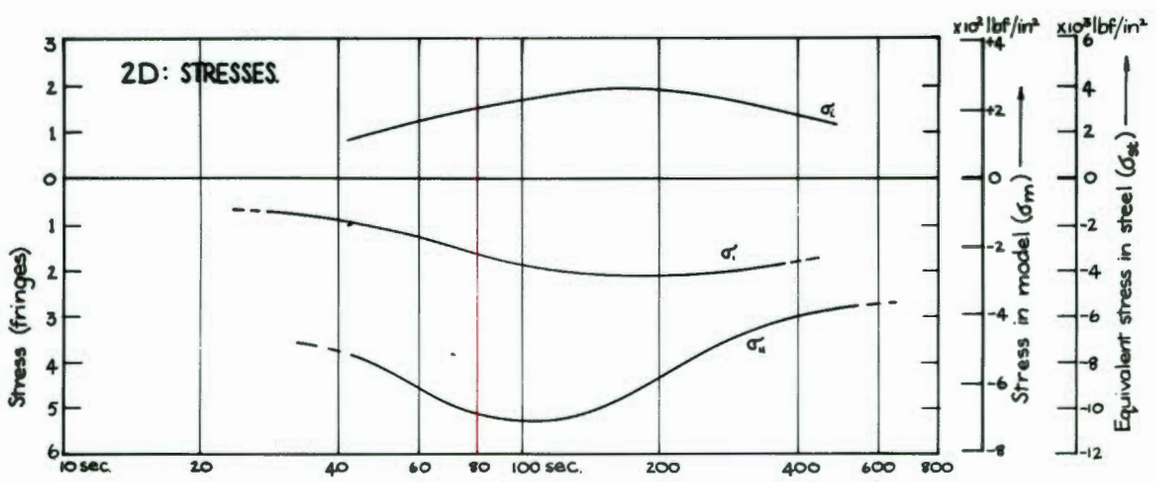

TEST Nº 3

THERMOCOUPLES : Iron/Constantan.
SCALE: 1mV/cm. REFERENCE: Melting Ice (0°C)

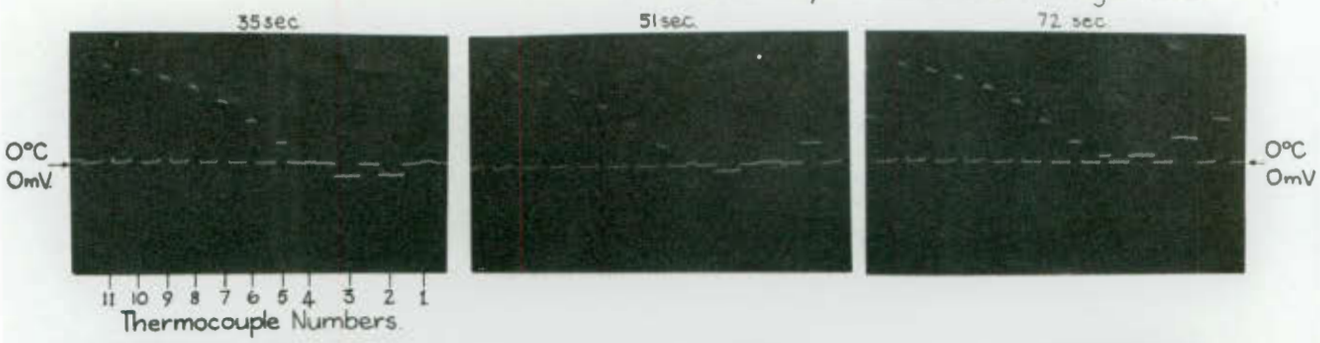

Grid showing positions of thermocouples.

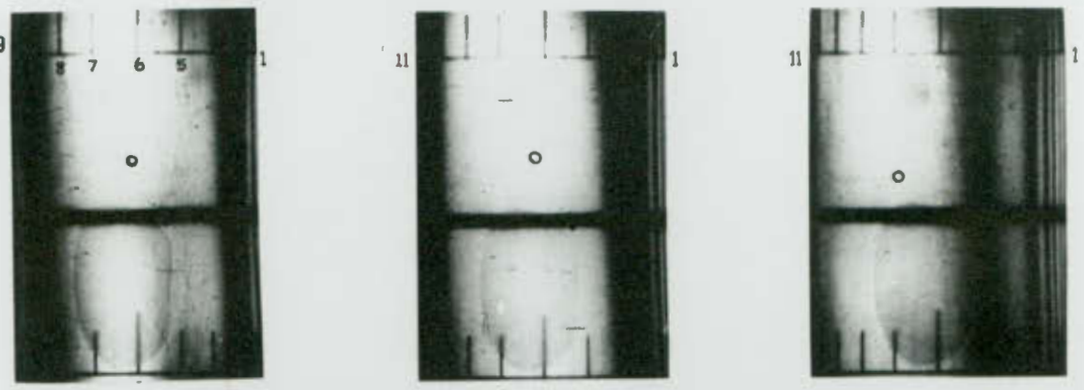

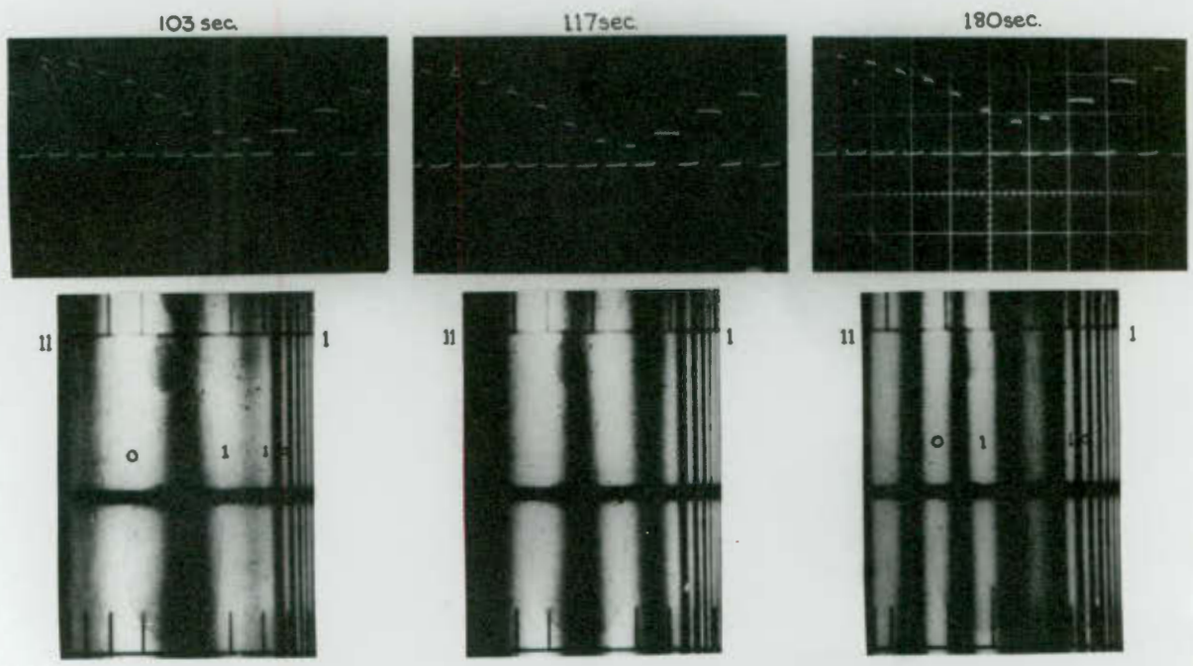

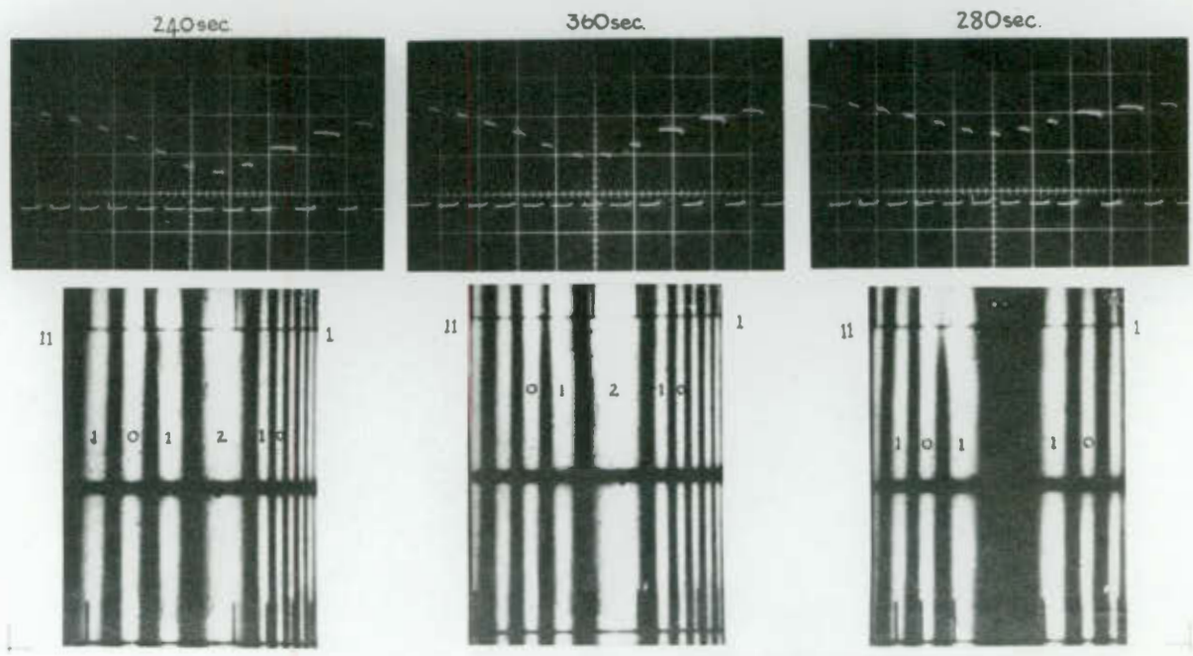

TEST Nº 3.

NOTATION: page 82.

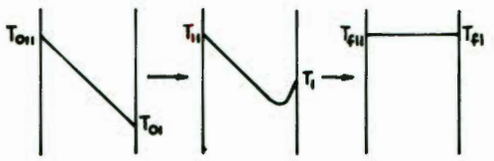

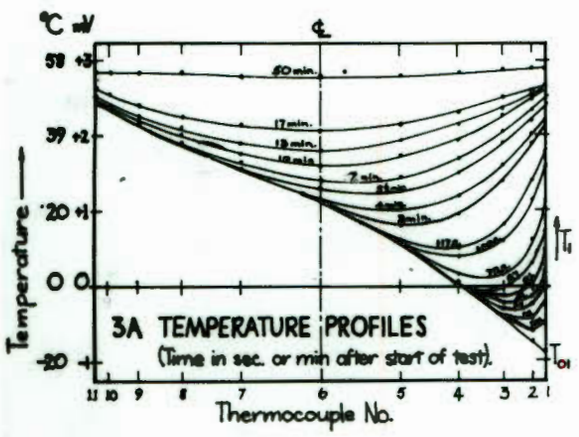

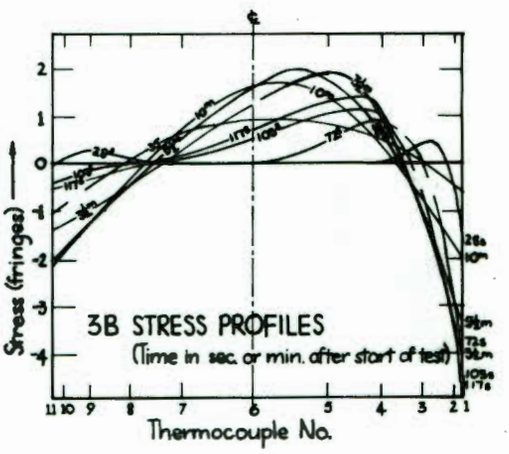

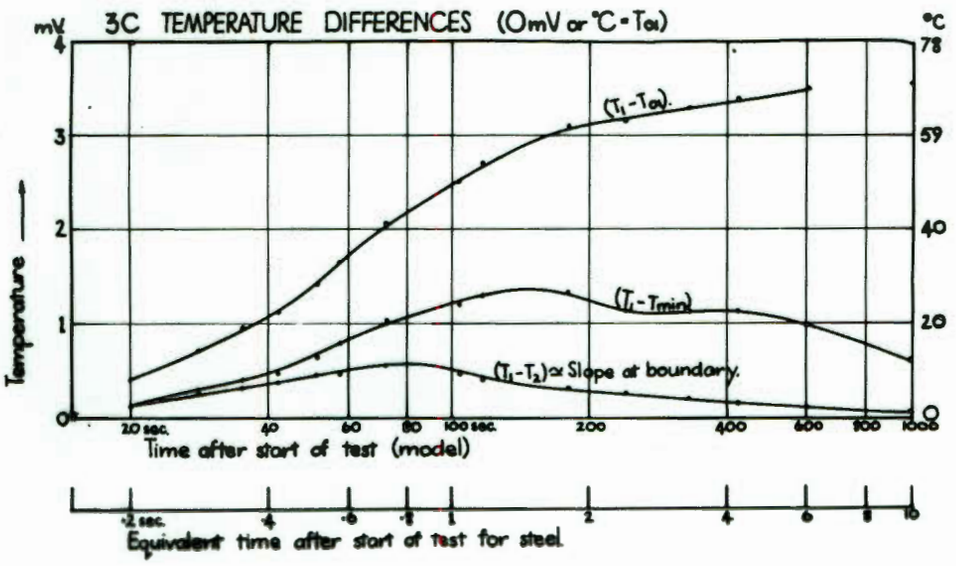

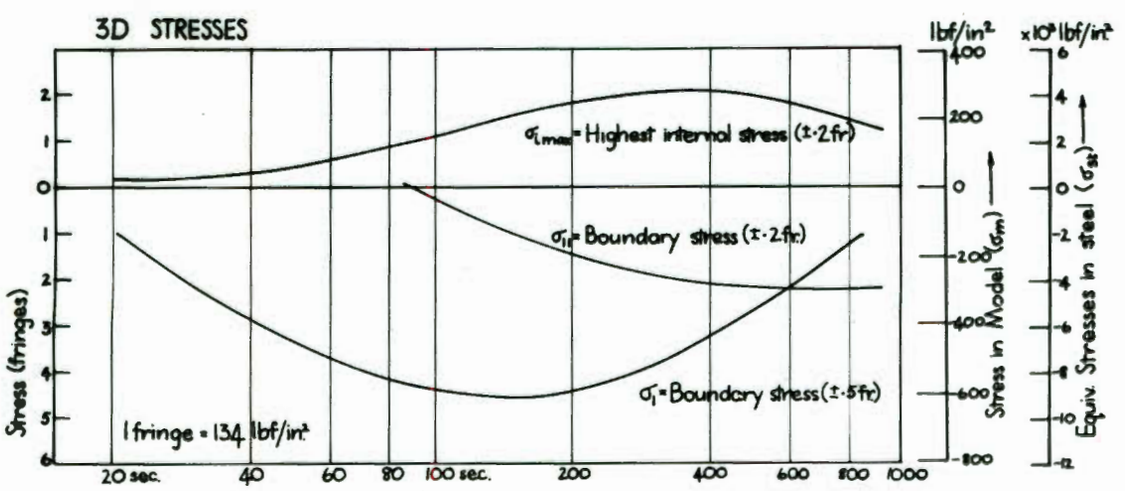

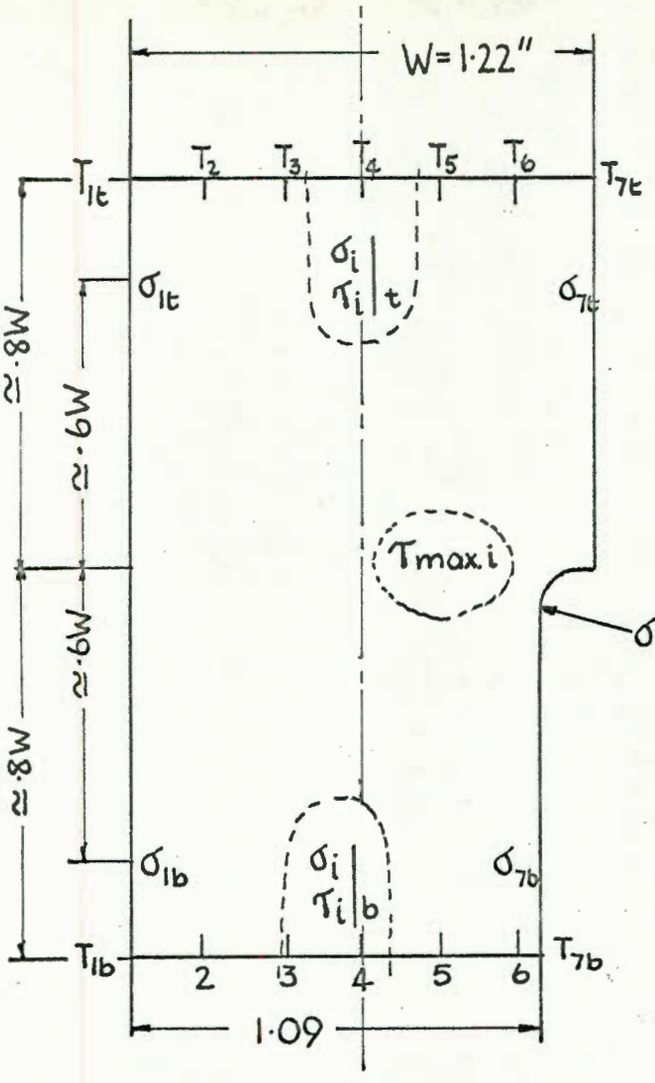

MODEL B.
TESTS 4,5,6,7.

NOTATION.

σ = Normal Stress
τ = Shear Stress
W = Model width
N = Fringe Count.
K = Stress concentrations factor.
σ_m = Model Stress
σ_{st} = Equivalent stress in steel prototype
σ_{max} = Highest boundary stress at radius
τ_{max} = Highest shear stress in region of radius.

Subscripts.

1-7 indicate points across width of model.
t indicates points above the radius in areas undisturbed by stress concentration ($\pm \simeq 0.6$ to .8W)
b is the same but below the radius.
i = internal
n = at radius or "notch".
o = starting condition at time zero.
m = model
st = Equiv. steel prototype

Examples: T_{o7} = Starting temperature at side 7.
T_{7t} = Temperature at side 7, 0.8W above radius.
τ_{ib} = highest shear stress inside model 0.6W below radius (i.e. in region undisturbed by the change in section).
σ_{it} = highest normal stress 0.6W above radius.
T_{min} = lowest temperature inside model at time of observation.

TEST 4. 4A: TEMPERATURE PROFILES.

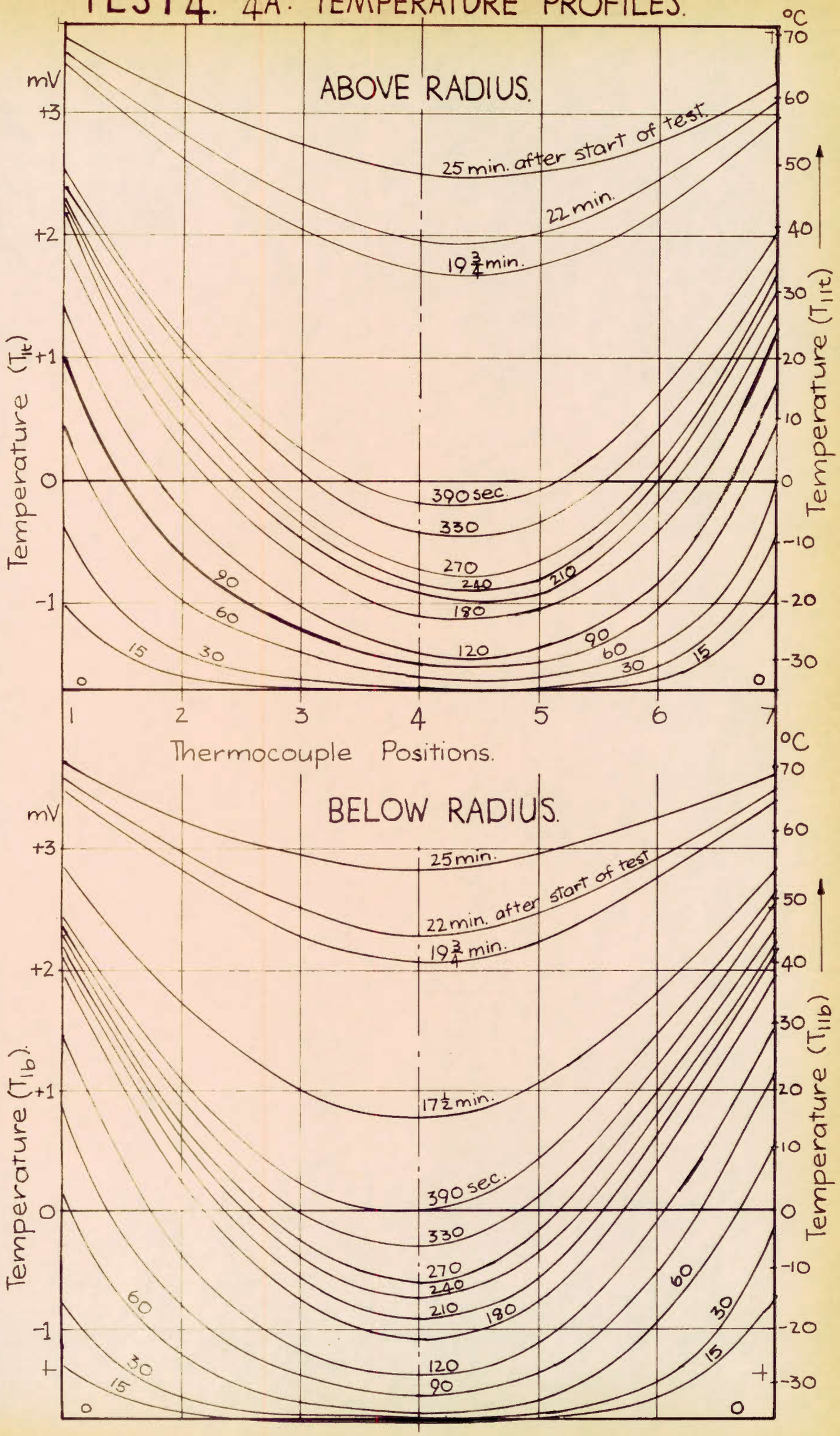

TEST Nº 4.

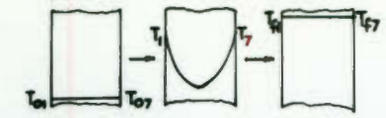

NOTATION: page 89.

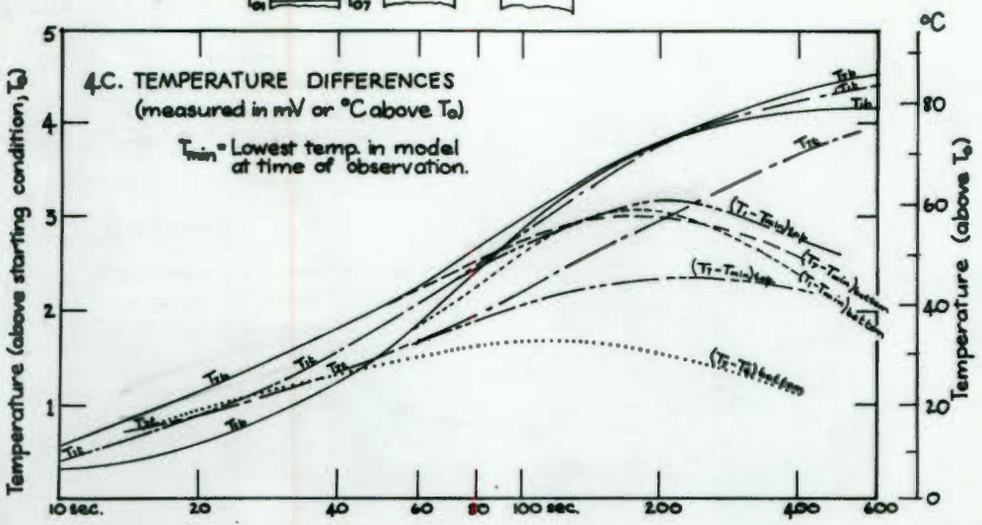

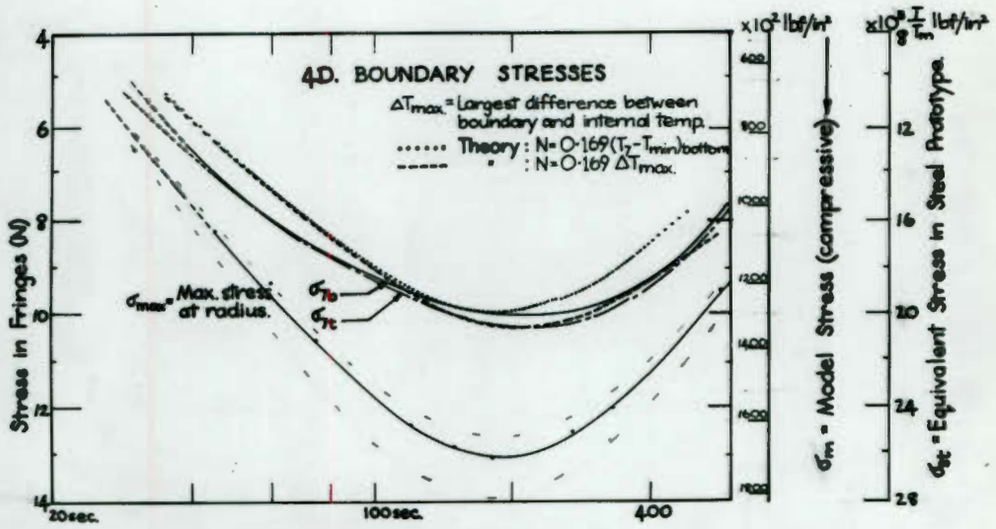

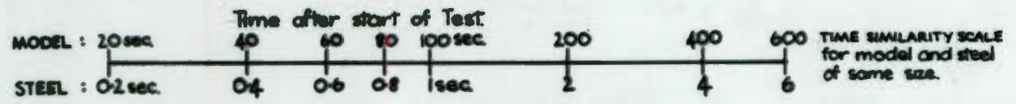

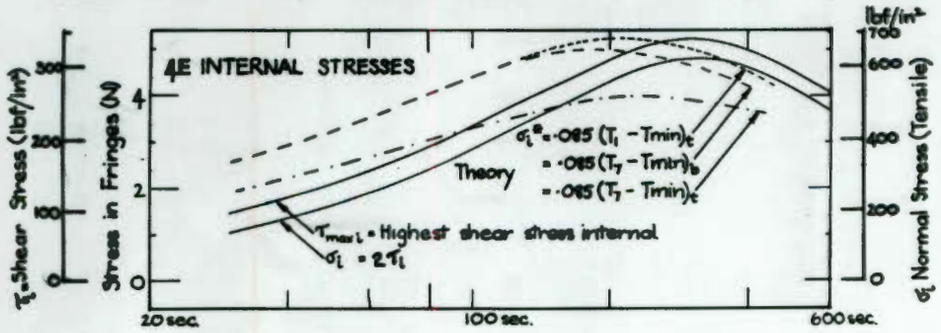

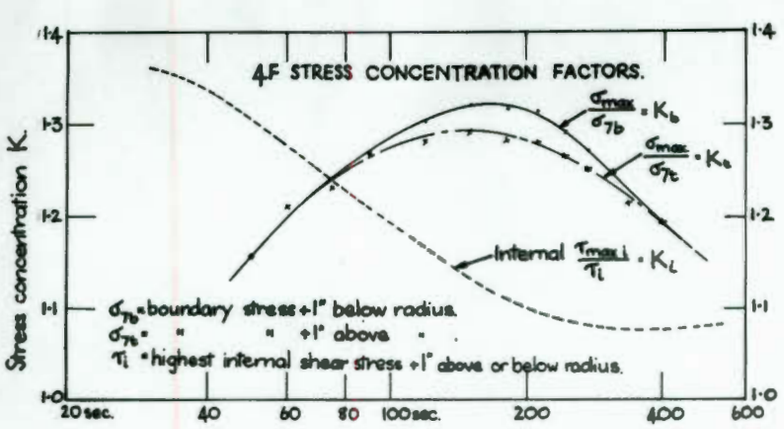

4G: DIMENSIONLESS STRESSES.

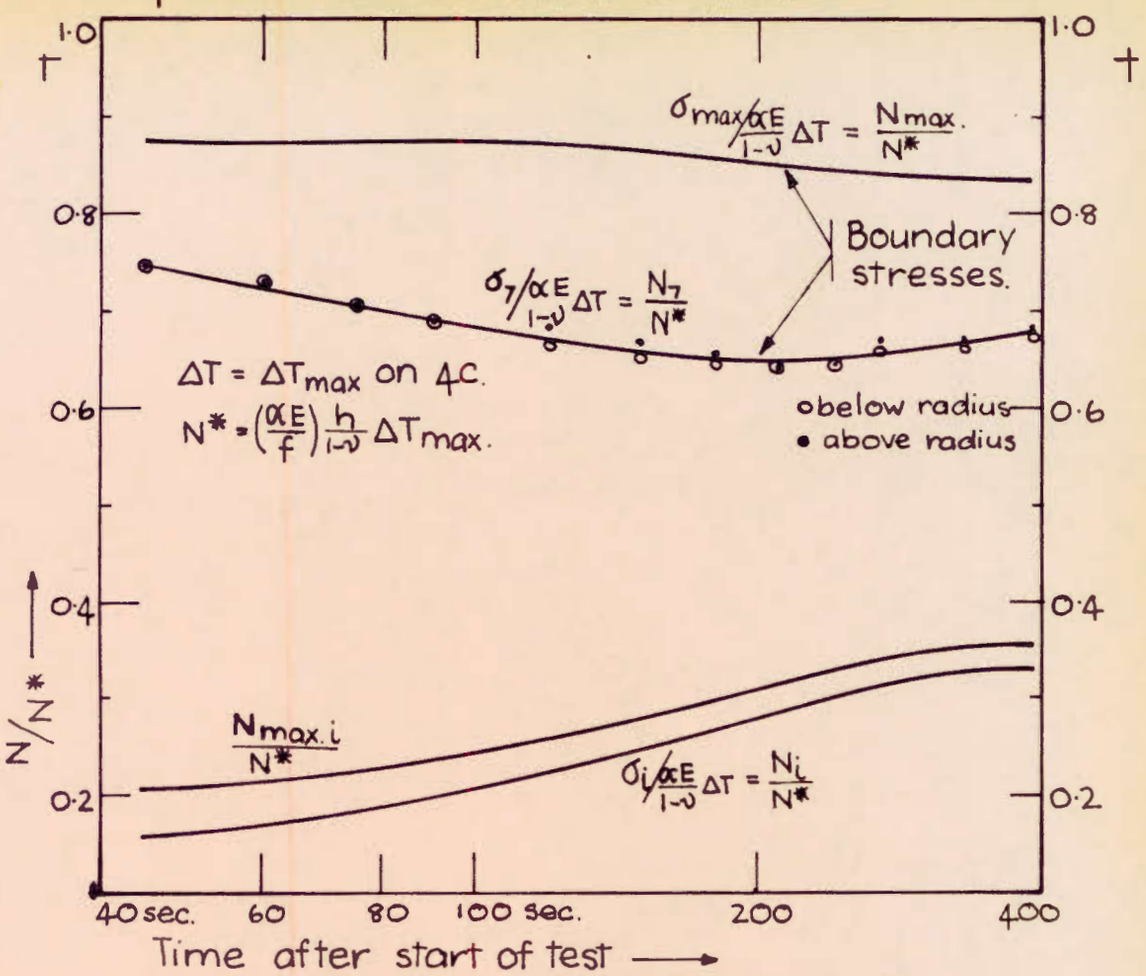

4H: FIGURE OF MERIT ($E\alpha/f$).

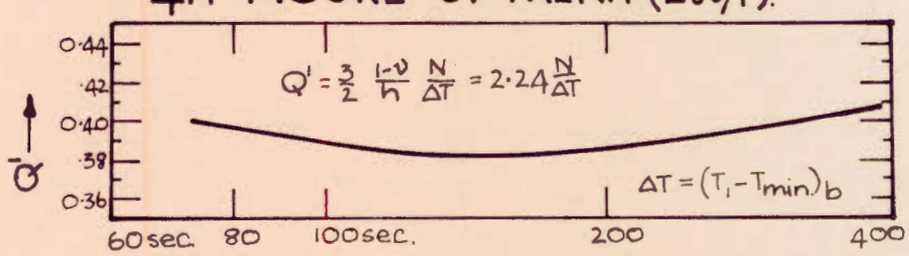

4J: STRESS vs. TEMPERATURE

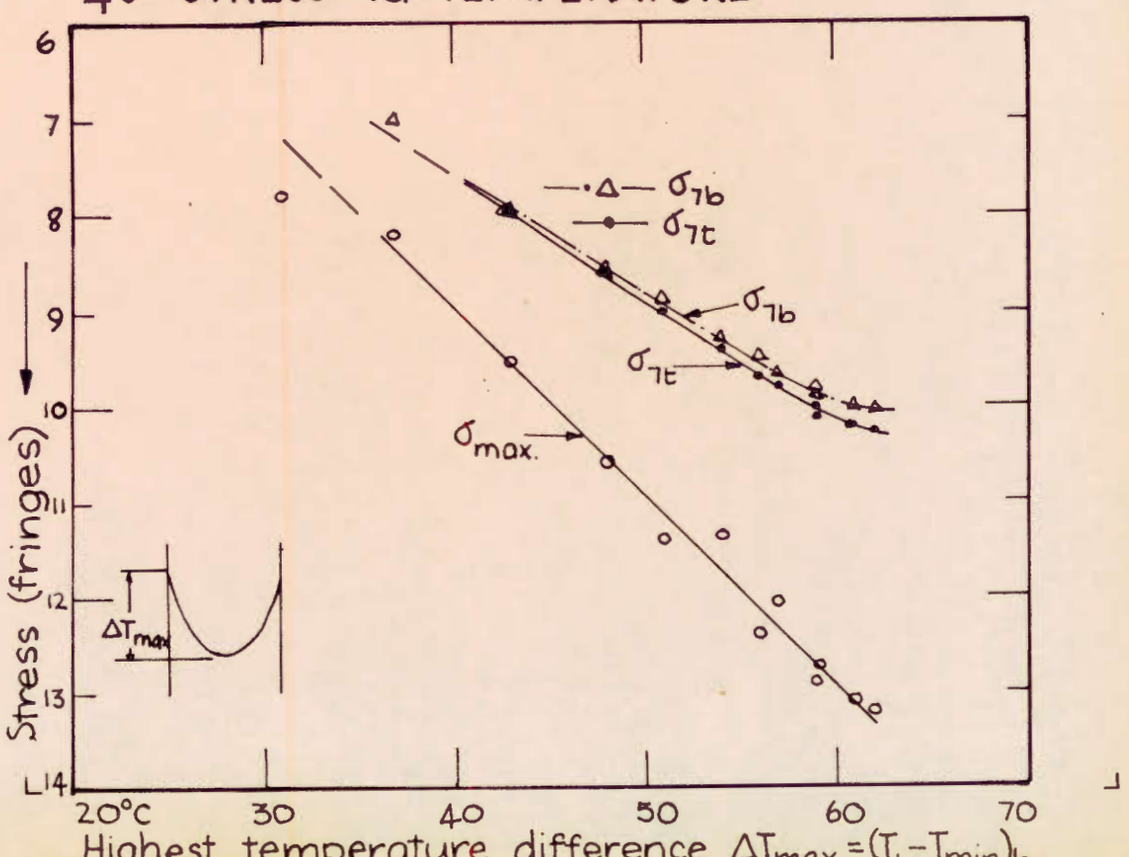

Time in seconds after start of test.

TEST 5

Above radius Below radius.

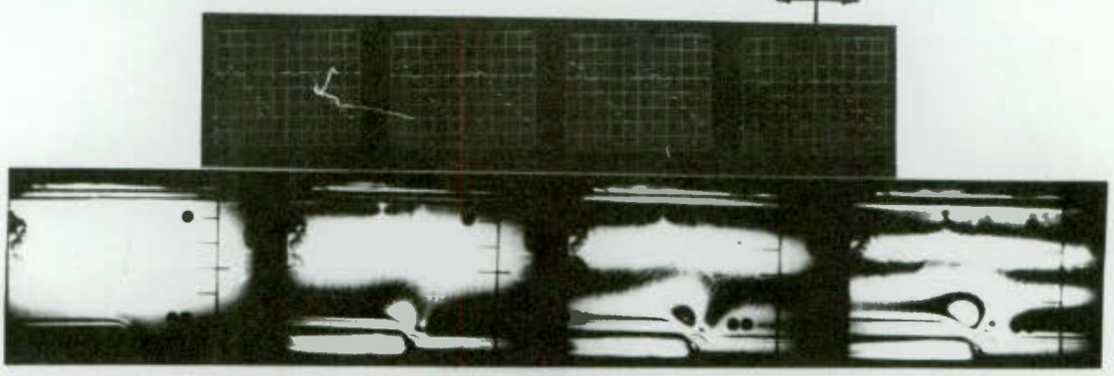

2 5 15 30

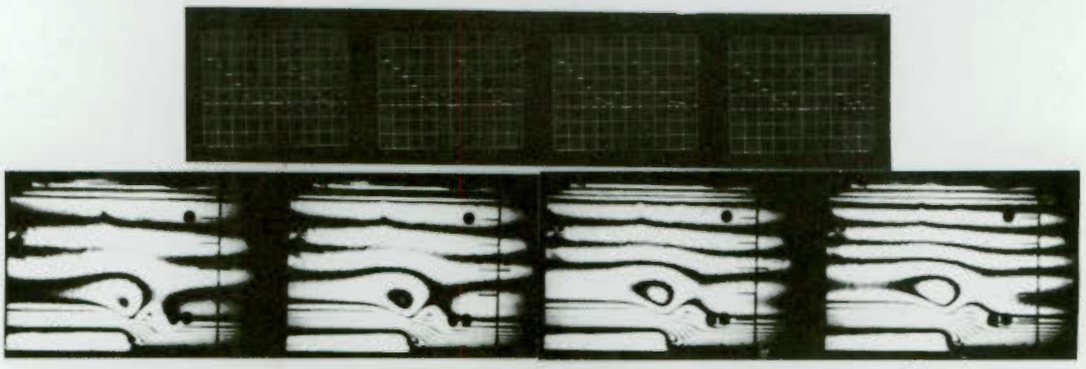

45 60 75 90

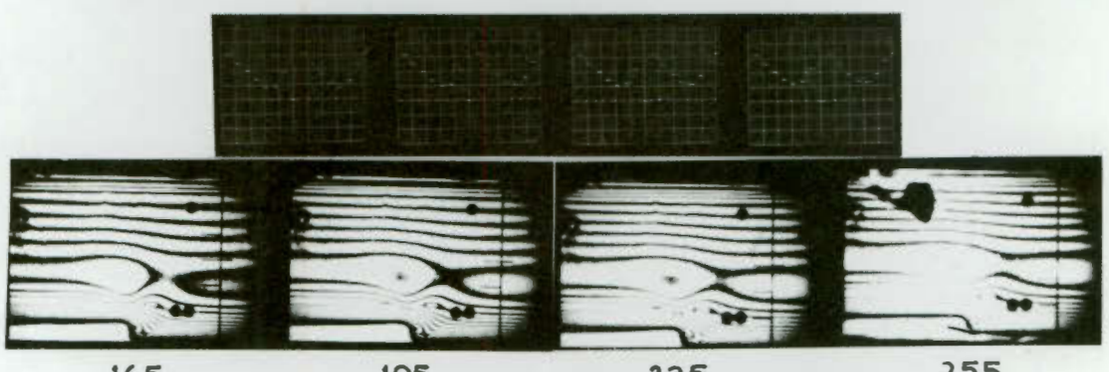

165 195 225 255

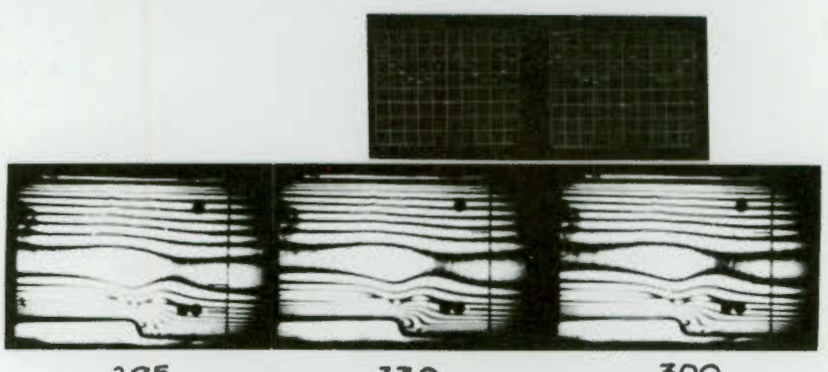

285 330 390

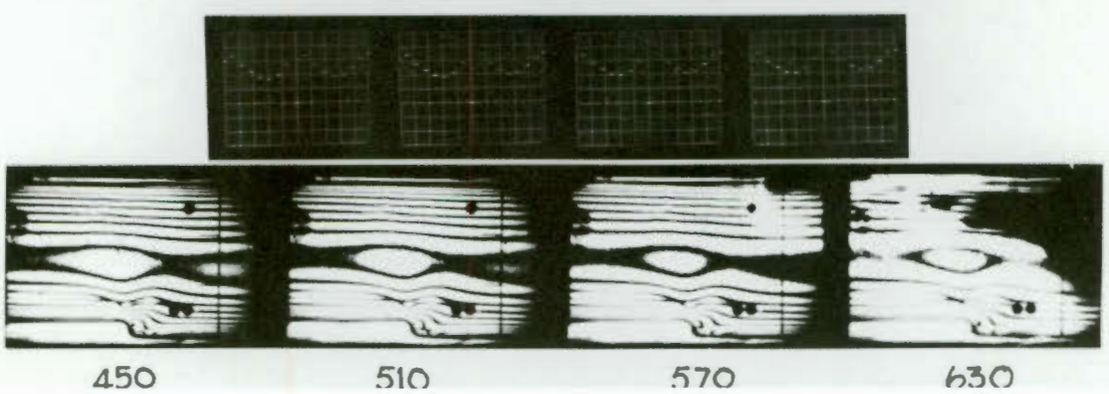

450 510 570 630

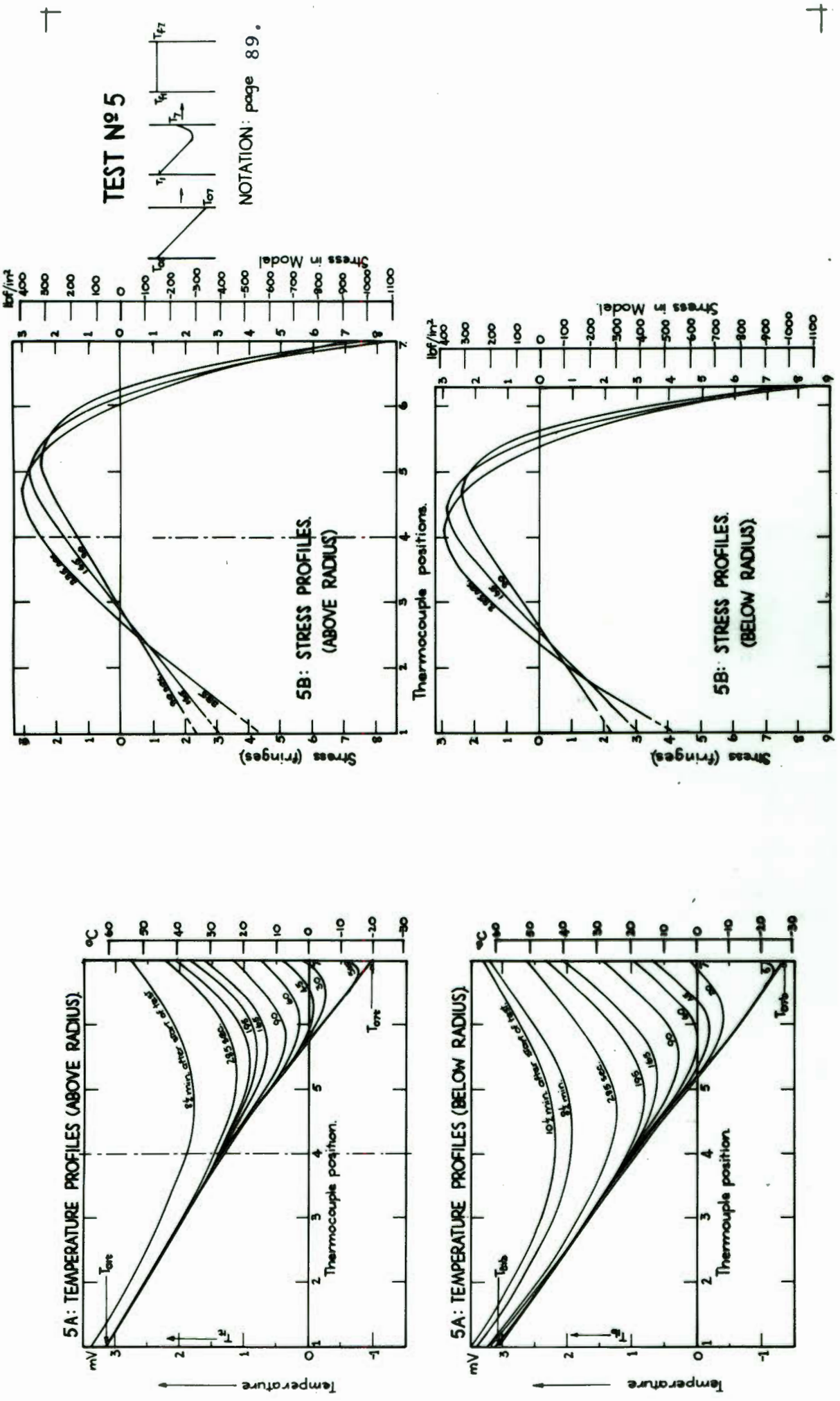
TEST Nº 5
NOTATION: page 89.
5B: STRESS PROFILES. (ABOVE RADIUS)
5B: STRESS PROFILES. (BELOW RADIUS)
Stress (fringes)
Stress in Model
Thermocouple positions.
5A: TEMPERATURE PROFILES (ABOVE RADIUS)
5A: TEMPERATURE PROFILES (BELOW RADIUS)
Temperature
Thermocouple position.

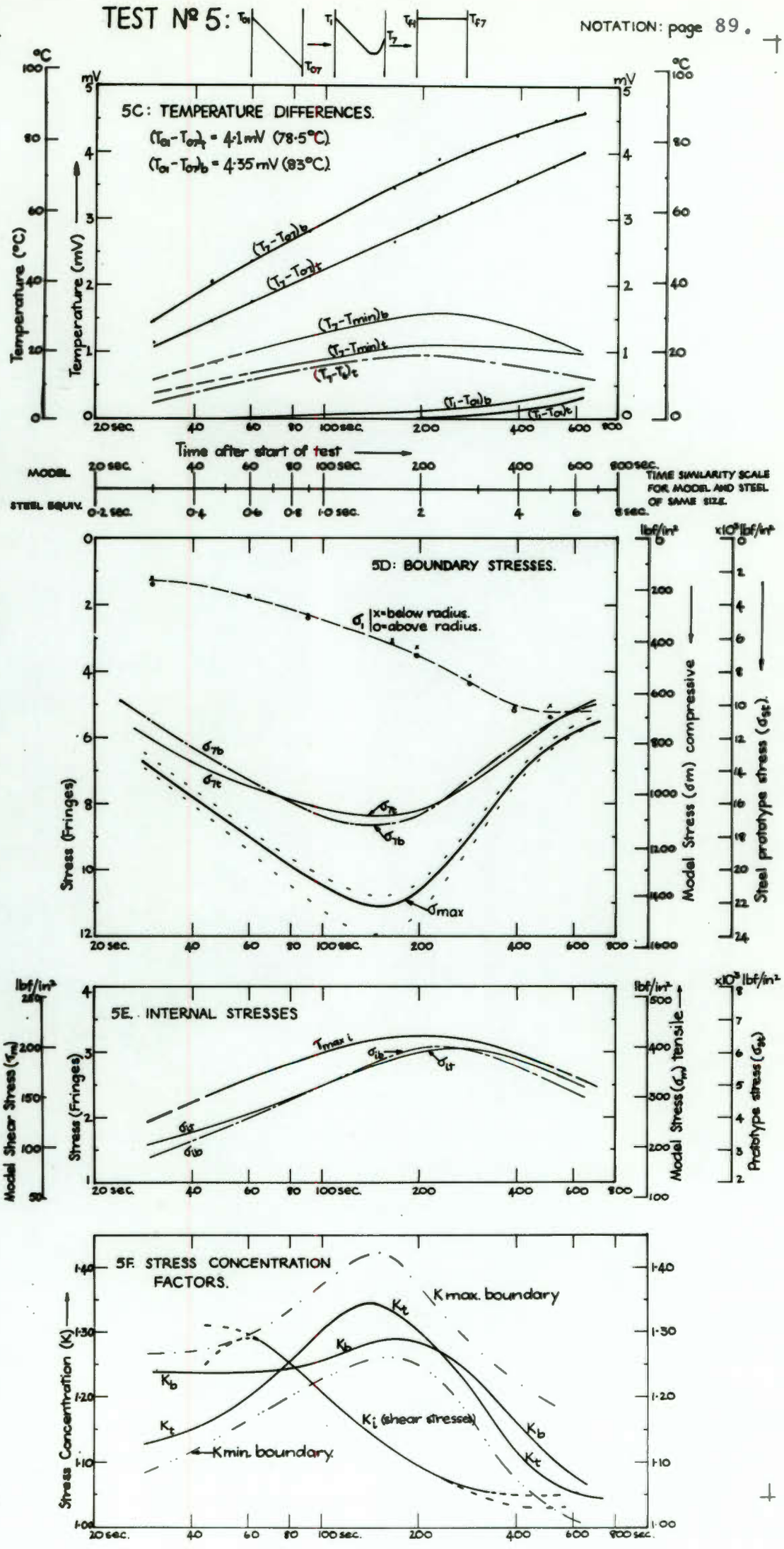
TEST Nº 5:
NOTATION: page 89.
5C: TEMPERATURE DIFFERENCES.
(T01 - T07)t = 4·1 mV (78·5°C)
(T01 - T07)b = 4·35 mV (83°C)
Temperature (°C)
Temperature (mV)
Time after start of test
MODEL
STEEL EQUIV.
TIME SIMILARITY SCALE FOR MODEL AND STEEL OF SAME SIZE.
5D: BOUNDARY STRESSES.
x=below radius.
o=above radius.
Stress (Fringes)
Model Stress (σm) compressive
Steel prototype stress (σst)
5E. INTERNAL STRESSES
Model Shear Stress (τm)
Model Stress (σm) tensile
Prototype stress (σst)
5F. STRESS CONCENTRATION FACTORS.
Kmax. boundary
Kmin. boundary
Ki (shear stresses)
Stress Concentration (K)

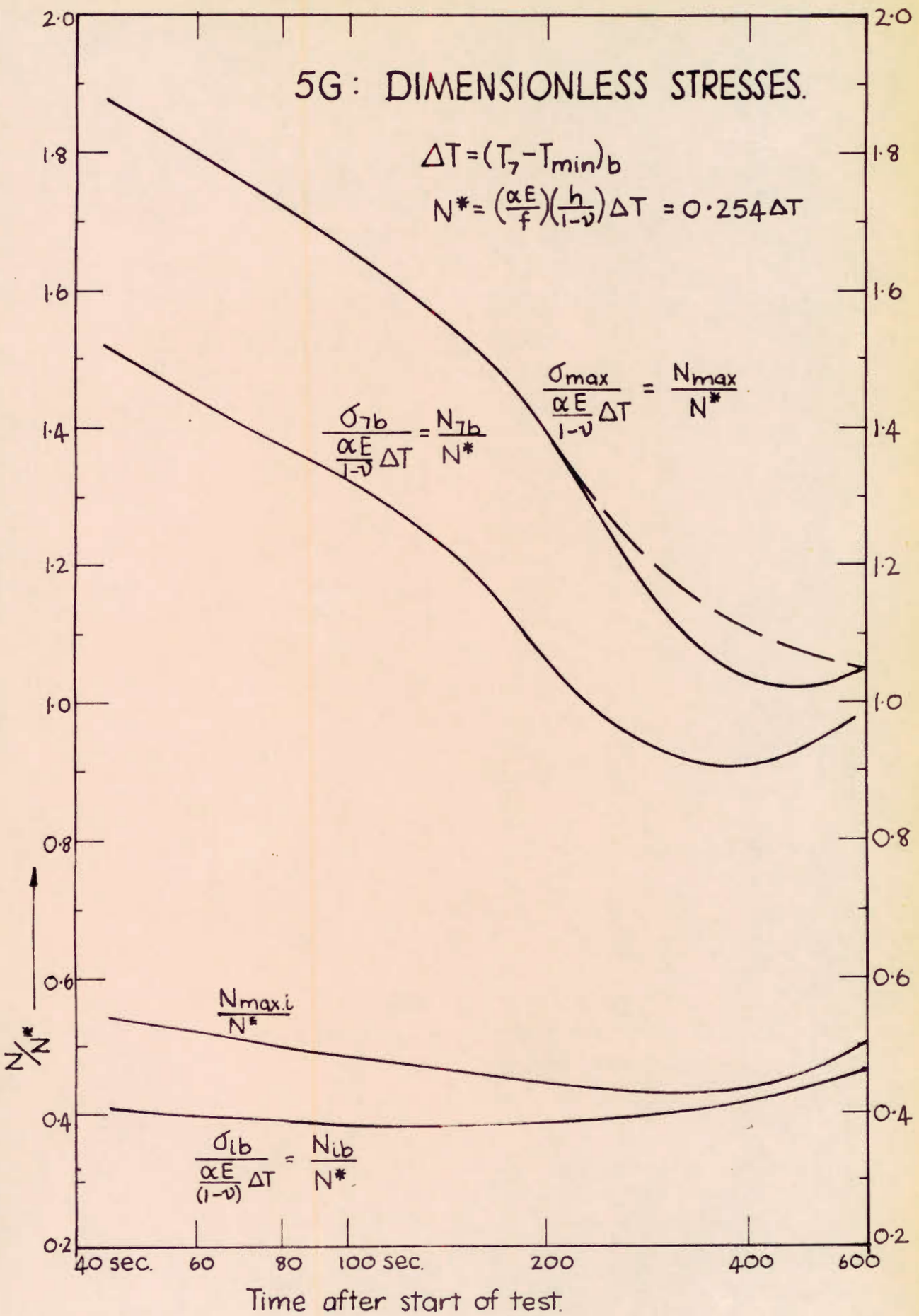
5G: DIMENSIONLESS STRESSES.
$\Delta T = (T_7 - T_{min})_b$
$N^* = \left(\frac{\alpha E}{f}\right)\left(\frac{h}{1-\nu}\right)\Delta T = 0{\cdot}254\,\Delta T$
$\frac{\sigma_{max}}{\frac{\alpha E}{1-\nu}\Delta T} = \frac{N_{max}}{N^*}$
$\frac{\sigma_{7b}}{\frac{\alpha E}{1-\nu}\Delta T} = \frac{N_{7b}}{N^*}$
$\frac{N_{max.i}}{N^*}$
$\frac{\sigma_{ib}}{\frac{\alpha E}{(1-\nu)}\Delta T} = \frac{N_{ib}}{N^*}$
N*/N
2·0
1·8
1·6
1·4
1·2
1·0
0·8
0·6
0·4
0·2
40 sec.
60
80
100 sec.
200
400
600
Time after start of test.

TEST 6

Time in seconds after start of test.

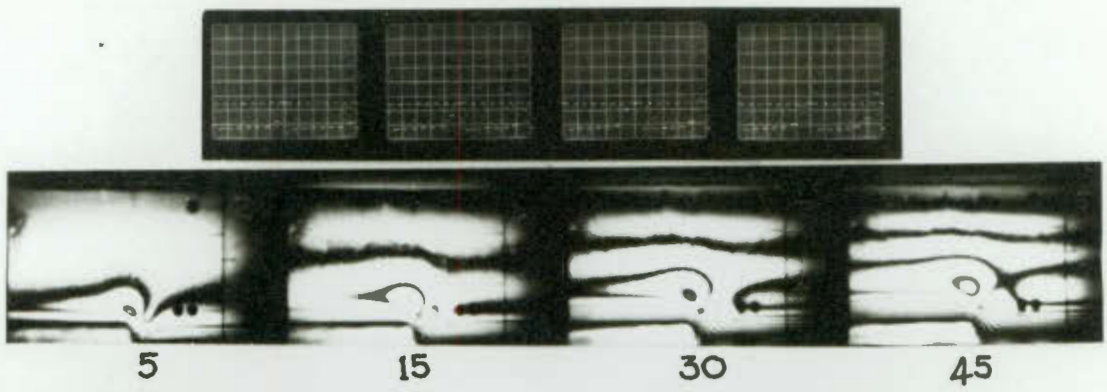

5 15 30 45

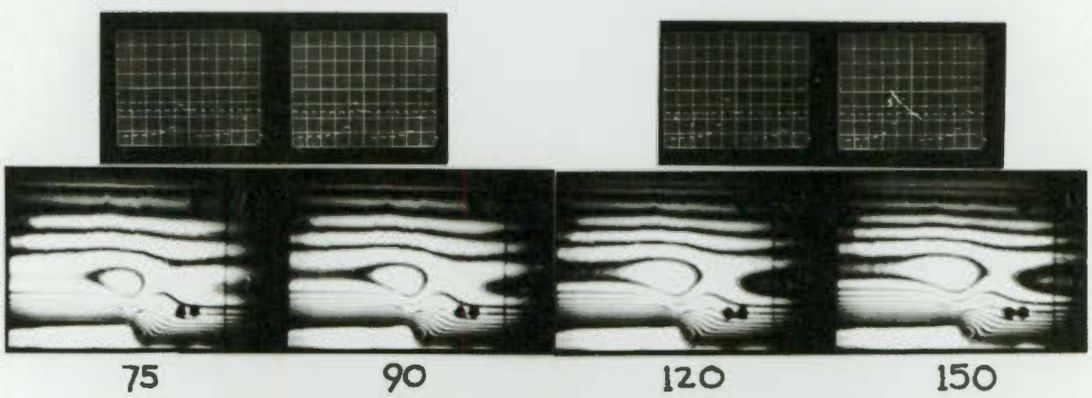

75 90 120 150

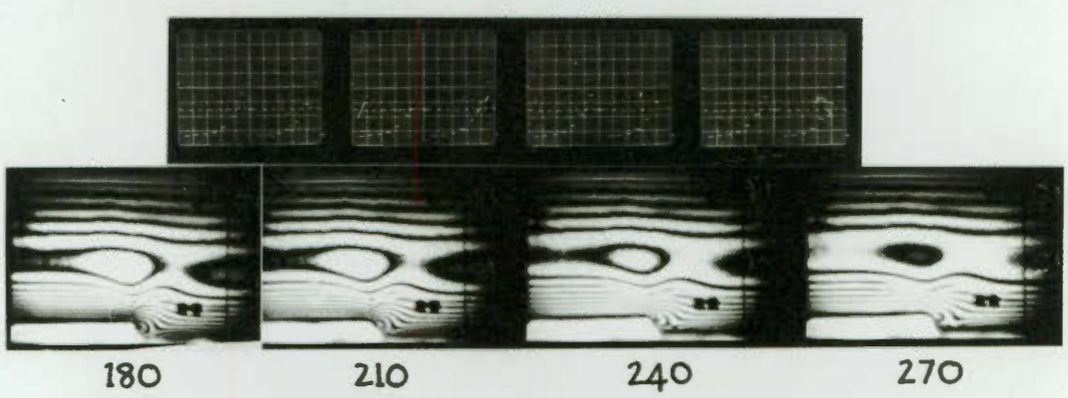

180 210 240 270

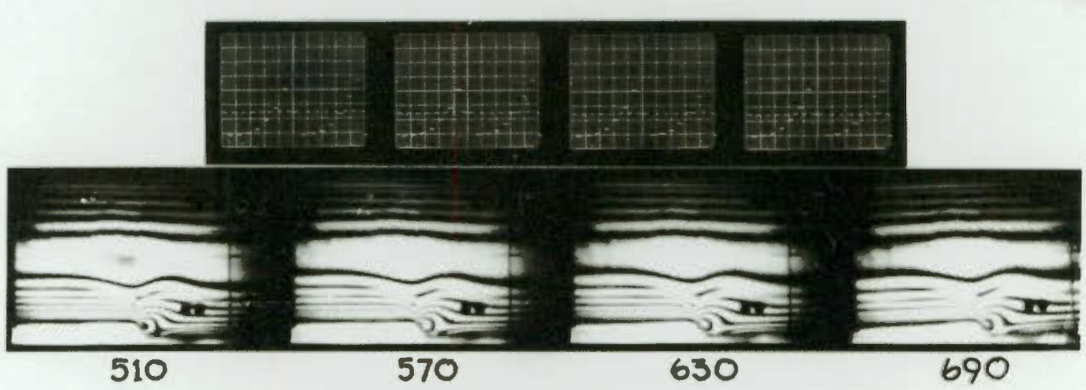

510 570 630 690

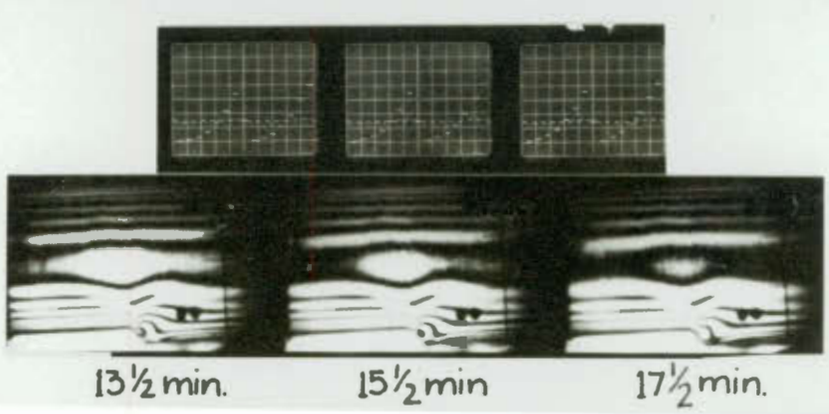

13½ min. 15½ min 17½ min.

6A: TEMPERATURE PROFILES.

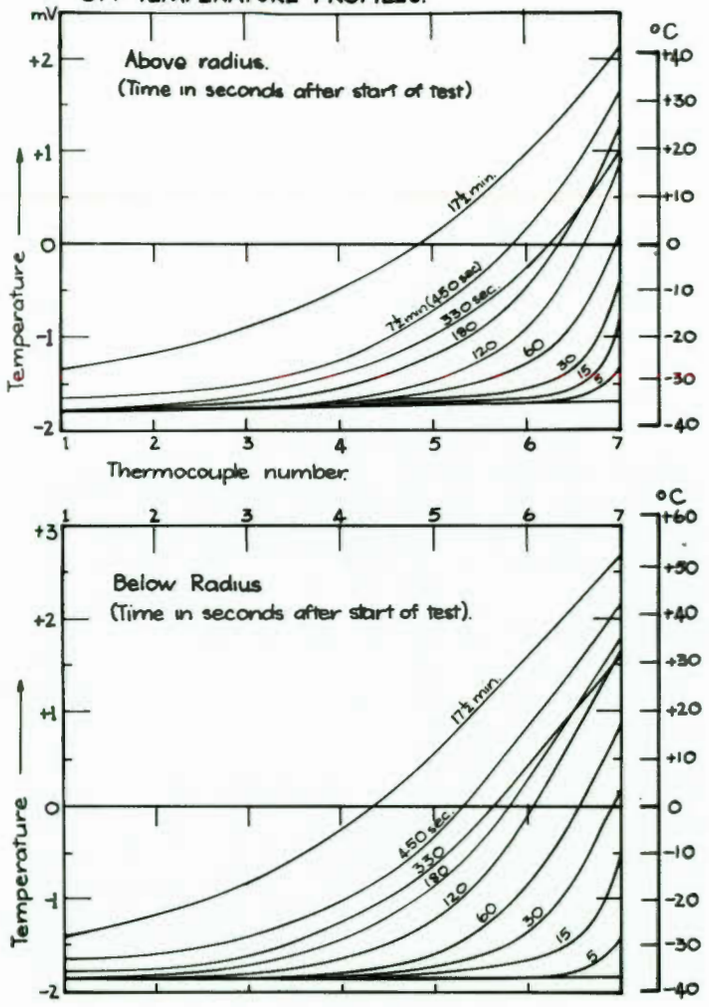

6B: STRESS PROFILES.

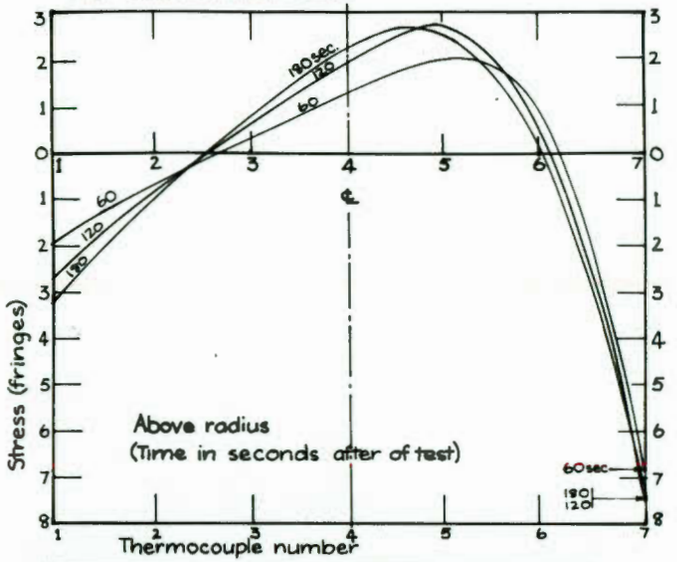

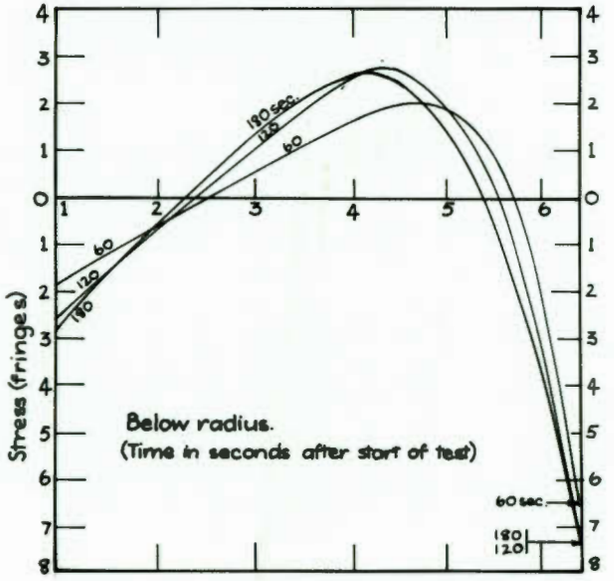

TEST Nº 6

NOTATION: page 89.

TEST Nº 6

NOTATION: page 89.

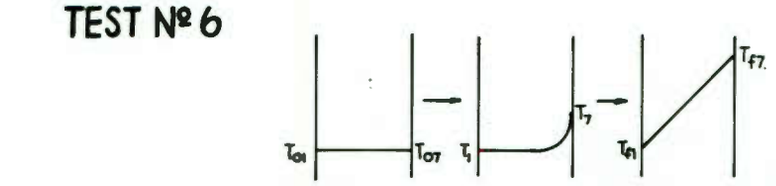

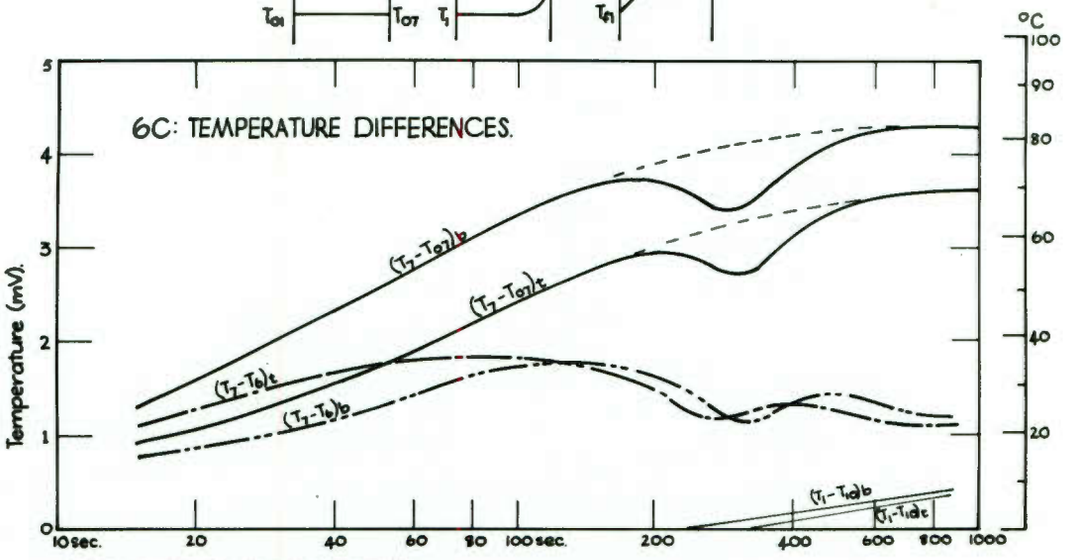

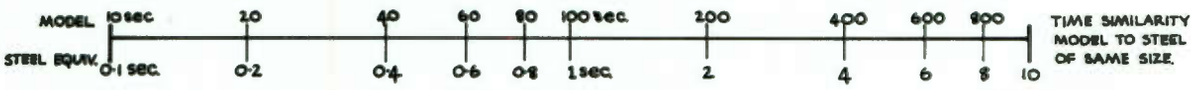

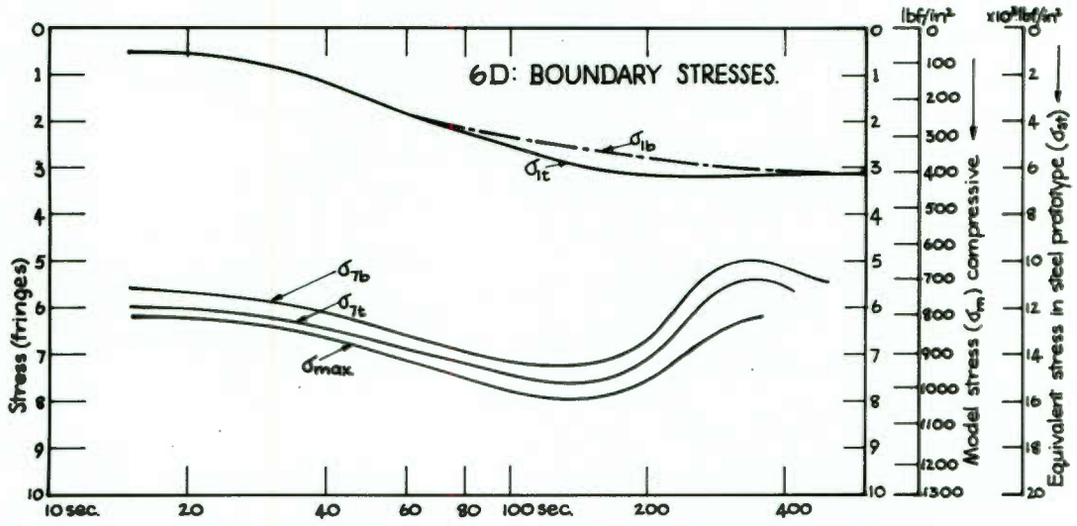

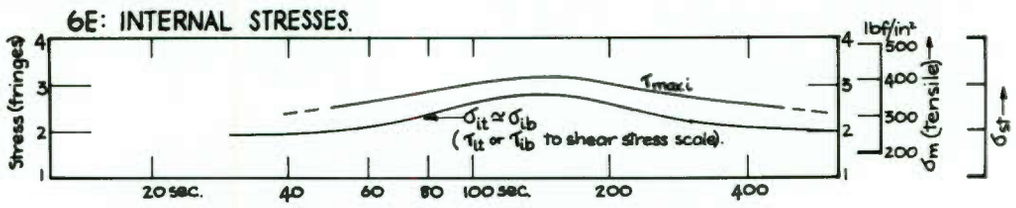

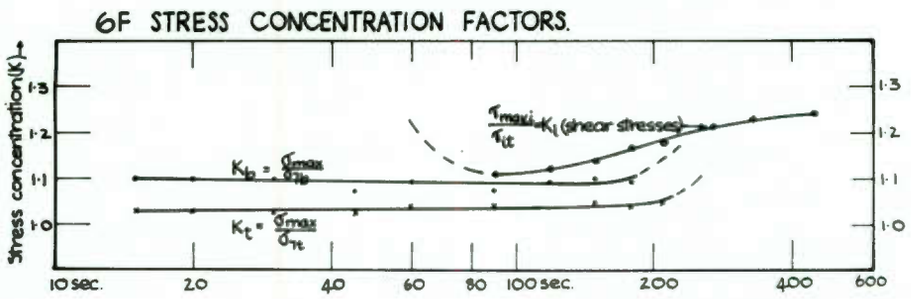

TEST 7

Time in seconds after start of test.

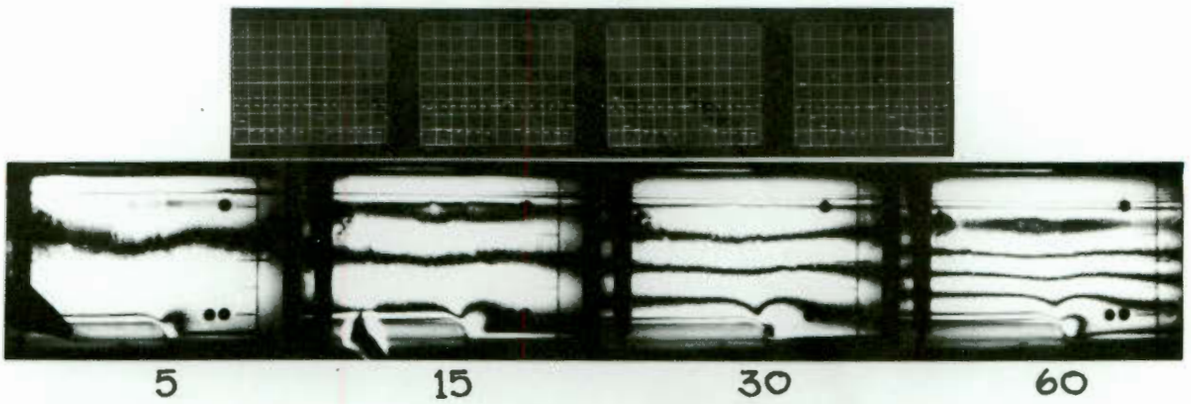

5 15 30 60

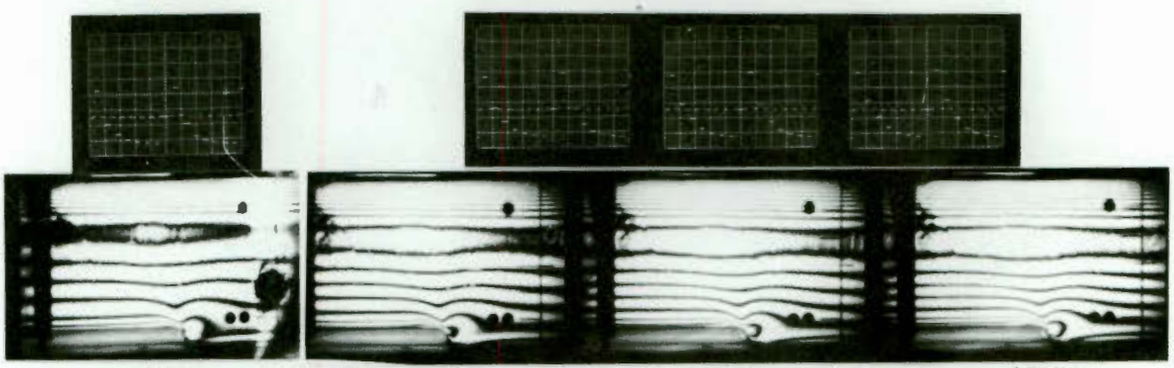

75 120 150 180

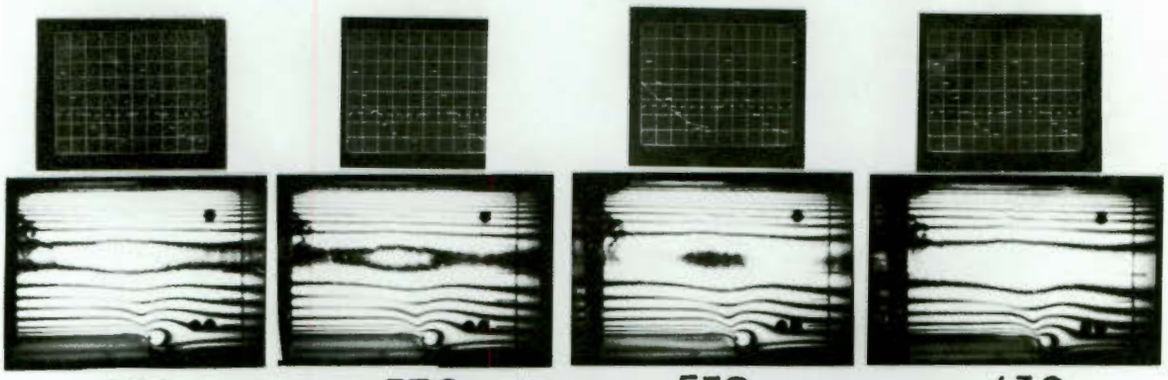

270 330 570 630

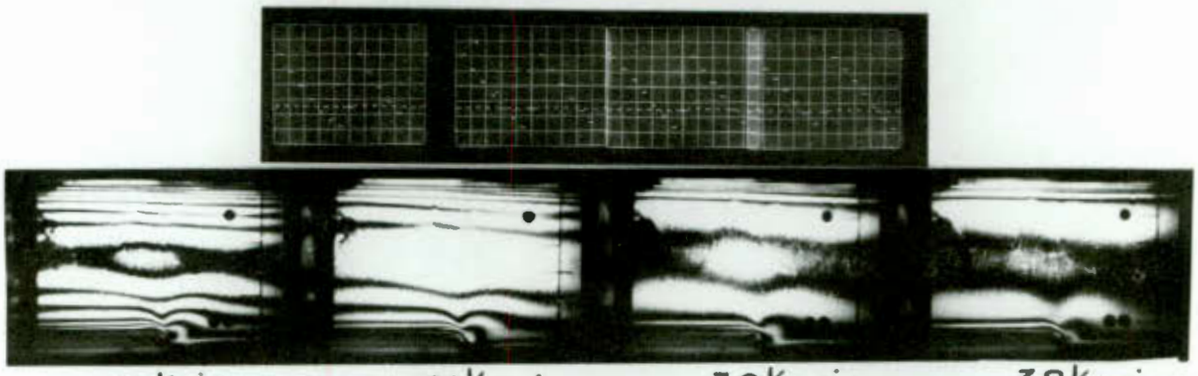

16½ min. 21½ min. 30½ min. 38½ min.

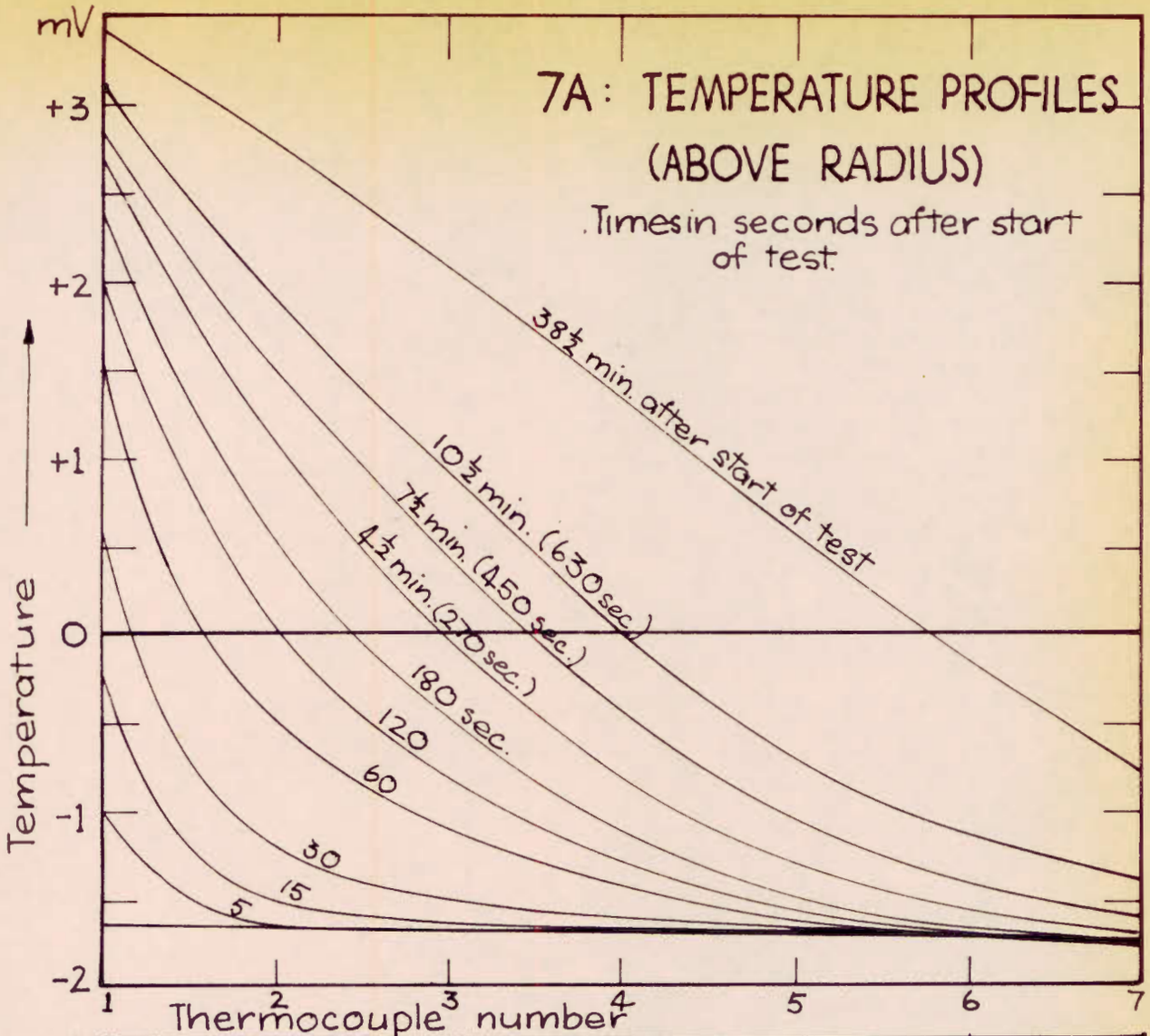
mV
+3
+2
+1
0
-1
-2
Temperature
7A: TEMPERATURE PROFILES
(ABOVE RADIUS)
Times in seconds after start of test
38½ min. after start of test
10½ min. (630 sec.)
7½ min. (450 sec.)
4½ min. (270 sec.)
180 sec.
120
60
30
15
5
1
2
3
4
5
6
7
Thermocouple number

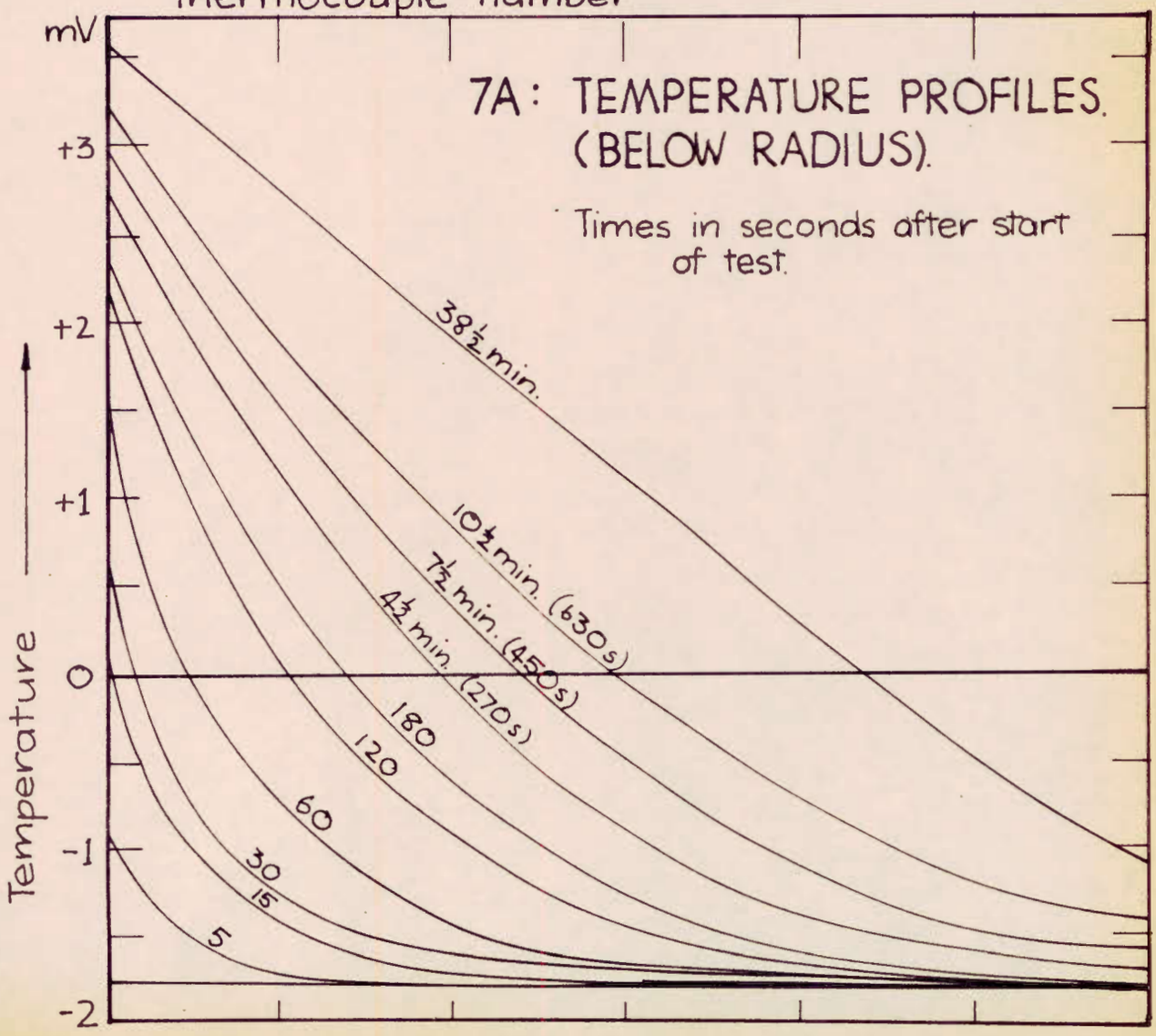
mV
+3
+2
+1
0
-1
-2
Temperature
7A: TEMPERATURE PROFILES.
(BELOW RADIUS).
Times in seconds after start of test.
38½ min.
10½ min. (630s)
7½ min. (450s)
4½ min. (270s)
180
120
60
30
15
5

TEST Nº 7

NOTATION: page 89.

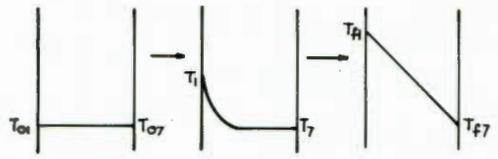

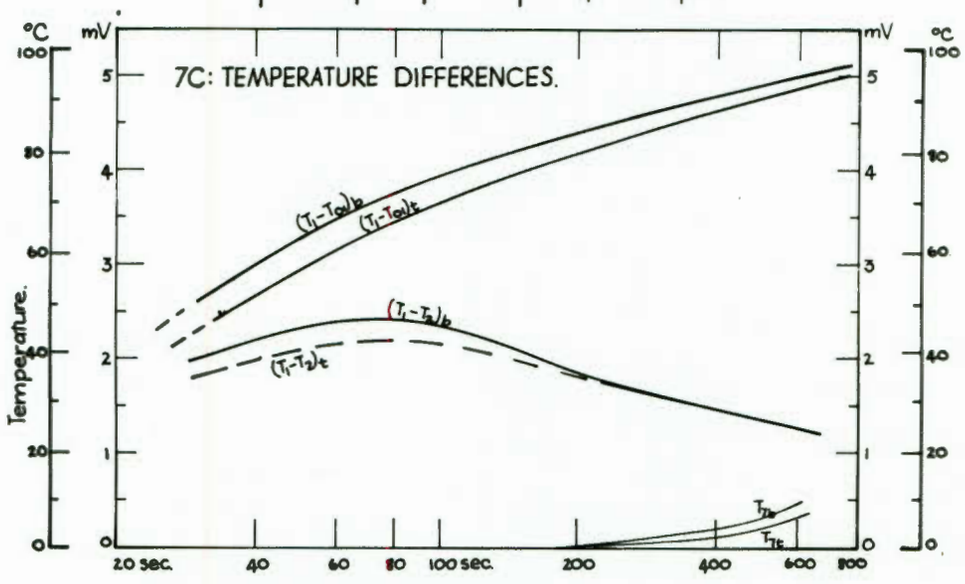

Time after start of test (seconds) ⟶

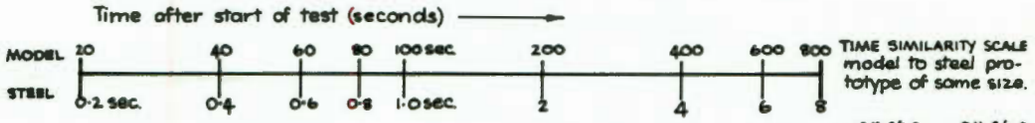

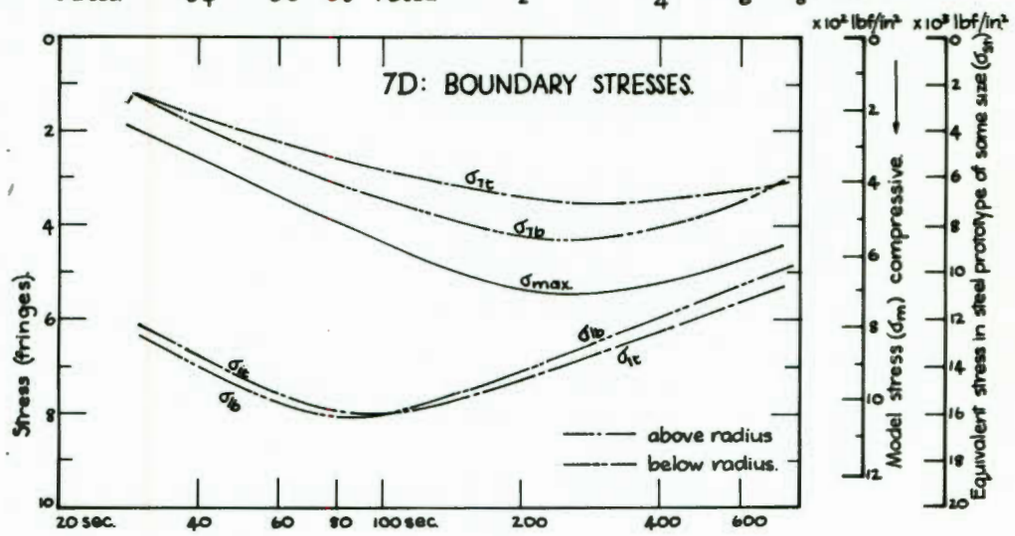

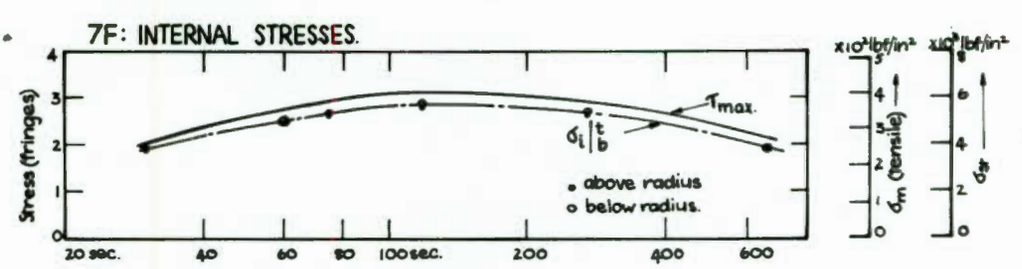

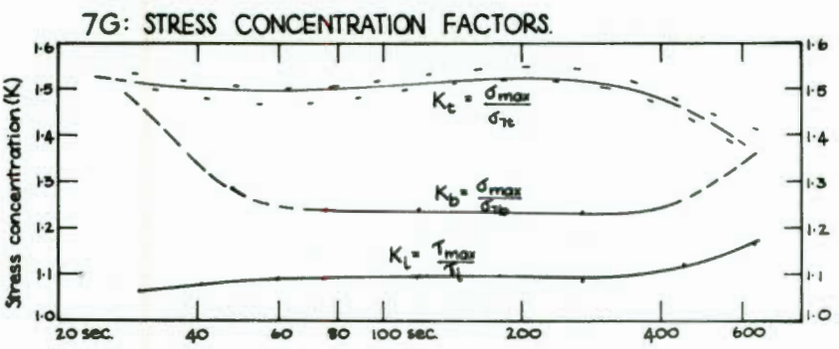

ISOCLINICS

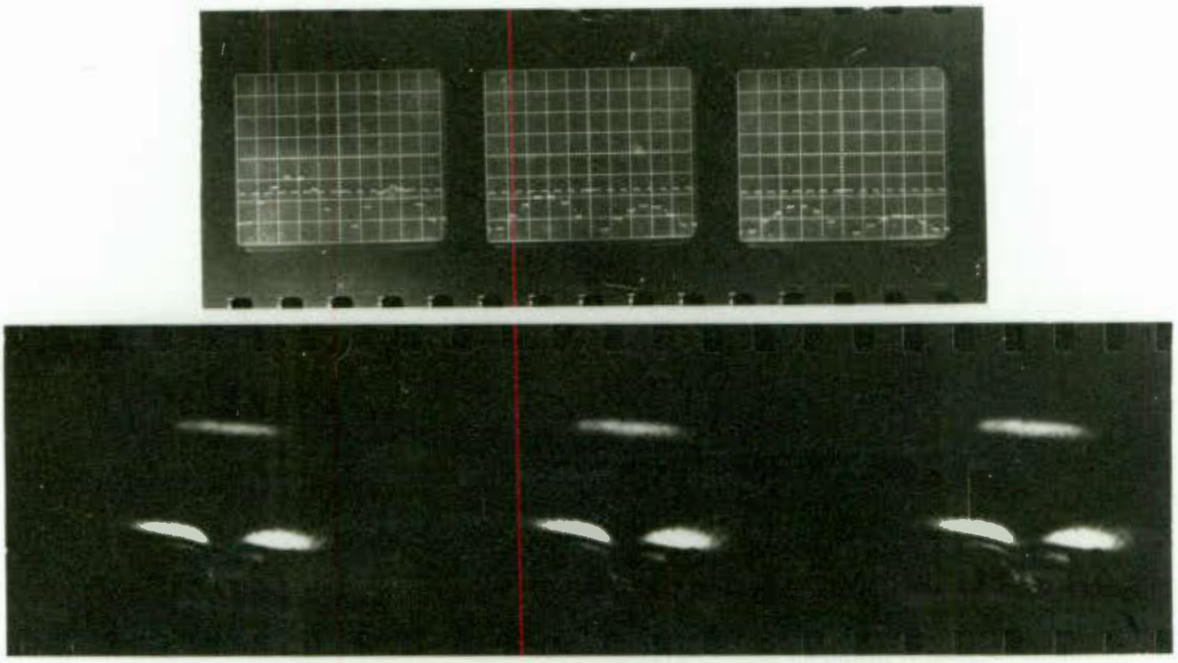

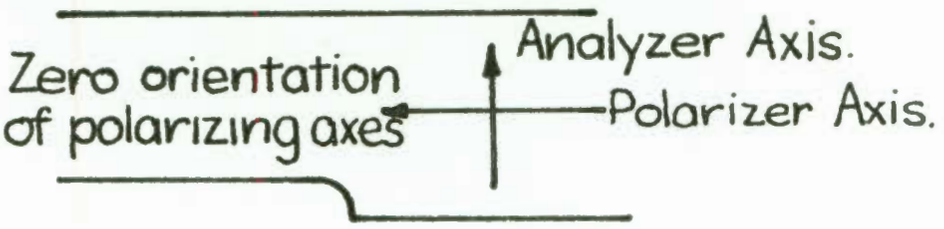

Therefore:

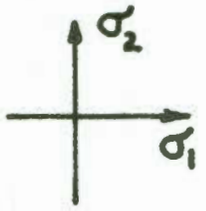

wherever model image is black
i.e. everywhere except at white
areas near radius.

After about 3 minutes, the temperature profiles should be symmetrical parabolas and the boundary stresses may be predicted by equation 15. With the correct values from table 2 this becomes:

$$N^{*}=0.155\,\Delta T_{max} \qquad (20)$$

where ΔT_{max} is the largest temperature difference between a boundary and the inside of the model at each instant. The values for ΔT_{max} are shown on graph 1C and the boundary stresses to equation (20) are drawn as a chain dotted line in 1D. Agreement with experimental values is generally closer than 5%.

The figure of merit, Q', is calculated by setting the correct values from table 2 into equation (16) so that

$$Q' = 2.26\ N/\Delta T_{max} \qquad (21)$$

The solution to this equation, using the mean value for the boundary stresses in 1D and ΔT_{max} from 1C, is drawn in graph 1F. Q' is seen to be nearly constant over the range where equation (21) can be applied.

The difference between the two boundary stresses σ_1 and σ_2 can be attributed to slight non symmetry of the temperature profiles.

The internal stresses fall within a band of probability which is drawn in outline on graph 1F.

Test 2(Model A): Plate initially at a uniform temperature, heated on the one side only.

The graphs can be interpreted directly. The drop in surface temperature T_{11} at about 200 seconds is due to an unexpected cross flow of cold paraffin into the hot system.

The difference between the readings of the two thermocouples T_{11} and T_{10} may be taken as an arbitrarily chosen indication of the slope of the temperature profile near the boundary which is being heated.

Test 3(model A): Plate, initially with a linear temperature gradient through its thickness, with the cold boundary being

heated: (At intermediate points in this test conditions similar to those which arise during internal heating of a plate, are found.)

The graphs speak for themselves. || No, no!

The highest stress occurs on the boundary subjected to the temperature change after about 160 seconds. (1.6sec. for steel). This would also be the worst stress condition for internal heating of a plate.

Tests on Model B:

Since the model is unsymmetrical observations are made of stresses and temperatures above and below the change in section. The highest stresses caused by the change in geometry are also recorded. There are therefore eight general points of interest: Two on the boundaries and one internally above, and the same number below the radius, in regions undisturbed by the stress concentration; plus the points of highest boundary and internal stresses in the region of the radius.

Test 4: Plate initially at a uniform temperature, heated equally on both sides:

As explained in section 5.6, the photographic record of the fringe patterns of this test was too dark to be adequately reproduced as positive prints. Details of the boundary stresses could be read so accurately that it was not necessary to consider plotting the full stress profiles in order to arrive at accurately extrapolated values of the stresses at the boundaries of the model.

Theoretical predictions of the stresses were made in the same way as for test 1, but with the slightly different material properties of Model B, equations 20 and 21 became:

$$N^* = 0.169\Delta T \qquad (22)$$

$$Q' = 2.24\ N/\Delta T_i \qquad (23)$$

For the internal stresses $N_i^* = \frac{1}{2}N^* = 0.085\Delta T$ (24)

Agreement with the experimental curves for the boundary stresses are good over the section of the graph where equation 22 applies. The prediction of equation 24 does not agree as well with the experimental curves of 4E, the main error being a relative shift in time. The highest value of σ_i is 2.5% lower than the highest value for $\sigma_i^* = .085(T_7 - T_{min})b$. and occurs 100 seconds later. These stresses are obviously more sensitive to deviations from symmetry in the temperature distributions.

Graph 4F shows that the boundary stress concentrations increase to maxima coincident with the occurrence of maximum stresses. The difference between the internal shear stresses $(\tau_{maxi} - \tau_i)$ remains approximately constant throughout the time represented by 4E. This means that the stress concentration K_i starts at a high value early in the test and reduces as the test progresses to a minimum at about the time when the absolute values of the stresses reach their maxima.

The value of Q', as calculated from the experimental results (eq. 23) is once more nearly constant. This is shown in 4H.

Graph 4J shows that the relation between ΔT and stress is linear. This is in accordance with the theory of equations 9 and 22.

These same equations predict that the value for the dimensionless boundary stress should be constant and equal to 0.66. This is almost exactly so at the times when equation 9 applies.

Test 5: Plate initially in steady state condition, stepped side cold, the other hot, with the cold side being heated:

The very steep gradients in the radius made an accurate fringe count, very difficult. The actual count could, during the periods of maximum stress be as much as one fringe low.

This uncertainty is shown by the dotted lines alongside the σ_{max} curve of graph 5D.

The boundary and internal stress concentration factors behave in a similar way to those of test 4. The chain dotted lines in 4F show the extreme probabilities for the boundary stress concentration factor. K_{max} was found by dividing the upper probability boundary of σ_{max} by the lowest probability boundary of the two surface stresses σ_{7b} and σ_{7t}. K_{min} was found by dividing the lowest probability boundary for σ_{max} by the highest probable values for σ_{7b} and σ_{7t}.

Test 6: Plate initially at a uniform temperature, with the stepped side being heated.

Shortly after the occurrence of the highest stresses, some cold liquid was cross pumped into the hot system. This caused a drop of short duration in the surface temperature T_7, which was almost immediately reflected in the surface stress and temperature but had no obvious effect on the internal stress graphs of 6E, nor on the stresses σ_1. This shows clearly the effect of short time oscillations in the boundary temperatures on the stresses induced in a component.

The boundary stress concentration lines of 6F are constant up to the instant when the temperature disturbance occurred.

Test 7: Plate initially at a uniform temperature with the straight side being heated.

The results are similar to those for test 6, except that the highest stresses now no longer occur on the radius.

5.8: Experimental errors.

With carefully controlled and consistent temperature variations on the model boundaries, The largest single area of uncertainty in the experimental results was the exact

reading of the highest fringe order on the boundaries of the model at places where the stress gradient was either very steep or changing rapidly with time. Under these conditions the error in the fringe count could be 1 fringe, i.e. about 10% of the stress levels pertaining at such times. Good negatives of fringe pattern taken at times when the stresses do not vary so rapidly, (i.e. at about the time of maximum surface stresses) can be read with a reliability better than $\frac{1}{2}$ fringe, i.e. 5%.

In the vicinity of the highest internal stresses the stress gradient changes slowly, so that, the fringes are generally broad. Under such conditions it is difficult, without the use of compensation technique (which cannot be used in this kind of polariscope set up) to estimate accurately the partial fringe order at the point of highest stress. The total area of uncertainty could, at most, be about 0.3 fringe (10% at the stress levels considered) but is normally less than 0.2 fringe, i.e. about 7%.

In tests which are set up to study specific conditions such as the stresses which occur with a given profile for internal heating, errors should not be larger than 5%. With improved illumination and the use of large plate films accuracies better than 2% can be expected.

Other sources of error which may be present, singly, or in various combinations, are due to:

(i) Difficulties in defining accurately the boundary of the model. This is especially troublesome during the early stages of a test when thermal shock conditions prevail and the rapidly moving fringes blur the image of the model near the boundary. This can virtually be eliminated by improved illumination which will allow shorter exposure. times and sharper focusing onto the edges of the model.

(ii) Residual edge stresses in the model. These are

serious in areas of high stress concentration, but can be reduced or even eliminated by careful preparation and handling of the model.

(iii) Variations in the elastic and photoelastic properties of the model material with temperature.

The sum of these errors is estimated to be about 4%.

Recording of the temperature in the model is subject to a few small errors. These are:

(i) Errors in the placement of the thermocouples.

(ii) Thermocouple lag.

(iii) Drift in switching and recording equipment.

These errors are small and the sum of them is estimated to be not more than 2%. The resolution which was possible in the reading of the oscilloscope records was 50 micro volts, or $1^{o}C$. This is a constant value, which under conditions of small temperature change may be significant. With the normally used temperature differences, it introduced an error of 2% or less.

5.9 General discussion of the results:

The good agreement between the predictions of simple theory and the experimental results of tests 1 and 4 confirm the validity of the experimental results. The elastic, heat and optical constants of the model material is shown to be correct and the assumption of a constant value for the figure of merit of the material proved to be reasonable.

Of the three basic types of loading used, the highest stresses were caused by equal changes of temperature on the two boundaries of the model. (Tests 1 and 4). Such conditions do not occur very often in practice, but arise when a part is suddenly removed from a heated area, or when it is suddenly immersed in a hot or a cold liquid, e.g. quenching of plates, scram procedures in nuclear reaction and

various emergency conditions.

The temperature cycles of tests 3 and 5 induced stresses which were nearly as high as in the previous discussion. Such sequences are of great practical importance. They arise whenever the load in a power generating or heat transfer process is changed. In certain cases, especially when the heat transfer medium is a liquid metal, or at the pinch point in a once through boiler tube, the rate at which the surface temperature changes as well as the magnitude of the change may be very high. The resultant stresses can be predicted by tests similar to numbers 3 and 5. The temperature profiles set up in the early stages of these tests are furthermore similar to those which pertain in the steady state in components subjected to internal heating - a general design condition in nuclear reactors. From the worstepoints in graphs 3D and 5D to F these stresses are shown to be very high indeed. In considering creep and stress rupture full account should be taken of these stresses.

Tests 2, six and seven, represent conditions which occur during the start-up of thermal plant. The stresses in the absence of stress concentrations are of the same order as in the previous discussion, but the highest stresses at the shoulder are much lower. Conditions of this kind occur frequently in the life of most plant and may put a serious limit to the short term fatigue life of many critical parts.

All the model to prototype correlations on the graphs were made for a steel prototype of the same size as the model and subjected to the same temperature changes. The range of temperatures used in the tests never exceeded 100°C. The largest temperature difference in the model at any instant was slightly lower (from 60° to 80°C). An average rate of change of the model surface temperature up to the times of

highest stress was about 0.5°C/sec. Translated to steel this represents a change of 50°C/sec.

In design situations where thermal stresses are important a one to one ratio for geometric and temperature scaling will seldom apply. The stress scales will then generally be much higher than those given on the graphs.

In most of the tests the highest stresses occurred after about 200 seconds (i.e. about 2 seconds for a steel component). For the steel prototype this represents a rate of loading of the order of 6000 lbf/in^{2}sec., increasing to 10,000 lbf/in^{2}sec. at the point of highest stress concentration in the radius. With such high loading rates the ductile to brittle transition temperature of most materials is quite high and a brittle mode of failure has to be considered. Inertia effects also become important and the adiabatic, rather than the isothermal stress/strain relations apply.

The stress concentration caused by the geometric change in section of model B is a comparatively mild one. The two ends are still of nearly equal thickness so that the thermal inertia of the thin part differs only very little from that of the thick portion. With larger changes of section the thermal stresses tend to concentrate in the light section so that the stress concentration is much higher. Yet, even model B shows stress concentration factors, as high as 1.3. This is certainly high enough to be an important design consideration.

The same stress concentration applies to a plate like model B subjected to internal heating.

Structural concrete is a poor thermal conductor so that under conditions of internal heating the greater part of the heat is generated near the inner wall. This condition can

be studied with the same techniques as those used in tests 3 and 5 because the model material has a conductivity of the same order as concrete.

The graphs and photographs then illustrate the value of the test method as a design aid for the determination of thermal stresses under a wide variety of thermal loads. The same methods as were used here may be applied to the study of thermal stresses - transient and steady state - in many geometrical shapes and to find stress concentration factors for such cases as may be necessary. With correct scaling it is applicable to an infinite number of prototypes.

Manson (R30) reports a vast amount of experimental information in thermal stress cycling, plastic flow, creep and shock. Towards the end of this excellent book he says: "Sharp changes in cross section have long been known to introduce stress concentrations in mechanical loading. When loading is thermal, the effect may be even more deleterious--. It is thus especially important to consider the common situation in which stress and strain concentrations arise, as well as the methods of overcoming their deleterious effects." These tests have illustrated a very versatile way of acquiring such information.

Section 6: Conclusions.

The ever increasing role of photoelasticity in engineering achievements depends upon the extension of available techniques, and the development of new techniques for application to new problems. Great advances have been made in the short history of experimental photoelasticity, and the present work is presented as yet another step in this evolution which will widen the scope of investigation.

The test method and apparatus described in section 4 was specially developed to extend known methods for the experimental study of thermal stresses into new regions. It is particularly suitable for the simulation of a wide variety of transient thermal stress conditions; in fact, by careful manipulation of the controls almost any one dimensional and a limited number of two dimensional temperature gradients can be induced in suitably designed models.

In section 5 this experimental technique is applied to the study of thermal stresses generated in a thick plate by transient temperature conditions through its thickness. The validity of the results is confirmed by comparison with simple theory, and the versatility of the method is illustrated by its application to a number of thermal sequences. A typical model-to-prototype correlation is used to present scales on the graphs which would indicate the order of magnitude of the stresses in a steel plate, as well as the equivalent times when they would appear.

Apart from the general study of the stresses under changing temperature conditions, the results include the special case of the stresses in components subjected to internal heating.
This is the first time such stresses have been analysed by photoelasticity.

Thermal stress concentrations are found for a flat plate with a change in thickness (ratio of thicknesses used is 1.1 to 1). This has not previously been done for flat plates, nor for the general temperature cycles used here. The same tests also provide, for the first time, the stress concentrations in similar parts with internal heating.

Section 7: Acknowledgements.

Without the help and encouragement of several persons and organisations, this study would never have reached the present stage of development. Their assistance is gratefully acknowledged.

The South African Atomic Energy Board, Pelindaba, Transvaal and The Southern Universities Nuclear Institute, Faure, Cape, provided financial support for the purchase of some of the more expensive equipment. Special thanks are due to Dr. W.L. Grant, Director of the Reactor Design Division at Pelindaba, whose ideas initiated this research and whose interest remains a constant source of encouragement.

All the work for this thesis was performed in the Department of Mechanical Engineering of the University of Cape Town. The Foucade Bequest and Staff Research Fund contributed generously towards the project. Much of the apparatus was built in the departmental workshops, where Messrs. J. Busbridge, J.R. Gordon, M.A. Betterworth, and W.K. Betterworth all contributed valuable suggestions and help in its design and construction.

Messrs. W. Baerecke and L. Wheeler of the Photographic Department, University Library, gave valuable advice on the many photographic problems which arose.

The constant help and sound advice of Mr. R.M. Stegen of the Department of Mechanical Engineering, saved this programme from having a much rougher passage than it did.

Finally thanks are due to my wife, who did most of the lettering on the drawings, and my mother-in-law, Mrs. M.A.E. Kenyon, who did all the typing.

REFERENCES.

1. M.M. Frocht, "Photoelasticity", vol.1, 1941, vol.2, 1948, John Wiley and Son, New York.

2. E.E. Weibel, "Thermal Stresses in Cylinders by the Photoelastic Method", Proc. Fifth International Congress Applied Mechanics, Cambridge 1938, pp 213-20.

3. G. Gerard and A.C. Gilbert, "Photothermoelasticity: An exploratory Study", Jnl. of Applied Mechanics, v24, Trans. ASME, v79, 1957, pp 355-60.

4. H. Tramposch and G. Gerard, "Physical Properties of Plastics for Photothermoelasticity Investigations", Jnl. of Applied Mechanics, v25, Trans. ASME, v80, 1958, pp 525-28.

5. G. Gerard and H. Tramposch, "Photothermoelastic Investigation of Transient Thermal Stresses in a Multiweb Wing Structure", Jnl. of Aero/Space Sciences, v26, 1959, pp 783-6.

6. H. Tramposch and G. Gerard, "Correlation of Theoretical and photothermoelastic Results in Thermal Stresses in idealized Wing Structures", Jnl of Applied Mechanics, v27, 1960, pp 79-86.

7. H. Tramposch and G. Gerard, "An exploratory Study of Three Dimensional PHOTOTHERMOELASTICITY", Jnl. of Applied Mechanics, v28, March 1961, pp 35-40.

8. G. Gerard, "Progress in Photothermoelasticity", Int. Symp. on Photoelasticity, Chicago, Oct. 1961, Pergamon Press 1963, Ed. M. Frocht.

9. R.C. Samson, "A three-dimensional photoelastic method for analysis of differential contraction stresses", Experimental Mechanics v3, n9, 1963 pp 225-37.

10. A.J. Durelli and V.J. Parks, "New method to determine restrained shrinkage stresses in propellant grain models", Experimental Mechanics, v3, n 11, 1963, pp 263-8.

11. A.J. Durelli and V.J. Parks, "Photoelasticity Methods to determine Stresses in Propellant-grain Models", Experimental Mechanics, v5, n2, 1965, pp 33-46.

12. R.J. Rothstein and W.F. Kirkwood, "Photothermoelastic Analysis of Stresses in Multiconnected Flat Circular Rings", Experimental Mechanics, v4, n8, 1964, pp 237-43.

13. A.F. Emery, C.F. Barrett and A.S. Kobayaski, "Temperature Distributions and Thermal Stresses in a Partially Filled Annulus", Experimental Mechanics, v6, n12, Dec. 1966.

14. H. Becker, "An Exploratory Study of Stress Concentrations in Thermal Shock Fields", Jnl. of Engineering for Industry (ASME Ser. B), v84, 1962, pp 343-8.

15. G.A. Gurtman and A.A. Colao, "Photothermoelastic Investigation of Stresses around a Hole in a Plate subjected to Thermal Shock", Experimental Mechanics, v5, n4, 1965, pp 97-104.

16. M.M. Leven and R.L. Johnson, "Thermal Stresses on the Surface of Tube-sheet Plates of 10 and 33⅓ percent Ligament Efficiency", Experimental Mechanics v4, n12, 1964 pp 356-65.

17. T. Slot, "Photoelastic Simulation of Thermal Stresses by Mechanical Pre-Straining", Experimental Mechanics, v5, n9, 1965, pp 273-82.

18. S. Timoshenko and J.N. Goodier, "Theory of Elasticity", McGraw-Hill Book Co., New York, 2nd. Edition, 1951.

19. W. Nowacki, "Thermoelasticity", Pergamon Press, Oxford, (PWN Warszawa 1962).

20. B.A. Boley and J.H. Weiner, "Theory of Thermal Stresses", John Wiley and Sons, New York, 1960.

21. A.J. Durelli and W.F. Riley, "Introduction to Photomechanics", Prentice Hill Inc., Englewood Cliffs, 1965.

22. I.M. Daniel and A.J. Durelli, "Photothermoelastic Analysis of bonded propellant grains", Experimental Mechanics, v 1, n3, 1961, pp 97-104.

23. S.S. Manson, "Thermal Stresses in Design-Measurements by Photoelasticity", Machine Design v13, 1959, pp143-51.

24. L.F. McCalvery, "Measurement of Thermal Stresses during start-up of turbo-generators", Strain v2, n4, Oct. 1966, pp 3-10.

25. C.J. Smithells, "Metals reference Book", Vol 2, Butterworth, London, (3rd. Ed.) 1962.

26. J.W. Dally and W.F. Riley, "Experimental Stress Analysis", McGraw Hill Book Co., New York, 1965.

27. ASME Handbook: "Metals Engineering Design", McGraw Hill Book Co., New York, 1965.

28. P.P. Benham and R.D. Hoyle (editors), "Thermal Stress". Symposium at Imperial College, London, Sir Isaac Pitman, London, 1964.

29. The Franklin Institute Research Laboratories, "Thermal Stress Technique in the Nuclear Industry", Elsevier Publishing Co., New York, 1965.

30. S.S. Manson, "Thermal Stress and Low Cycle Fatigue", McGraw Hill Inc., New York, 1966.

31. A. Nadai, "Theory of Flow and Fracture of Solids", McGraw Hill Book Co., New York, v2, 1963, v1, 1950.

32. I.I. Gol'denblatt and N.A. Nikolaenko, "Calculation of Thermal Stresses in Nuclear Reactors", original Russian text 1962, translated into English, Consultants Bureau, New York, 1964.

33. D.J. Johns, "Thermal Stress Analysis", Pergamon Press, Oxford, 1965.

34. B.E. Gatewood, "Thermal Stresses", McGraw Hill Inc., New York, 1957.

35. J.D. Hovanesian and H.C. Kowalski, "Similarity in Thermoelasticity", Experimental Mechanics v7, n2, Feb. 1967, pp 82-4.

36. S.F. Borg, "Matri-Tensor Methods in Continuum Mechanics", D. van Nostrand Co., New York, 1963.

37. A.J. Durelli and Ferrer, "New Methods to Determine Elastic Constants", Materials Research and Standards, (ASTM) v3, n12, 1963, pp 98.

38. D.W. Robinson, "An Apparatus for the Measurement of Dynamic Mechanical Properties of Polymers over a wide Temperature Range", Jnl. of Scientific Instruments, v 32, n2, 1955

39. P. Reichner, "Stress Concentration in Multiple-notched rim of disc." Experimental Mechanics, v1, n 11, pp160-6.

40. M. Lessen, "On Similarity of Thermal Stresses in Elastic Bodies", Jnl. of the Aeronautical Sciences, v20, 1953, pp 716-7

41. J. Dugundji and J.M. Calligeros, "Similarity of Laws for Aerothermoelastic Testing", Jnl. of Aero-Space Sciences, v29, n8, 1962, pp 935-50.

42. N.H. Goldstein, "A Critical Analysis of Thermal Stresses", Data for Designers, Engineering Materials and Design Special Publication, London.

43. N.H. Polakowski and E.J. Ripling, "Strength and Structure of Engineering Materials", Prentice Hall Inc., Englewood Cliffs, 1966.

44. P. Dantu, "Extension of Moiré Method to Thermal Problems", Experimental Mechanics, v4, n3, 1964, pp 64-69.

45. P.S. Theocaris, "The Moiré Method in Thermal Fields", Experimental Mechanics, v4, n8, 1964, pp 223-31.

46. A.W. Hendry, "Photoelastic Analysis", Pergamon Press, Oxford, 1966.

47. C.R. Wylie, "Advanced Engineering Mathematics", McGraw Hill Book Co., New York, Third Edition, 1966.